The Astrophysical Journal, 665:265–294, 2007 August 10
© 2007. The American Astronomical Society. All rights reserved. Printed in U.S.A.

# GALAXY LUMINOSITY FUNCTIONS TO $z \sim 1$ FROM DEEP2 AND COMBO-17: IMPLICATIONS FOR RED GALAXY FORMATION[1]

S. M. Faber,[2] C. N. A. Willmer,[3,4] C. Wolf,[5] D. C. Koo,[2] B. J. Weiner,[3] J. A. Newman,[6,7] M. Im,[8] A. L. Coil,[3] C. Conroy,[9] M. C. Cooper,[9] M. Davis,[9] D. P. Finkbeiner,[10] B. F. Gerke,[11] K. Gebhardt,[12] E. J. Groth,[13] P. Guhathakurta,[2] J. Harker,[2] N. Kaiser,[14] S. Kassin,[2] M. Kleinheinrich,[15] N. P. Konidaris,[2] R. G. Kron,[16] L. Lin,[2,17] G. Luppino,[14] D. S. Madgwick,[6,7] K. Meisenheimer,[15] K. G. Noeske,[2] A. C. Phillips,[2] V. L. Sarajedini,[18] R. P. Schiavon,[19] L. Simard,[20,21] A. S. Szalay,[22] N. P. Vogt,[23] and R. Yan[9]

*Received 2005 June 1; accepted 2007 March 20*

## ABSTRACT

The DEEP2 and COMBO-17 surveys are compared to study luminosity functions of red and blue galaxies to $z \sim 1$. The two surveys have different methods and sensitivities, but nevertheless results agree. After $z \sim 1$, $M_B^*$ has dimmed by 1.2–1.3 mag for all colors of galaxies, $\phi^*$ for blue galaxies has hardly changed, and $\phi^*$ for red galaxies has at least doubled (our formal value is $\sim$0.5 dex). Luminosity density $j_B$ has fallen by 0.6 dex for blue galaxies but has remained nearly constant for red galaxies. These results imply that the number and total stellar mass of blue galaxies have been substantially constant since $z \sim 1$, whereas those of red galaxies (near $L^*$) have been significantly rising. To explain the new red galaxies, a "mixed" scenario is proposed in which star formation in blue cloud galaxies is quenched, causing them to migrate to the red sequence, where they merge further in a small number of stellar mergers. This mixed scenario matches the local boxy-disky transition for nearby ellipticals, as well as red sequence stellar population scaling laws such as the color-magnitude and Mg-$\sigma$ relations (which are explained as *fossil relics* from blue progenitors). Blue galaxies enter the red sequence via different quenching modes, each of which peaks at a different characteristic mass and time. The red sequence therefore likely builds up in different ways at different times and masses, and the concept of a single process that is "downsizing" (or upsizing) probably does not apply. Our claim in this paper of a rise in the number of red galaxies applies to galaxies near $L^*$. Accurate counts of brighter galaxies on the steep part of the Schechter function require more accurate photometry than is currently available.

*Subject headings:* galaxies: distances and redshifts — galaxies: evolution — galaxies: luminosity function, mass function

## 1. INTRODUCTION

A major handicap in look-back studies of galaxy evolution is the inability to follow the evolution of any one galaxy over time. Instead, we see only snapshots of the galaxy population at different epochs, and it is difficult to identify objects at one epoch with their precursors and descendants at different epochs. One of the most important tools to solve this problem is precision counts of galaxies, which can quantify the "flow" of galaxies in parameter space as masses, morphologies, and stellar populations change. The luminosity function of galaxies was historically the first such tool, but the concept is rapidly being broadened to include counts as a function of mass, internal velocity, color, and other parameters.

[1] Based on observations taken at the W. M. Keck Observatory, which is operated jointly by the University of California and the California Institute of Technology, and on observations made with the NASA/ESO *Hubble Space Telescope*, obtained from the data archives at the Space Telescope Science Institute, which is operated by the Association of Universities for Research in Astronomy, Inc., under NASA contract NAS5-26555, and from the Canadian Astronomy Data Centre.

[2] University of California Observatories/Lick Observatory, University of California, Santa Cruz, CA 95064; faber@ucolick.org, koo@ucolick.org, raja@ucolick.org, jharker@ucolick.org, kassin@ucolick.org, npk@ucolick.org, lihwai@ucolick.org, kai@ucolick.org, phillips@ucolick.org.

[3] Steward Observatory, University of Arizona, Tucson, AZ 85721-0065; cnaw@as.arizona.edu, bjw@as.arizona.edu, acoil@as.arizona.edu.

[4] On leave from Observatório Nacional, Rio de Janeiro, Brazil.

[5] Department of Physics, Oxford University, Oxford, UK; cwolf@astro.ox.ac.uk.

[6] Lawrence Berkeley Laboratory, Berkeley, CA 94720; janewman@lbl.gov.

[7] Hubble Fellow.

[8] Department of Physics and Astronomy, FPRD, Seoul National University, Seoul, Korea; mim@astro.snu.ac.kr.

[9] Department of Astronomy, University of California, Berkeley, CA 94720; cconroy@astron.berkeley.edu, cooper@astron.berkeley.edu, mdavis@astro.berkeley.edu, renbin@astro.berkeley.edu.

[10] Department of Astrophysical Sciences, Princeton University, Princeton, NJ 08544; dfink@astro.princeton.edu.

[11] Department of Physics, University of California, Berkeley, CA 94720; bgerke@astro.berkeley.edu.

[12] Department of Astronomy, University of Texas, Austin, TX 78712; gebhardt@hoku.as.utexas.edu.

[13] Department of Physics, Princeton University, Princeton, NJ 08544; groth@pupgg.princeton.edu.

[14] Institute for Astronomy, Honolulu, HI 96822-1897; kaiser@ifa.hawaii.edu, ger@ifa.hawaii.edu.

[15] Max-Planck-Institut für Astronomie, D-69117 Heidelberg, Germany; meise@mpia.de.

[16] Department of Astronomy, University of Chicago, Chicago, IL 60637; rich@oddjob.uchicago.edu.

[17] Department of Physics, National Taiwan University, Taipei 106, Taiwan.

[18] Astronomy Department, University of Florida, Gainesville, FL 32611; vicki@astro.ufl.edu.

[19] Astronomy Department, University of Virginia, Charlottesville, VA 22904-4325; ripisc@virginia.edu.

[20] Herzberg Institute of Astrophysics, National Research Council of Canada, Victoria, BC V9E 2E7, Canada; luc.simard@nrc.ca.

[21] Guest Observer, Canadian Astronomy Data Centre.

[22] Department of Physics and Astronomy, Johns Hopkins University, Baltimore, MD 21218; szalay@jhu.edu.

[23] Department of Astronomy, New Mexico State University, Las Cruces, NM 88003-8001; nicole@nmsu.edu.

However, nearly all these functions are *unimodal* and lack clear features that demarcate one class of galaxies from another. In other words, galaxies tend to populate one big "cloud" in most parameter spaces rather than separate clumps. This makes interpretation difficult, as subcounts depend on how boundaries within these clouds are defined, and it is not clear whether (or how) the boundaries should be adjusted to follow galaxy evolution. As a result, we often cannot tell whether a change in the number of galaxies in any particular bin is due to a change in the overall number of galaxies or to the motion of galaxies in and out of that bin from neighboring bins. The latter problem is further exacerbated by the fact that samples are usually size or brightness limited and population numbers on the other side of these limits are not known. Finally, uncertain errors can smear counts from one bin to another. It will be possible to model all of these problems when a full theory of galaxy formation is available that predicts how galaxies should evolve in every measured parameter. In the meantime, it is hard to break the population into well-motivated subpopulations, and we therefore lack the means to obtain more finely divided knowledge.

Amid this sea of unimodal functions, one function stands out on account of its uniquely bimodal character, namely, the color function. This is visible in the color-magnitude diagram (CMD) of nearby galaxies, where early-type E/S0s populate a narrow red sequence that is separated from bluer, star-forming spirals by a shallow valley (Strateva et al. 2001; Hogg et al. 2003; Balogh et al. 2004; Baldry et al. 2004 and references therein). A similar division extends to at least $z \sim 1$ (Lin et al. 1999; Im et al. 2002; Bell et al. 2004b, hereafter B04; Weiner et al. 2005, Willmer et al. 2006, hereafter Paper I) and possibly beyond (Giallongo et al. 2005). A bimodal distribution is also seen in other parameters such as spectral class (Madgwick et al. 2002, 2003) and morphologies, metallicities, and star formation rates (Kauffmann et al. 2003a, 2003b), but color is by far the easiest to measure. Thus, not only does color sort galaxies cleanly into bins, it is also highly relevant to the emergence of the Hubble sequence.

However, to exploit this opportunity requires highly accurate counts, as the expected effects over recent look-back times are not large. For example, counts of red galaxies in the COMBO-17 survey were seen to evolve by a factor of a few since $z = 1$ (B04). Even this small number has important implications for galaxy formation (see § 6), but confirming and improving the measurement clearly requires accuracies of order 10%–20%. Few previous measurements of distant luminosity functions have attained this accuracy. Red galaxies are especially difficult because of their high clustering, which necessitates large samples over a large number of statistically uncorrelated regions. We are only just now coming to appreciate how formidable the problem of cosmic variance is (e.g., Somerville et al. 2004).

The present paper addresses these challenges by comparing two large surveys, DEEP2 and COMBO-17, to create the largest database yet of distant galaxies with accurate redshifts, containing 39,000 galaxies in total with 15,600 beyond $z = 0.8$. The entire sample is large enough and dispersed enough over the sky that cosmic variance and Poisson fluctuations are reduced to 7%–15% per redshift bin. The samples were selected and measured in different ways—DEEP2 redshifts are spectroscopic, while COMBO-17's are photometric—and thus provide an important check on one another. Finally, color bimodality is used to divide red galaxies from blue galaxies at all epochs. The red luminosity function is rederived and compared to previous results by B04 from COMBO-17. The blue function offers an important foil for considering the behavior of the red function; it is derived here for the first time based on DEEP2 data from Paper I combined with data reanalyzed from COMBO-17. The two surveys are found to agree well for both red and blue functions in all major respects.

Our most important result is to confirm the recent rise in the number of massive red galaxies around $L^*$ found by B04. In contrast, the number density of massive blue galaxies has remained essentially constant since $z \sim 1$. This rise implies that a significant fraction of early-type galaxies assumed their final form at relatively late times, below $z = 1$, *where the process can be studied in detail*. The late emergence of many $L^*$ spheroidal galaxies disagrees with the classic high-redshift, monolithic collapse model for spheroid formation (Eggen et al. 1962; Larson 1975) but seems to be consistent with large amounts of other data, as reviewed in § 6.

The remainder of this introduction reviews previous measurements of luminosity functions through 2005 June, when this paper was first submitted; more recent work is discussed in § 6.4. The subject has a venerable history (e.g., Binggeli et al. 1988; Tresse 1999; de Lapparent et al. 2003), with determinations ranging from low to high redshift for field and cluster galaxies. Accurate determinations of *nearby* field luminosity functions have finally become available from the Two Degree Field Galaxy Redshift Survey (2dFGRS; Norberg et al. 2002) and the Sloan Digital Sky Survey (SDSS; Blanton et al. 2003; Bell et al. 2003), providing local benchmarks against which evolution can be measured.

That the luminosity function varies with the properties of galaxies has been known since Sandage et al. (1985) showed that the shape and magnitude of luminosity functions in the Virgo Cluster depend on galaxy morphology and luminosity class. This dependence on internal characteristics is also seen in local field galaxies when morphologies (Marzke et al. 1994, 1998; Marinoni et al. 1999), colors (Lilly et al. 1995b; Marzke & da Costa 1997; Lin et al. 1999; Blanton et al. 2001), and spectral types (e.g., Heyl et al. 1997; Bromley et al. 1998; Folkes et al. 1999; Cohen 2002; Madgwick et al. 2002; de Lapparent et al. 2003) are considered.

Early studies of the evolution of the galaxy luminosity function contained only a few hundred galaxies beyond $z = 0.5$ (e.g., Cowie et al. 1996; Brinchmann et al. 1998; Lin et al. 1999; Cohen 2002; Im et al. 2002; de Lapparent et al. 2003). In a landmark paper using the Canada-France Redshift Survey (CFRS), Lilly et al. (1995b) claimed that the evolution of the luminosity function is coupled to internal properties, being strongly correlated with color and, to a lesser extent, with luminosity. Dividing red galaxies from blue ones using the median spectral type of the sample (type Sbc), the authors found a steepening in faint-end slope for blue galaxies at redshifts beyond $z > 0.5$, whereas red galaxies showed little change in either luminosity or number density over the redshift range covered, $0.05 \leq z \leq 1$. The implication was that red galaxies had formed early before those epochs but that blue galaxies were still evolving, in agreement with the early monolithic collapse picture.

The conclusion that evolution depends on internal properties of galaxies was also reached by Cowie et al. (1996) based on a sample reaching to $z \sim 1.6$. Star formation rates were estimated from [O II] fluxes, and $K$-band photometry was used to estimate stellar masses. Cowie et al. (1996) found that most of the luminosity function evolution since $z \sim 1$ is due to blue galaxies with small masses but high star formation rates. More massive galaxies were relatively stable in number, particularly in the $K$ band, while the $B$ band showed modest number evolution. They concluded that the characteristic mass of galaxies undergoing intense star formation decreases over time, which they termed

"downsizing." This and other kinds of downsizing relevant to the evolution of red spheroidal galaxies are discussed in § 6.2.

Lin et al. (1999) measured evolution in the luminosity function out to $z = 0.55$ using redshifts from the Canadian Network for Observational Cosmology Field Galaxy Survey (CNOC2). They divided galaxies by rest-frame color into early, intermediate, and late types and were the first to detect color bimodality at significant redshifts. They stressed the different evolution among the various types and claimed that early-type galaxies had fairly constant number density but were brighter in the past, while late types were much more frequent in the past but not much brighter. The luminosity density of early types stayed constant, while that of late types fell.

Cohen (2002) measured galaxies in a region centered on the Hubble Deep Field and Flanking Fields and, in contrast to CFRS, found that the luminosity functions of several different spectral classes of galaxies showed no strong evidence of change in faint-end slope to $z \sim 1$, and further that the value of this slope is comparable to the local value. Galaxies with spectra dominated by absorption lines at $z = 1$ were brighter by $\sim$1.5 mag relative to local ones, while galaxies with strong [O II] were brighter by $\sim$0.75 mag at $z \sim 1$.

Im et al. (2002) measured evolution in the luminosity function of morphologically normal red early-type galaxies by selecting distant galaxies in the DEEP1 survey to match local E/S0s in both morphology and color. This work also noted color bimodality and used it to separate red galaxies from blue ones. The luminosity function of early-type galaxies was found to brighten by 1.1–1.9 mag in rest-frame $B$ from $z = 0$ back to $z \sim 0.8$, but the number density of red galaxies appeared to be relatively constant over that time. This paper is related to the present one, as DEEP1 redshifts were employed and several authors are also authors of the present paper. However, the constant number of red galaxies found there disagrees with our current results. Possible reasons for this are discussed in § 4.2.

A similar degree of brightening was obtained by Bernardi et al. (2003) for early-type galaxies in the SDSS, where a brightening of $\sim$1.15 mag per unit redshift back in time was extrapolated based on a sample reaching to $z \sim 0.3$.

In a later study going 2 mag fainter than Im et al. (2002), Cross et al. (2004) studied the faint end of the luminosity functions of a few dozen red-selected galaxies and morphologically selected early-type galaxies using Advanced Camera for Surveys (ACS) images and photometric redshifts. The red-selected luminosity function was found to turn over steeply at faint magnitudes near $z \sim 1$, whereas the morphologically selected sample was flat. The difference was attributed to blue spheroids, which filled in the counts at faint levels in the morphologically selected sample.

The evolution of the luminosity function as a function of color since $z \sim 1$ was also investigated by Pozzetti et al. (2003), who used the near-infrared–selected K20 survey of Cimatti et al. (2002b) and divided the sample using the color of nearby Sa galaxies. They found a modest rise of at most 30% in the number of red galaxies near $L^*$ after $z = 1$ and concluded that most bright red galaxies were already in place by $z \sim 1.3$.

The distant surveys just cited clearly disagree on many points, including the number of galaxies, shapes of luminosity functions, and degree of fading over time. However, it is important to note that most of them typically cover only a few tens of square arcminutes, for which the rms cosmic variance is $\sim$50% per $\Delta z = 0.2$ at $z = 1$ and is even greater for highly clustered galaxies (Somerville et al. 2004). Modest growth of factors of a few in galaxy numbers cannot be detected with errors this large. More recent surveys containing several thousand galaxies are now beginning to provide more robust measurements of distant luminosity functions. One of the first is a large survey by Ilbert et al. (2005; VVDS) using the VIMOS spectrograph on the ESO Very Large Telescope, which has measured the evolution of the total galaxy luminosity function to $z \sim 2$ using a sample of $\sim$11,000 galaxies to $I_{\rm AB} = 24.0$ with spectroscopic redshifts. They found that $M_B^*$ for the global luminosity function has faded by 1.6–2.2 mag from $z = 2$ to now but that global number density has remained nearly constant over that time. They also suggested a possible steepening of the faint-end slope beyond $z = 1$. This study is compared to ours in § 4.1, and the overall agreement is fairly good (down to our magnitude limit).

A second large survey is DEEP2 (Davis et al. 2003), which has employed spectroscopic redshifts to measure distances and internal kinematics for $\sim$40,000 galaxies in four regions of sky. To enhance the yield of distant objects, galaxies were preselected in three of these regions to have $z > 0.7$ using *BRI* colors (the fourth region, the extended Groth strip [EGS], is not preselected). The luminosity function analysis for the first third of DEEP2 was presented in Paper I, which used $U - B$ color bimodality to divide red from blue galaxies. A fall with time in the number density of bright blue galaxies at fixed absolute magnitude was detected that was well modeled by assuming constant number density, fading in $M_B^*$ of $\sim$1.3 mag, and constant faint-end slope. Counts for red galaxies showed little change in number density (near $L^*$), a similar degree of fading to the blue function, but a formally significant rise in number density with time. The data from this paper are a major component of the present paper.

An alternative to spectroscopic surveys is photometric redshifts. In spite of lower precision, photometric redshifts yield a larger number of redshifts per unit telescope time and enable distances to be measured for galaxies that are too faint for spectroscopy. This approach has been pursued using both space-based (e.g., Takeuchi et al. 2000; Poli et al. 2001; Bolzonella et al. 2002) and ground-based data (e.g., Fried et al. 2001; Drory et al. 2003; Wolf et al. 2003, hereafter W03; Chen et al. 2003; Gabasch et al. 2004). Of the photometric redshift surveys, the ones most comparable to the present work are COMBO-17 (W03) and the FORS Deep Field (FDF; Gabasch et al. 2004). The latter used a sample of more than 5500 galaxies down to $I_{\rm AB} = 26.8$ to measure the total rest-frame $B$-band luminosity function from $z \sim 0.4$ to $\sim$4. Like DEEP2 and VVDS, FDF found a constant number of galaxies back to $z \sim 1$ but, unlike VVDS, did not find a steepening of faint-end slope despite the fact that their sample went 10 times fainter.

The largest survey of precision photometric redshifts yet is COMBO-17 (Wolf et al. 2001, hereafter W01; W03), which contains $\sim$28,000 galaxies in four fields. In terms of depth, area, and sample size it is very similar to DEEP2. The first luminosity function analysis of COMBO-17, by W03, divided the sample into bins of fixed spectral energy distribution (SED) type that did not evolve with redshift. Some of the evolutionary trends that were discovered may have reflected color evolution between these fixed spectral bins rather than actual changes in numbers. The approach was changed in B04, who used an evolving color cut based on bimodality to study red galaxies only. As noted earlier, this work obtained the important result that red galaxies were not only brighter in the past (by >1 mag) but were also fewer in number, by at least a factor of 2 at $z = 1$. This claim, which was based on $\phi^*$, was buttressed by a separate argument based on the luminosity density, $j_B$, of red galaxies. This can be measured more accurately than either $L^*$ or number density alone

TABLE 1
Survey Characteristics

| Survey (1) | Area ($deg^2$) (2) | $N_{field}$ (3) | $N_{gal}$ (4) | $N_z$ (5) | $N_z > 0.8$ (6) | $m_l$ (7) | $m_u$ (8) | $z_{min}$ (9) | $z_{max}$ (10) | System (11) |
|---|---|---|---|---|---|---|---|---|---|---|
| EGS | 0.28 | 1 | 9115 | 4946 | 2026 | 18.5 | 24.1 | 0.2 | 1.4 | $R_{AB}$ |
| Fields 2+3+4 | 0.85 | 3 | 18756 | 6338 | 4820 | 18.5 | 24.1 | 0.8 | 1.4 | $R_{AB}$ |
| DEEP1 | 0.04 | 1 | 2438 | 621 | 241 | 16.5 | 23.5 | 0.2 | 1.0 | $I814_{Vega}$ |
| COMBO 17 | 0.78 | 3 | 40210 | 27947 | 8792 | 17.0 | 24.0 | 0.2 | 1.2 | $R_{Vega}$ |

Notes.—Col. (1): Surveyed region. Col. (2): Area in square degrees. Col. (3): Number of noncontiguous fields in surveyed region. Col. (4): Number of galaxies in source catalog. Col. (5): Number of good quality redshifts. Col. (6): Number of good quality redshifts above $z = 0.8$. Col. (7): Bright apparent magnitude limit. Col. (8): Faint apparent magnitude limit. Col. (9): Lower redshift limit. Col. (10): Upper redshift limit. Col. (11): Apparent magnitude system of catalog.

and was found to hold roughly constant since $z \sim 1$. Since both data and stellar population models indicate a strong *fading* of red stellar populations by 1–2 mag between $z = 1$ and now (see § 5), the authors reasoned that the total stellar mass bound up in red galaxies must be *increasing* by the same factor, which provided additional evidence for growth of stellar mass in red galaxies since that time. A specific evolutionary scenario proposed by B04 had the majority of present-day massive E/S0s moving onto the red sequence after $z \sim 1$. The stellar populations of such galaxies would age passively once galaxies were on the red sequence, but individual galaxies could continue to increase their stellar masses via mergers *along* the red sequence, as predicted by the hierarchical model of galaxy formation. We explore and extend this model in this paper.

Aside from B04, few works have as yet used color bimodality to measure the luminosity functions of red and blue galaxies separately. One of these is by Giallongo et al. (2005), who used a mixture of deep and shallow data in four fields containing 1434 galaxies. Dividing galaxies both by $U - V$ color and by star formation rate, they found that color bimodality persists to $z \sim 2$ but that the number density of red galaxies falls steeply at epochs before $z = 1$. No numbers were provided for $z = 1$ specifically, making quantitative comparison impossible with our work, but their trends agree at least qualitatively with ours.

The foregoing summary illustrates that information on distant luminosity functions is still fragmentary and often contradictory. In particular, the important claim by B04 for the rise in red galaxies after $z = 1$ has not yet been thoroughly checked. A major obstacle has been cosmic variance, as reliably detecting number density evolution by a factor of a few requires samples covering *whole square degrees* on the sky, not tens of square arcminutes, and broken up into several well-separated areas. DEEP2 and COMBO-17 meet both requirements: each sample is large enough and diverse enough to give statistically meaningful results on its own, and the results can be intercompared. The goal of this paper is to compare these samples to determine the global luminosity function out to $z \sim 1$ and to measure functions separately for red and blue galaxies.

This paper is organized as follows. Section 2 presents the data, which include not only COMBO-17 (W03) and DEEP2 (Paper I) but also data from the smaller DEEP1 pilot survey (see references below), which are presented here for the first time. Section 3 briefly summarizes methods used to measure the luminosity functions and their evolution, referring the reader to Paper I and W03 for more details. Readers wanting results quickly can skip directly to § 4, which presents the luminosity functions, computes values of $M_B^*$, number density, and $j_B$ from fitting to Schechter functions, and compares the results to low- and high-redshift values from the literature. These are our core results on evolution. A detailed discussion of possible errors is presented in § 5, which is used to establish a *minimum doubling* in the number of red galaxies near $L^*$ since $z = 1$, in agreement with B04.

Implications for galaxy formation, especially for red galaxies, are discussed in § 6, which draws heavily on the properties of local E/S0s, as well as distant ones. We ultimately favor a stepwise, "mixed" scenario in which red sequence galaxies are descended from blue cloud galaxies that experience a shutdown in star formation, migrate to the red sequence, and then undergo a limited number of further stellar mergers to attain their final masses. This scenario is similar to the one outlined by B04 and seems to have the right ingredients to explain the boxy-disky "structure sequence" of local ellipticals, as well as their locally narrow stellar population scaling relations. A discussion of quenching and downsizing mechanisms closes the scientific discussion. Lastly, we review recent work by other groups *after* our paper was submitted and show that it supports our claim of at least a doubling in the number of red galaxies (near $L^*$) after $z = 1$. A final summary is presented in § 7.

Throughout this work, an $(H_0, \Omega_M, \Omega_\Lambda) = (70, 0.3, 0.7)$ cosmology is used. Unless indicated otherwise, all magnitudes and colors are on the Vega system. Necessary conversions to AB magnitudes are given in Table 1 of Paper I. Luminosity functions are specified per unit comoving volumes.

## 2. DATA

The main data analyzed in this paper come from the DEEP2 and COMBO-17 surveys, with supporting data from DEEP1. Detailed background information on these surveys appears in other references, but core information needed to understand the samples and their selection effects is provided in the next subsections. Basic properties of the surveys (area, number of galaxies, magnitude and redshift limits) are summarized in Table 1.

### 2.1. *DEEP2*

The DEEP2 survey strategy, data acquisition, and data reduction pipeline are described in Davis et al. (2003), S. M. Faber et al. (2007, in preparation), and J. A. Newman et al. (2007, in preparation). A detailed summary was provided in Paper I (§ 2) as background to computing the DEEP2 luminosity functions; the functions from Paper I (Tables 3–5) are adopted here without change. DEEP2 catalogs are derived from Canada-France-Hawaii Telescope (CFHT) images taken with the $12K \times 8K$ mosaic camera (Cuillandre et al. 2001) in $B$, $R$, and $I$ in four different regions of the sky. Reduction of the photometric data, object detection, photometric calibration, and construction of the star-galaxy catalogs are described in Coil et al. (2004).

*R*-band images used to define the galaxy sample have a limiting magnitude for image detection at $R_{AB} \sim 25.5$. Apparent magnitude cuts of $R_{AB} \geq 18.5$ and $R_{AB} \leq 24.1$ and a surface brightness cut of $\Sigma_R \leq 26.5$ were applied (see Paper I, § 2). Separation between stars and galaxies is based on magnitude, size, and color, which were used to assign each object a probability of being a galaxy; star-galaxy separation efficiency is discussed in Coil et al. (2004) and Paper I (§§ 2 and 3.4). In fields 2, 3, and 4, the spectroscopic sample is preselected using *B*, *R*, and *I* to have estimated redshifts greater than 0.7, which approximately doubles the efficiency of the survey for galaxies near $z \sim 1$. The fourth field, the EGS, does not have this preselection applied but instead has roughly equal numbers of galaxies above and below $z = 0.7$, which were selected using a well-understood algorithm. Redshifts were measured spectroscopically using DEIMOS (Faber et al. 2003) on the Keck II telescope. Slitlets are placed (nearly) randomly on 60% of all galaxies after preselection (70% without preselection in EGS), of which 70% yield successful redshifts (80% in EGS), with a catastrophic failure rate of 1%.

The DEEP2 sample used here combines data from the first season of observations in fields 2, 3, and 4 with $\frac{1}{3}$ of the total EGS data, which provides an initial sample at low redshifts. The total number of galaxies is 11,284, with 4946 (44%) in EGS, 3948 (35%) in field 4, 2299 (20%) in field 3, and 91 (1%) in field 2. Since the photometric redshift cut at $z \sim 0.7$ provides a soft boundary for the selection of galaxies, only EGS is used to probe the lower redshift realm $z < 0.8$, while data in all four fields are used for $z \geq 0.8$. CMDs illustrating the sample binned by redshift are shown in Figure 4 of Paper I.

### 2.2. *COMBO-17*

The COMBO-17 survey consists of multicolor imaging data in 17 optical filters covering a total of 1 deg$^2$ of sky at high Galactic latitudes. The filter set contains five broadband filters (*UBVRI*) plus 12 medium-band filters stretching from 400 to 930 nm. All observations were obtained with the Wide Field Imager (WFI; Baade et al. 1999) at the MPG/ESO 2.2 m telescope on La Silla, Chile. The total exposure time is ~160 ks per field, which includes a ~20 ks exposure in the *R* band with seeing below 0.8″ FWHM. The WFI provides a field of view of $34' \times 33'$ on a CCD mosaic consisting of eight 2K × 4K CCDs with ~67 million pixels providing a scale of 0.238″ pixel$^{-1}$. The observations began during the commissioning phase of the WFI in 1999 January and are continuing as the area is extended to cover more fields. The data used here are from three fields covering an area of 0.78 deg$^2$, providing a catalog of ~200,000 objects found by SExtractor (Bertin & Arnouts 1996) on *R*-band images with a 5 $\sigma$ point-source limit of $R \sim 26$.

SEDs created from these 17 passbands were used to classify all objects into stars, galaxies, and QSOs by comparison with template SEDs. Less than 1% of the sources have spectra that are peculiar, not yielding an object class (W03), and star-galaxy separation is highly efficient. A first analysis of the COMBO-17 luminosity function was published by W03, but the galaxy catalog has changed slightly since then. Basic details of the classification algorithm and choice of templates were given in W01. In 2003, an improved set of SED templates was introduced after it was found that the accuracy of galaxy redshifts was limited by template mismatch for bright galaxies, for which more subtle SED details could be seen. The new set of galaxy templates contains a grid of synthetic spectra based on the PEGASE code for population synthesis models (Fioc & Rocca-Volmerange 1997), whereas in the past the redshift determination relied only on the observed templates by Kinney et al. (1996). The new redshifts are accurate to within $\delta z/(1+z) < 0.01$ at $R < 21$ and to within 0.05 down to $R < 24$ (Wolf et al. 2004, hereafter W04). The changes from the old redshifts are relatively small (see Fig. 4 in W04) and are within the errors of the old estimates, but residual errors were reduced by up to a factor of 3 for galaxies with selected SED shapes. Typical catastrophic failure rates for COMBO-17 galaxies are ~1% in the magnitude range used for the luminosity functions, as measured using galaxies in common between W04 and Le Fèvre et al. (2005) in Chandra Deep Field–South (CDF-S). The resulting luminosity functions of galaxies are also unchanged within the errors published in W03 if the same color divisions are used. The luminosity functions of red sequence galaxies published by B04 were already based on the new redshift catalog.

In this paper we recalculate luminosity functions from the COMBO-17 galaxy sample using different color divisions than before. The red sequence cut is similar to the one in B04, with a small difference: B04 measured the mean color of the red sequence, which is affected to a small degree by *K*-correction errors that vary in a nonstochastic way with redshift. They then fitted a smooth evolution to the measured colors to identify the most likely trend. Here we adjust the cut to match the color valley as determined by the measured colors in each individual redshift bin. As stated by B04, the difference this makes to luminosity functions is small. However, we consider it preferable to follow the small but systematic variations in the data for the purpose of splitting the population. The new method is identical in spirit to that used for DEEP2 (see Paper I, § 4.1).

In COMBO-17, a galaxy redshift measurement is considered successful when the error expected from the probability distribution is below a threshold of $\sigma_z/(1+z) \lesssim 0.1$. The completeness of successful redshifts depends on galaxy rest-frame color, and simulated completeness maps are shown in W03 and W04. The large redshift incompleteness among blue galaxies at the faint end of the COMBO-17 sample would lead to unreliable completeness corrections in the last few luminosity function bins just above the survey limit. These bins have thus been dropped, and all correction factors used in the remaining bins (plotted data points) are below 1.5. For red sequence galaxies at $z < 1.2$, which are the special focus of this paper, redshifts are measured successfully for the *entire* sample at $R < 24$ used for the luminosity function. This claim can be tested by identifying likely red sequence galaxies from an apparent CMD like that in Figure 1*a*. In COMBO-17, galaxies with failed redshifts occupy solely the region of blue galaxies. This is consistent with (1) the known lower COMBO-17 completeness for redshifts of blue galaxies close to the faint limit and (2) the zero completeness (by design) of COMBO-17 with respect to $z > 1.4$ galaxies. Blue galaxies with $z > 1.4$ are expected to be a much larger part of a flux-limited sample with $R < 24$ than red sequence galaxies at $z > 1.4$. Owing to their red colors and faint near-UV (NUV) fluxes, only red sequence galaxies of extremely high luminosity could pass the flux limit at high redshift, of which there are evidently very few.

### 2.3. *DEEP1*

DEEP1 was a pilot survey for DEEP2 that was conducted using the Low Resolution Imaging Spectrometer (LRIS) on the Keck telescopes in 1995–1999. Since the only published luminosity function using DEEP1 data treated E/S0s above $I814 = 22$ (Im et al. 2002), a more detailed description of DEEP1 data is presented here. Readers not interested in these details should skip to § 3.

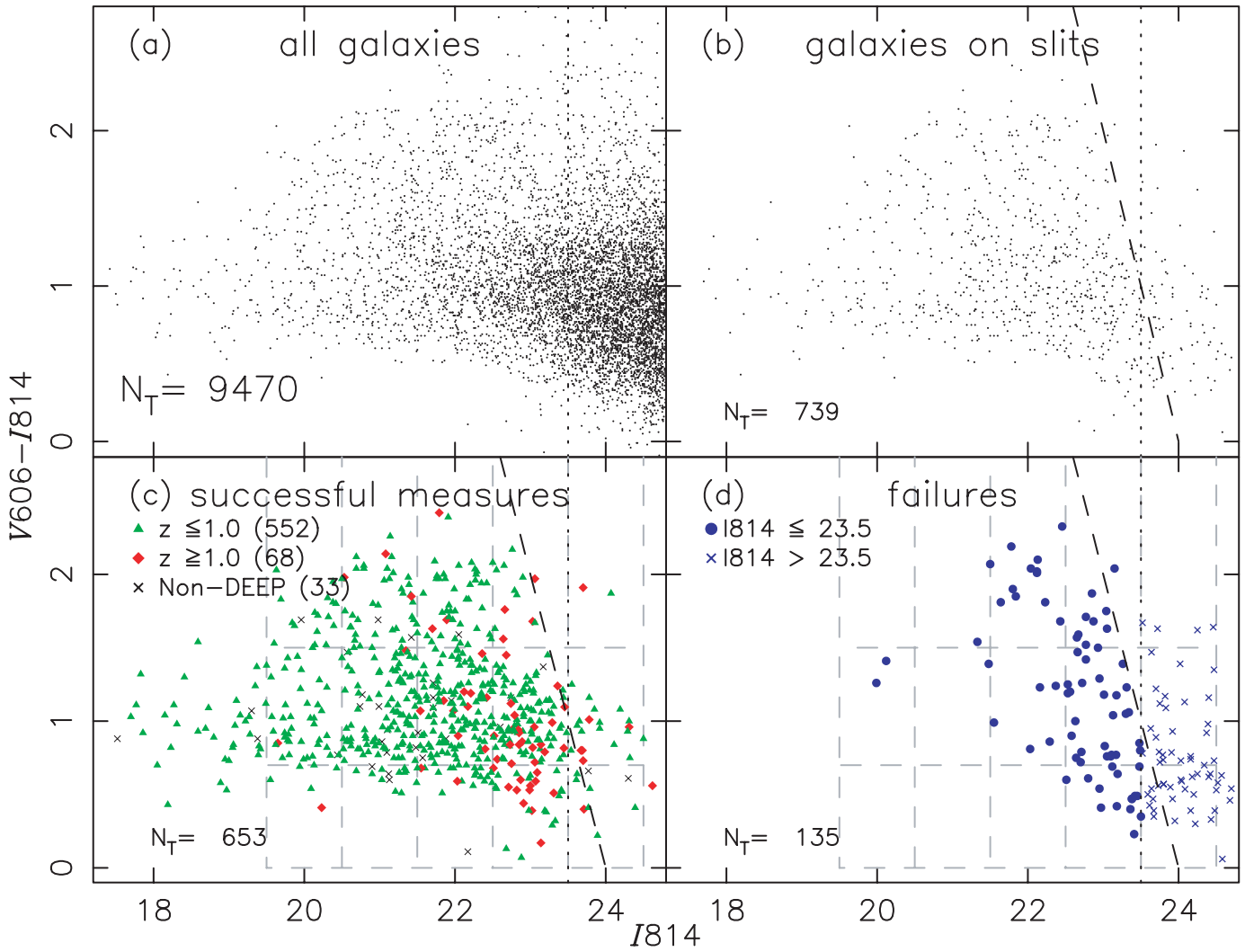


FIG. 1.—Apparent color-magnitude distribution of galaxies in the DEEP1 GSS. (*a*) Full sample; (*b*) distribution of galaxies placed on slits; (*c*) distribution of successful redshifts, where galaxies in the main DEEP1 redshift interval are shown as green triangles and galaxies lying beyond the upper redshift limit are shown as red diamonds. Galaxies with redshifts coming from Lilly et al. (1995a) and Brinchmann et al. (1998) are the black crosses. (*d*) Distribution of failed redshifts. The limit $I814 = 23.5$ adopted for the luminosity function analysis is shown as the vertical dotted line, while the black dashed line represents the limit $(V606 + I814)/2 = 24$ actually used to select galaxies for observation. The dashed gray lines show the boundaries in color and magnitude used for the redshift histograms in Fig. 2.

Background on the DEEP1 sample selection and photometry is presented in Vogt et al. (2005), photometry and bulge-disk decompositions by Simard et al. (2002), and spectroscopy and redshifts by Weiner et al. (2005). The DEEP1 sample is drawn from objects detected in a set of 28 contiguous Wide Field and Planetary Camera (WFPC2) pointings, termed the Groth Strip Survey (GSS), located at approximately $14^h16^m30^s$, $+52^\circ15'50''$ (J2000.0) (PIs E. Groth [GTO 5090] and J. Westphal [GTO 5109]). The solid angle covered by the GSS is 127 arcmin$^2$.

The DEEP1 photometric catalog was created by Groth et al. (1994) and contains several parameters measured using FOCAS (Tyson & Jarvis 1979). To this catalog were added total magnitudes and colors measured fitting two-dimensional bulge+disk models using the GIM2D package (Simard et al. 1999, 2002). For galaxies without GIM2D measurements, magnitudes and colors measured by Ratnatunga et al. (1999) in the Medium Deep Survey (MDS) were used, which have comparable quality to GIM2D measurements (Simard et al. 2002). When neither GIM2D nor MDS had magnitudes and colors, the FOCAS measurements were transformed into the same system as the GIM2D magnitudes by adding the median offset between GIM2D and FOCAS magnitudes in each color [$I814 = I_{\rm FOCAS} - 0.295$ and $V606 - I814 = (V - I)_{\rm FOCAS} + 0.106$; all *HST* magnitudes are on the Vega system].

DEEP1 spectroscopic data were obtained over several observing runs using LRIS (Oke et al. 1995) on the Keck I and II telescopes. Most galaxies were observed using two different gratings, with a blue side ranging from 4500 to 6500 Å and a red side from 6000 to 9500 Å. Total exposure times ranged from 50 minutes for galaxies observed on one mask to ~500 minutes for galaxies placed on several masks. In the analysis in § 4, the DEEP1 sample is restricted to galaxies with $16.5 \leq I814 \leq 23.5$ and with redshift quality A or B, as explained in Weiner et al. (2005) (no surface brightness cut was applied). Galaxies generally have more than one identified spectral feature, and the redshift confidence level is better than 90%. The total number of galaxies in the region that satisfy the apparent magnitude limit is 2438, of which 621 have good quality redshifts. The typical sampling rate of DEEP1 redshifts is ~40%, and the typical redshift success rate is ~70%, for a final overall sampling density of ~25%.

The apparent CMD of DEEP1 galaxies is shown in Figure 1. The spectroscopic sample was selected from a "pseudo-*R*" band

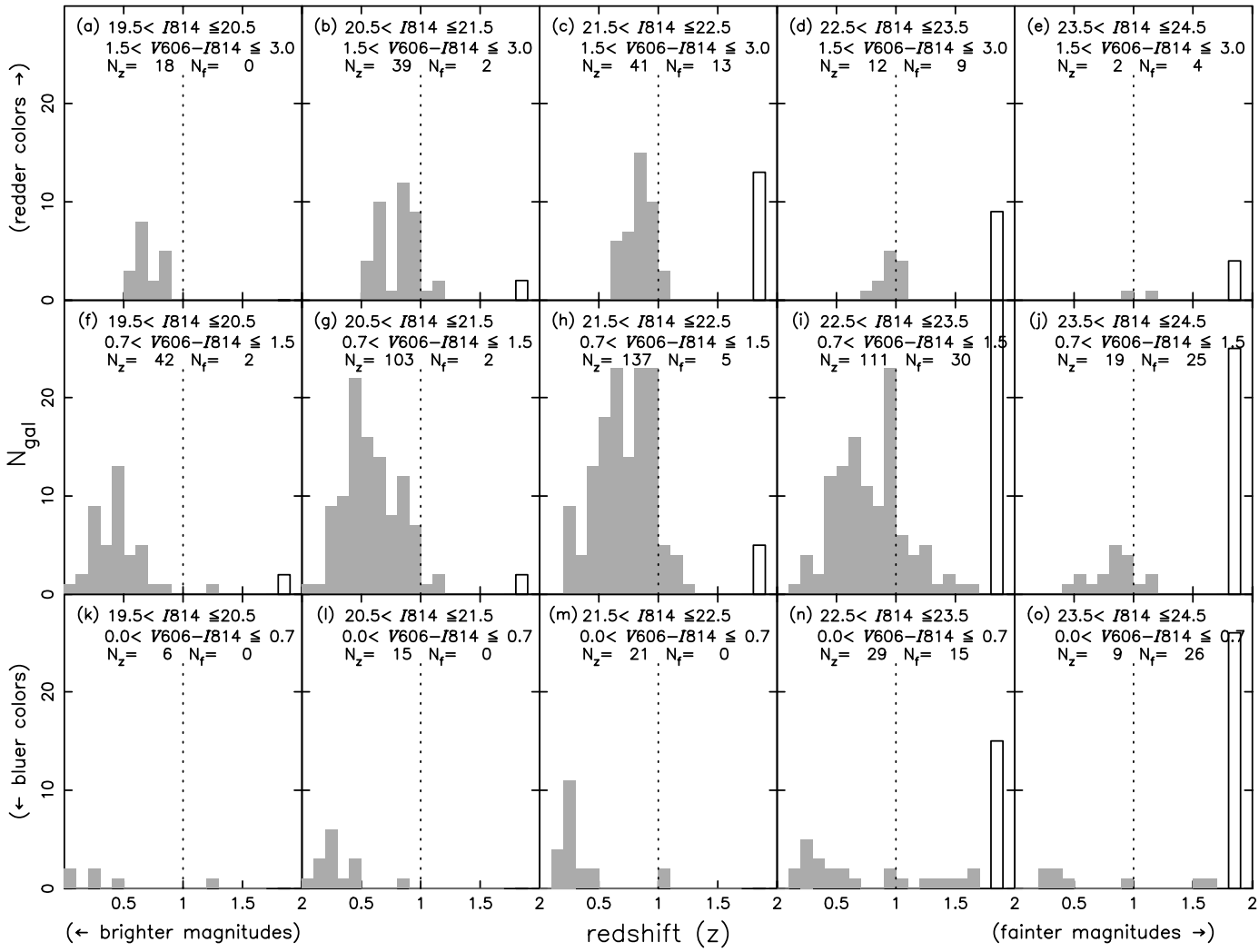


FIG. 2.—Distributions of measured DEEP1 redshifts in the apparent color-magnitude bins indicated in Fig. 1. The display is such that magnitudes become fainter toward the right and colors redder toward the top. $N_z$ in each panel is the number of successful redshifts in that bin; $N_f$ is the number of attempted galaxies that failed to yield successful redshifts. The dashed line represents the high-$z$ cut for DEEP1 ($z = 1.0$), while the bar at the right of each diagram shows the number of failed redshifts. For $I814 \geq 22.5$, the number of failures increases significantly, being slightly larger for blue galaxies.

magnitude: $(V606 + I814)/2 \leq 24.0$; this has been converted to an approximate $I814$ magnitude shown as the vertical dotted line in all four panels. Figure 1*a* shows the full sample of galaxies, and Figure 1*b* shows the distribution of galaxies placed in slits. Because of the $R$-band selection, shown as the inclined dashed line, there is a dearth of red galaxies fainter than $I814 = 23.5$; brighter than this, the sample of galaxies placed on masks is a good representation of the total galaxy sample. Figure 1*c* presents the distribution of galaxies that were successfully measured; green symbols show galaxies below the adopted high-$z$ cutoff (described in § 3), while red symbols show galaxies beyond the cutoff, which were not used. Black crosses show galaxies with redshifts from CFRS (Lilly et al. 1995b) and from Brinchmann et al. (1998), for which DEEP1 measured no spectrum. Figure 1*d* shows the distribution of galaxies with failed redshifts. The few bright cases of failed redshifts resulted from short integrations or spectra of galaxies at mask edges, while the majority of failures are of faint and generally blue galaxies. As in DEEP2 and COMBO-17, most failures are likely beyond the adopted high-redshift cutoff of the survey, here taken to be $z_h = 1.0$. This is the cutoff for the DEEP1 analysis and is the redshift where O II $\lambda$3727 becomes heavily confused with strong OH sky lines in the LRIS data (Weiner et al. 2005).

Figure 2 divides the apparent CMD into magnitude and color bins. For each bin, the histogram of the distribution of galaxies as a function of redshift is shown, where the filled histogram represents successful measures and the open bar at the right the number of failures inside each bin. The number of failed redshifts increases at magnitudes fainter than $I814 \sim 22.5$.

Figure 3 shows the distribution of rest-frame $U - B$ versus redshift. The method used to measure $U - B$ is described in Weiner et al. (2005) and in Appendix A of Paper I and uses the two observed WFPC2 filters $V606$ and $I814$. A bimodal color distribution is clearly seen, as well as large-scale structure fluctuations due to galaxy clustering (vertical stripes). The number of successful redshifts above $z = 1$ falls drastically owing to OH confusion (see above).

Rest-frame CMDs for different redshift intervals are shown in Figure 4. Similar diagrams were shown for DEEP2 in Figure 4 of Paper I and for COMBO-17 in Figure 1 of B04. The solid line in each panel represents the limiting absolute magnitude that corresponds to apparent magnitude $I814 = 23.5$ at the far edge of the bin as a function of rest-frame color. The color dependence was calculated using the $K$-correction code from Paper I (Appendix A). The changing slope of the line as a function of redshift is caused by the fact that the mean wavelength

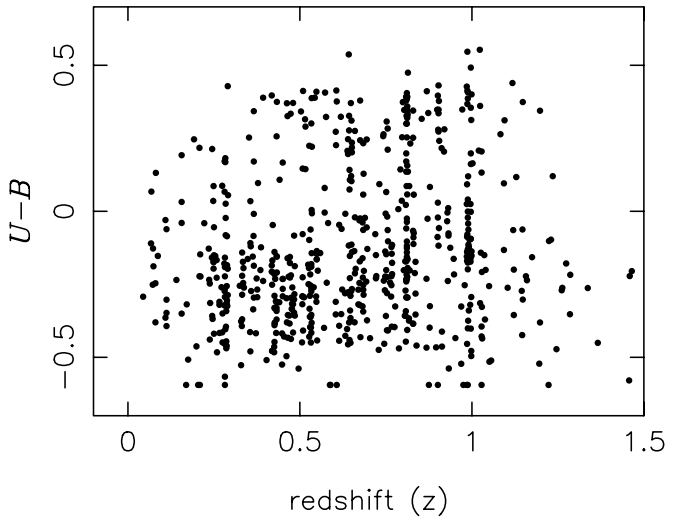


FIG. 3.—Rest-frame ($U - B$) colors as a function of redshift for DEEP1 galaxies. The bimodal distribution of rest-frame colors is clearly evident. The lack of very low-redshift red galaxies is due to the small volume covered by DEEP1 and the rarity of faint red field galaxies.

of the $I606 + I814$ filter average used to select the sample coincides with rest-frame $B$ at $z \sim 0.7$ but differs from it increasingly as the redshift is either greater or smaller than that.

The upper dashed line in each panel represents the cut used to separate red from blue galaxies. This line is identical to that used for DEEP2 in Paper I (eq. [19]) since the rest-frame colors and magnitudes are on the same system. The equation of that line is

$$U - B = -0.032(M_B + 21.52) + 0.454 - 0.25, \quad (1)$$

which is taken from the van Dokkum et al. (2000) color-magnitude relation for red galaxies in distant clusters, converted to the cosmological model used in this paper, and corrected empirically downward by 0.25 mag in order to pass through the valley between red and blue galaxies. Although the colors of red galaxies may evolve with redshift, this effect is not strongly seen in either DEEP1 or DEEP2 colors, and a line with constant zero point independent of redshift is used for all redshift bins.

We conclude this section by comparing the strengths and weaknesses of our two major data sets, DEEP2 and COMBO-17. Both surveys go to nearly the same apparent magnitude, $R \sim 24$, and have comparable numbers of galaxies beyond $z = 0.8$ (see Table 1). The square roots of cosmic variance are shown for each sample in Tables 2–4 by galaxy color and by redshift bin. They are comparable beyond $z = 0.8$ and range between 10% and 20% for all redshifts and color classes. When combined, the two surveys have a total (square root) cosmic variance of ~7%–15% per color-redshift bin at $z \sim 1$. The strengths of DEEP2 are rock-solid redshifts and high completeness for blue galaxies all the way to $z = 1.4$ owing to the sensitivity to [O II] $\lambda$3727, which is strong in distant blue galaxies. The strengths of COMBO-17 are higher completeness overall at all redshifts, particularly for distant red galaxies near $z \sim 1$. This is offset by a tendency to lose redshifts for blue galaxies toward the faint limits of the survey, which has forced us to cut off the COMBO-17 All and Blue luminosity functions at a shallower point than DEEP2 to keep completeness corrections small. The two data sets thus complement each other well at high $z$, making a parallel, head-to-head comparison useful.

## 3. METHODS

The methods used for the DEEP2 luminosity function (and DEEP1 here) were described in Paper I (§ 3); the methods used for COMBO-17 were described in W03 and are very similar. Two statistical estimators are used, the parametric maximum likelihood method of Sandage et al. (1979, hereafter STY79; see also Efstathiou et al. 1988; Marzke et al. 1994) and the nonparametric $1/V_{\rm max}$ method of Schmidt (1968; see also Felten 1976; Eales 1993). The STY79 method fits an analytic Schechter function to obtain $L^*$ and $\alpha$; $\phi^*$ is then estimated using the minimum variance density estimator of Davis & Huchra (1982). A visual check on both the shape and normalization for each redshift bin is provided by using $1/V_{\rm max}$ to calculate the average number density of galaxies in bins of absolute magnitude at each redshift. Formulae for both methods are given in Paper I (§§ 3.1 and 3.2).

Since the STY79 method does not yield $\phi^*$, it is not suitable for calculating errors, which are highly correlated between $\phi^*$ and $M_B^*$. For DEEP1 and DEEP2, these errors are calculated from the 1 $\sigma$ error ellipsoid (Press et al. 1992) gotten by fitting a Schechter function to the $1/V_{\rm max}$ data points (Paper I, § 4.2). These errors are then applied to the STY79 values of $M_B^*$. Additional cosmic variance errors are added in quadrature. For COMBO-17, the errors in parameters are calculated first for $M_B^*$ using STY79, and then $\phi^*$ errors are calculated using the field-to-field variations (W03).

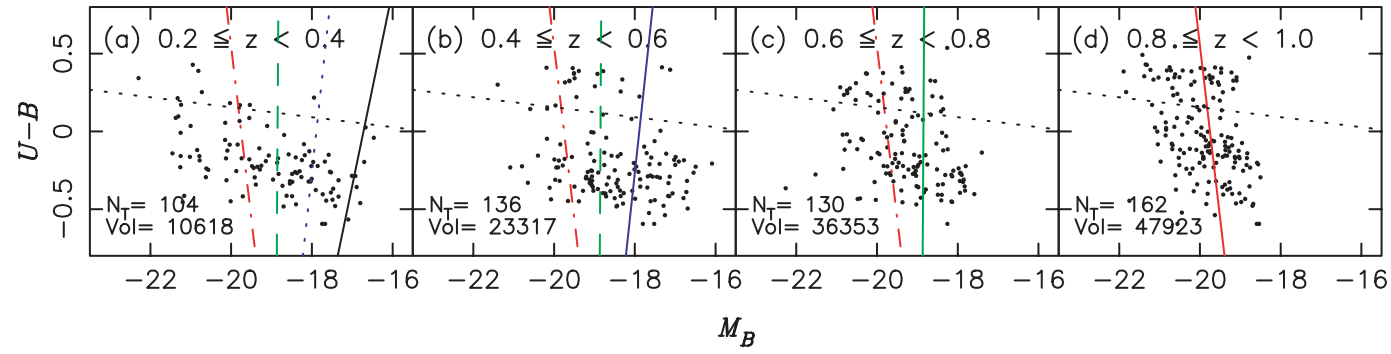


FIG. 4.—Rest-frame CMDs of DEEP1 galaxies for four redshift intervals. The solid line in each panel indicates the approximate faint absolute magnitude limit as a function of intrinsic color and redshift for a sample with a fixed apparent magnitude limit at $I814 = 23.5$. This line represents the faintest galaxy visible as a function of color at the upper redshift limit of each panel. The dashed lines repeat these solid lines from other panels. The dotted parallel line is the (fixed) cut used to define red sequence galaxies, calculated in the same manner as for DEEP2 galaxies in Paper I. The numbers at lower left show the number of galaxies plotted and the comoving volume in Mpc$^3$ for the $(H_0, \Omega, \Lambda) = (70, 0.3, 0.7)$ cosmology.

TABLE 2
SCHECHTER FUNCTION PARAMETERS FOR ALL GALAXY SAMPLES

| $\langle z \rangle$ (1) | $N_{\rm gal}$ (2) | $\alpha$ (3) | $M_B^*$ (4) | $\phi^*$ ($\times 10^{-4}$ Gal Mpc$^{-3}$) (5) | $\sqrt{\rm Var}$ (6) | $j_B$ ($\times 10^8\ L_\odot$) (7) | Weights (8) |
|---|---|---|---|---|---|---|---|
| 0.30 | 734 | −1.30 | $-21.07^{+0.13}_{-0.13}$ | $26.39^{+1.81}_{-1.62}$ | 0.20 | 1.43 ± 0.33 | DEEP2 optimal |
| 0.50 | 983 | −1.30 | $-21.15^{+0.06}_{-0.06}$ | $31.39^{+0.97}_{-1.04}$ | 0.18 | 1.83 ± 0.32 | DEEP2 optimal |
| 0.70 | 914 | −1.30 | $-21.51^{+0.03}_{-0.03}$ | $26.07^{+1.39}_{-1.14}$ | 0.16 | 2.11 ± 0.34 | DEEP2 optimal |
| 0.90 | 2561 | −1.30 | $-21.36^{+0.01}_{-0.02}$ | $33.04^{+0.90}_{-1.11}$ | 0.08 | 2.33 ± 0.20 | DEEP2 optimal |
| 1.10 | 844 | −1.30 | $-21.54^{+0.04}_{-0.04}$ | $24.94^{+2.20}_{-2.63}$ | 0.08 | 2.08 ± 0.27 | DEEP2 optimal |
| 0.30 | 6205 | −1.30 | $-21.00^{+0.17}_{-0.17}$ | $32.26^{+11.32}_{-11.32}$ | 0.11 | 1.50 ± 0.53 | COMBO-17 |
| 0.50 | 5828 | −1.30 | $-21.20^{+0.13}_{-0.13}$ | $33.32^{+4.73}_{-4.73}$ | 0.10 | 1.85 ± 0.26 | COMBO-17 |
| 0.70 | 7122 | −1.30 | $-21.52^{+0.14}_{-0.14}$ | $32.16^{+2.91}_{-2.91}$ | 0.10 | 2.41 ± 0.22 | COMBO-17 |
| 0.90 | 5795 | −1.30 | $-21.25^{+0.19}_{-0.19}$ | $41.26^{+14.84}_{-14.84}$ | 0.09 | 2.41 ± 0.87 | COMBO-17 |
| 1.10 | 2997 | −1.30 | $-21.38^{+0.19}_{-0.19}$ | $34.72^{+4.97}_{-4.97}$ | 0.09 | 2.30 ± 0.33 | COMBO-17 |

NOTES.—Col. (1): Central redshift of bin. Col. (2): Number of galaxies in bin. Col. (3): Value of the adopted faint-end slope. Col. (4): Value of $M_B^*$ and upper and lower 68% Poisson errors. Col. (5): Mean density $\phi^*$ and the 68% Poisson errors for DEEP2 and combined Poisson with cosmic variance estimates for COMBO-17. Col. (6): Square root of cosmic variance, based on field geometry, bin volume, and galaxy bias ($b$) as a function of color (see text). Col. (7): Luminosity density and a conservative error that combines Poisson errors in $M_B^*$ and $\phi^*$ with cosmic variance in quadrature; see text for further explanation. Col. (8): Weighting scheme used. Optimal weights mean that minimal weights were used for blue galaxies and average weights were used for red galaxies. Both these and the COMBO-17 weights are explained in § 3.

Weights are needed for every data set to correct for missing galaxies. The adopted weights take into account the fact that (1) objects may be missing from the photometric catalog, (2) stars may be identified as galaxies and vice versa, (3) not all objects in the photometric catalog are targeted for redshifts, and (4) not all targets yield successful redshifts. For DEEP1 and DEEP2, factors 1 and 2 are small or zero (see Paper I, § 3.3), and only factors 3 and 4 are important. The assumption to deal with factor 3 is that all unobserved galaxies share the same average properties as the observed ones in a given color-magnitude bin. Factor 4 is dealt with by assigning a model redshift distribution to the failed galaxies. We use two such models, as explained in § 3.3 of Paper I. The "minimal" model assumes that all failed galaxies lie entirely beyond the high-redshift cutoff of the survey, which is $z_h = 1.4$ for DEEP2 and $z_h = 1.0$ for DEEP1. Paper I argues that this model provides an adequate description for blue galaxies. The second model for failed redshifts is the "average" model, in which failed redshifts are assumed to have the same distribution as successful redshifts in the same color-color-magnitude bin. Paper I preferred this model for red galaxies, and we use it here. Luminosity functions calculated with the average model are typically 10%–20% higher than those using the minimal model. When the All galaxy sample is treated (sum of red and blue), an "optimal" model is used in which red galaxies are handled using the average model and blue galaxies are handled using the minimal model.

One alteration to this scheme was applied for DEEP1 based on *HST* images, which are available for this sample. Tests with these images showed that objects with angular half-light radius $r_{\rm hl} \geq 1''$ (from GIM2D) invariably lie within the legal redshift range $z \leq 1.0$, and the weights were modified to take this extra knowledge into account. Figure 5 plots the resultant sampling rates, redshift success rates, and weights for DEEP1; analogous results were shown for DEEP2 in Figures 5 and 6 of Paper I.

For COMBO-17, factor 1 is small since only galaxies close to very bright stars are lost from the object catalog. Factor 3 is zero, as the photo-$z$ code works on the entire catalog. Factors 2 and 4 are linked, since in COMBO-17 both object classification and redshift estimation are one process. In one direction, a few K stars are misidentified as galaxies, but their number is small. In the other direction, the misclassification of galaxies as stars is modeled together with redshift incompleteness using simulations

TABLE 3
SCHECHTER FUNCTION PARAMETERS FOR BLUE GALAXY SAMPLES

| $\langle z \rangle$ (1) | $N_{\rm gal}$ (2) | $\alpha$ (3) | $M_B^*$ (4) | $\phi^*$ ($\times 10^{-4}$ Gal Mpc$^{-3}$) (5) | $\sqrt{\rm Var}$ (6) | $j_B$ ($\times 10^8\ L_\odot$) (7) | Weights (8) |
|---|---|---|---|---|---|---|---|
| 0.30 | 627 | −1.30 | $-20.36^{+0.13}_{-0.11}$ | $31.78^{+2.15}_{-1.87}$ | 0.11 | 0.89 ± 0.20 | DEEP2 minimal |
| 0.50 | 812 | −1.30 | $-20.72^{+0.05}_{-0.07}$ | $33.40^{+1.39}_{-1.77}$ | 0.10 | 1.31 ± 0.23 | DEEP2 minimal |
| 0.70 | 764 | −1.30 | $-21.15^{+0.07}_{-0.07}$ | $24.67^{+1.35}_{-1.58}$ | 0.09 | 1.44 ± 0.26 | DEEP2 minimal |
| 0.90 | 2644 | −1.30 | $-21.21^{+0.00}_{-0.03}$ | $27.27^{+0.35}_{-0.42}$ | 0.09 | 1.68 ± 0.13 | DEEP2 minimal |
| 1.10 | 1224 | −1.30 | $-21.38^{+0.04}_{-0.05}$ | $20.84^{+1.08}_{-1.58}$ | 0.09 | 1.50 ± 0.16 | DEEP2 minimal |
| 1.30 | 448 | −1.30 | $-21.86^{+0.07}_{-0.08}$ | $13.44^{+2.00}_{-2.71}$ | 0.07 | 1.51 ± 0.31 | DEEP2 minimal |
| 0.30 | 5109 | −1.30 | $-20.74^{+0.20}_{-0.20}$ | $24.26^{+8.42}_{-8.42}$ | 0.11 | 0.88 ± 0.31 | COMBO-17 |
| 0.50 | 4649 | −1.30 | $-21.10^{+0.15}_{-0.15}$ | $23.20^{+3.48}_{-3.48}$ | 0.10 | 1.18 ± 0.18 | COMBO-17 |
| 0.70 | 5691 | −1.30 | $-21.30^{+0.16}_{-0.16}$ | $27.27^{+3.12}_{-3.12}$ | 0.09 | 1.67 ± 0.19 | COMBO-17 |
| 0.90 | 4903 | −1.30 | $-21.10^{+0.17}_{-0.17}$ | $37.32^{+12.80}_{-12.80}$ | 0.09 | 1.91 ± 0.65 | COMBO-17 |
| 1.10 | 2741 | −1.30 | $-21.25^{+0.18}_{-0.18}$ | $29.19^{+4.14}_{-4.14}$ | 0.09 | 1.71 ± 0.24 | COMBO-17 |

NOTES.—See Table 2 for meanings of columns. Minimal weights were used for blue galaxies and mean that all failed redshifts were assumed to lie beyond the upper limit of the survey, $zh = 1.4$ for DEEP2. Both these and the COMBO-17 weights are explained further in § 3.

TABLE 4
SCHECHTER FUNCTION PARAMETERS FOR RED GALAXY SAMPLES

| $\langle z \rangle$ (1) | $N_{gal}$ (2) | $\alpha$ (3) | $M_B^*$ (4) | $\phi^*$ ($\times 10^{-4}$ Gal Mpc$^{-3}$) (5) | $\sqrt{\mathrm{Var}}$ (6) | $j_B$ ($\times 10^8\ L_\odot$) (7) | Weights (8) |
|---|---|---|---|---|---|---|---|
| 0.30 | 109 | −0.50 | $-20.86^{+0.16}_{-0.17}$ | $18.89^{+1.89}_{-1.85}$ | 0.15 | 0.58 ± 0.18 | DEEP2 average |
| 0.50 | 173 | −0.50 | $-20.83^{+0.12}_{-0.09}$ | $17.71^{+1.03}_{-1.13}$ | 0.14 | 0.52 ± 0.13 | DEEP2 average |
| 0.70 | 196 | −0.50 | $-21.05^{+0.06}_{-0.06}$ | $17.63^{+1.29}_{-1.50}$ | 0.13 | 0.64 ± 0.15 | DEEP2 average |
| 0.90 | 535 | −0.50 | $-21.02^{+0.04}_{-0.02}$ | $13.47^{+0.60}_{-0.82}$ | 0.12 | 0.47 ± 0.06 | DEEP2 average |
| 1.10 | 178 | −0.50 | $-21.33^{+0.08}_{-0.07}$ | $7.51^{+1.31}_{-1.52}$ | 0.12 | 0.35 ± 0.08 | DEEP2 average |
| 0.30 | 1096 | −0.50 | $-20.63^{+0.16}_{-0.16}$ | $21.91^{+8.48}_{-8.48}$ | 0.15 | 0.50 ± 0.19 | COMBO-17 |
| 0.50 | 1179 | −0.50 | $-20.77^{+0.11}_{-0.11}$ | $19.97^{+3.21}_{-3.21}$ | 0.14 | 0.51 ± 0.08 | COMBO-17 |
| 0.70 | 1431 | −0.50 | $-21.10^{+0.12}_{-0.12}$ | $17.75^{+0.70}_{-0.70}$ | 0.13 | 0.62 ± 0.02 | COMBO-17 |
| 0.90 | 892 | −0.50 | $-21.18^{+0.14}_{-0.14}$ | $11.89^{+5.20}_{-5.20}$ | 0.12 | 0.45 ± 0.19 | COMBO-17 |
| 1.10 | 256 | −0.50 | $-21.58^{+0.16}_{-0.16}$ | $5.32^{+1.19}_{-1.19}$ | 0.12 | 0.29 ± 0.07 | COMBO-17 |

NOTES.—See Table 2 for meanings of columns. Average weights were used for red galaxies and mean that all failed redshifts were assumed to follow the same redshift distribution as successfully observed galaxies. Both these and the COMBO-17 weights are explained further in § 3.

described in W01 and W03. These take signal-to-noise ratio, SED shape, and redshift into account and are calibrated using Monte Carlo simulations. Weights are then applied as a function of apparent magnitude and color and are close to unity to the full sample depth for all red galaxies but increase rapidly for blue galaxies toward the survey limit. However, we do not use data points that involve corrections by more than a factor of 1.5, and as a result, COMBO-17 luminosity functions for blue galaxies do not quite reach to the corresponding apparent magnitude limit, $R = 24$.

## 4. ANALYSIS

### 4.1. *The DEEP and COMBO-17 Luminosity Functions*

This section compares the luminosity functions derived from DEEP2, DEEP1, and COMBO-17 with one another and with published data. The DEEP2 functions are "best estimates" from Tables 3–5 of Paper I and use weights based on the optimal missing redshift model for All galaxies, the minimal model for Blue galaxies, and the average model for Red galaxies (see § 3). For DEEP1, the minimal model is used for all weights, while

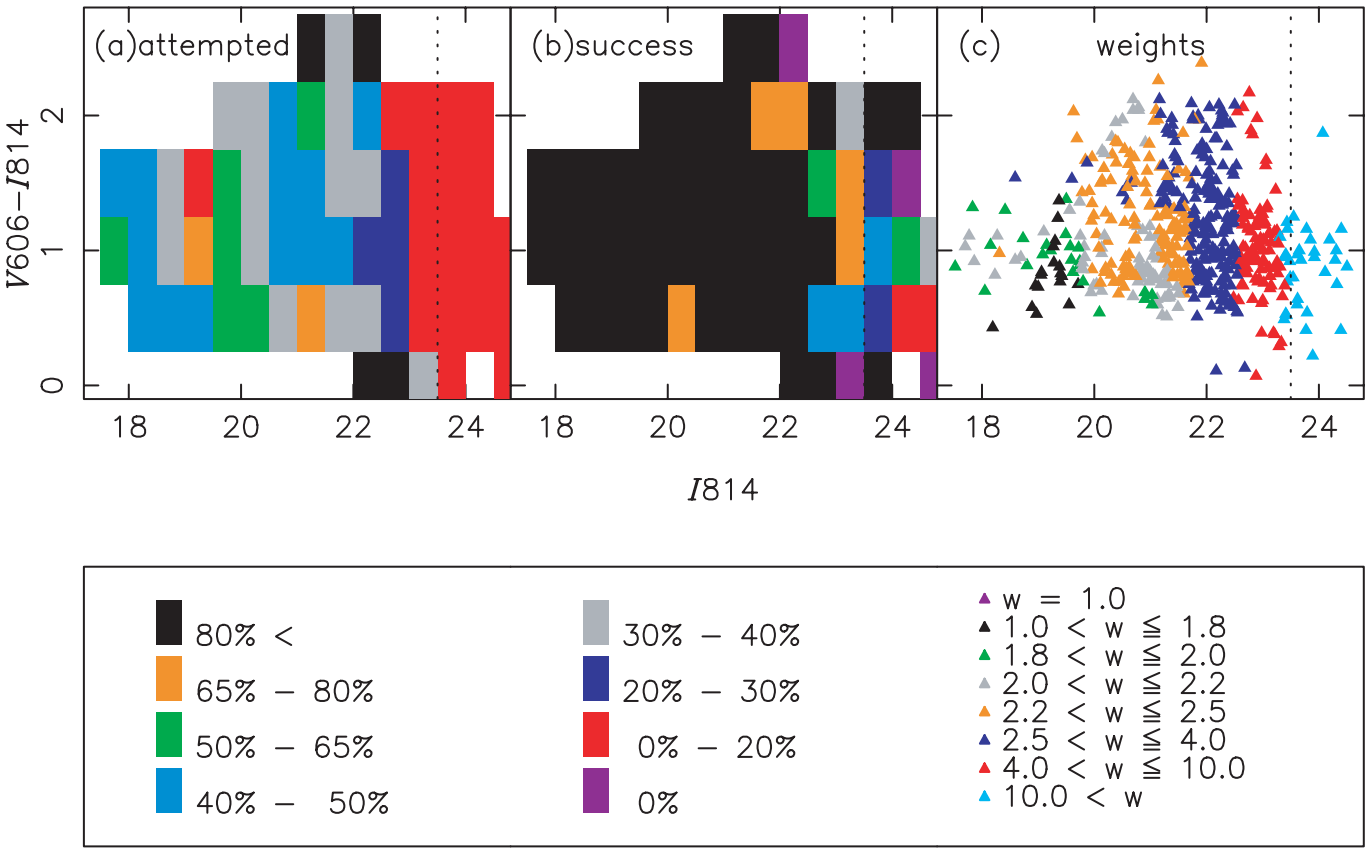


FIG. 5.—Sampling rate as a function of apparent magnitude and color for DEEP1. The vertical dotted line represents the $I814 = 23.5$ magnitude limit. (*a*) Percentage of galaxies placed on slits relative to the total sample; (*b*) success rate for obtaining good redshifts among those attempted; (*c*) weight of each galaxy used to correct for incomplete sampling as a function of color and apparent magnitude. The weighting scheme for all of DEEP1 uses the minimal model in which all failures correspond to galaxies beyond the upper redshift limit of the survey ($z > 1.0$).

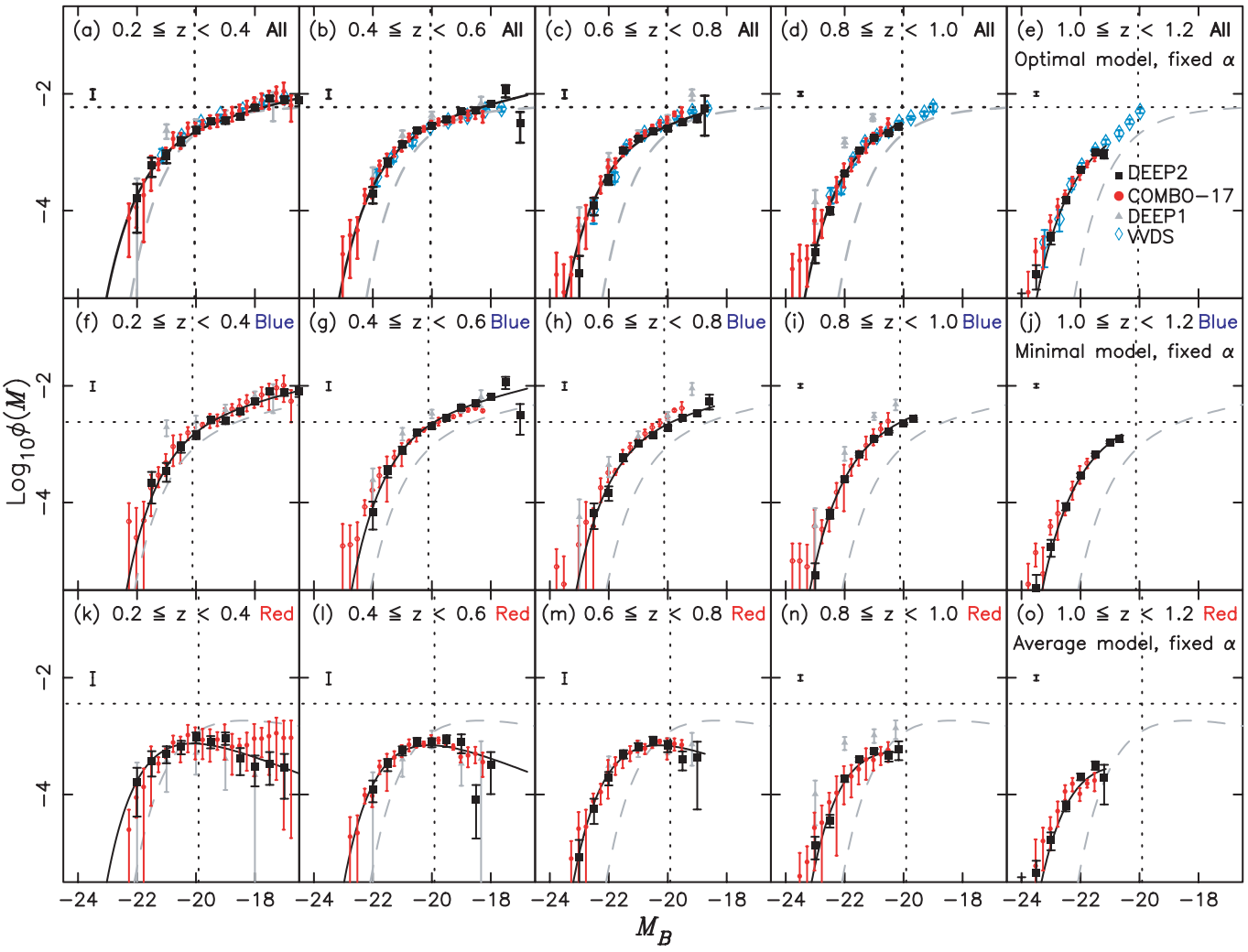


FIG. 6.—Luminosity functions measured in different redshift bins for All galaxies (*top row*), Blue galaxies (*middle row*), and Red galaxies (*bottom row*). Points determined using the $1/V_{\rm max}$ method are shown in black for DEEP2, gray for DEEP1, and red for COMBO-17. COMBO-17 data come from new calculations by C. Wolf using the revised bimodality method to separate blue and red galaxies. Points for All galaxies from VVDS (Ilbert et al. 2005) are shown in blue. Error bars for DEEP2 are 68% Poisson values; those for COMBO-17 combine Poisson and cosmic variance. Cosmic variance for DEEP2 is shown at the top left of each panel based on theoretical values using the method described in the text; cosmic variance for COMBO-17 based on actual field-to-field measurements is similar (see Tables 2–4). The solid black lines represent Schechter functions fitted to DEEP2 data using the STY79 method. For these, $\alpha$-values were kept fixed at those measured from the COMBO-17 "quasi-local" sample in bins extending from $z = 0.2$ to 0.6. The values used are $\alpha = -1.3$ (All), $\alpha = -1.3$ (Blue), and $\alpha = -0.5$ (Red). Schechter functions for local samples are shown as the dashed gray lines, using results from SDSS measurements by Bell et al. (2003) as tabulated in Table 5. The dotted lines serve as a visual reference and are plotted at the values of $M_B^*$ and $\phi^*$ for the local data. Overall agreement between DEEP2, COMBO-17, and VVDS is very good where data overlap.

COMBO-17 weights are as described in § 3 and W03. Galaxies are analyzed all together (the "All" sample) and also divided into "Red" and "Blue" subsamples using color-magnitude bimodality. The method used to divide blue and red galaxies in DEEP2 and DEEP1 is based on the slanting line that goes through the color valley in the $U - B$ versus $M_B$ CMD (see eq. [1] and Fig. 4 of Paper I and Fig. 4 here). The line used for COMBO-17 is similar to the one used by B04 based on $U - V$ versus $M_V$ except that the smoothly evolving zero point of the line through the color valley has been replaced by zero points tuned to make the line go through the valley in each redshift bin separately.

Figure 6 shows the resulting luminosity functions for the All data (*top row*), Blue data (*middle row*), and Red data (*bottom row*). Redshift increases from left to right across a row. Nonparametric $1/V_{\rm max}$ data points are shown for DEEP2 by the filled black squares, for DEEP1 by the gray triangles, and for COMBO-17 by the red circles. For all samples, the calculation of the luminosity function is truncated at the faint end using dashed lines analogous to those in Figure 4, taking the limiting absolute magnitude at each color and in each redshift bin into account; details are given in Paper I (§ 4). Blue galaxies are further trimmed in COMBO-17, as described above in § 3 to allow for greater redshift incompleteness.

The error bars on each DEEP2 and DEEP1 point represent Poisson statistics only. Cosmic variance estimates are shown as the separate error bar at the top left corner of each panel and are estimated using the procedure of Newman & Davis (2002) to account for the evolution of the correlation function. The bias factors derived by Coil et al. (2004) for red galaxies ($b = 1.32$) and blue galaxies ($b = 0.93$) relative to dark matter halos are included in these estimates. The values plotted are for DEEP2. To first order, Poisson variance is random from point to point, whereas cosmic variance should mainly move all points in a given bin up and down together. Since these effects are different, they are shown separately. For COMBO-17, the error bars

TABLE 5
SCHECHTER FUNCTION PARAMETERS FROM THE LITERATURE

| Sample (1) | $z_{med}$ (2) | $\alpha$ (3) | $M_B^*$ (4) | $\phi^*$ ($\times 10^{-4}$ Gal Mpc$^{-3}$) (5) | $j_B$ ($\times 10^8\ L_\odot$) (6) | References (7) | Notes (8) |
|---|---|---|---|---|---|---|---|
| A | 0.07 | $-1.21 \pm 0.03$ | $-20.22^{+0.10}_{-0.10}$ | $55.22^{+4.46}_{-4.46}$ | $1.27 \pm 0.12$ | 1 | a |
| | 0.07 | $-1.03 \pm 0.10$ | $-20.04^{+0.10}_{-0.10}$ | $59.00^{+0.34}_{-0.34}$ | $0.98 \pm 0.03$ | 2 | b |
| | 0.10 | $-0.89 \pm 0.01$ | $-19.73^{+0.02}_{-0.02}$ | $74.77^{+2.74}_{-2.74}$ | $1.27 \pm 0.04$ | 3 | |
| | 0.30 | $-1.16 \pm 0.03$ | $-20.88^{+0.18}_{-0.18}$ | $48.74^{+5.87}_{-5.87}$ | $1.92 \pm 0.23$ | 4 | c |
| | 0.50 | $-1.26 \pm 0.05$ | $-21.31^{+0.16}_{-0.16}$ | $28.54^{+5.14}_{-5.14}$ | $1.85 \pm 0.33$ | 4 | c |
| | 0.70 | $-1.10 \pm 0.11$ | $-21.14^{+0.19}_{-0.19}$ | $49.87^{+11.46}_{-11.46}$ | $2.38 \pm 0.55$ | 4 | c |
| | 0.90 | $-1.30 \pm 0.11$ | $-21.53^{+0.18}_{-0.18}$ | $32.10^{+8.16}_{-8.16}$ | $2.66 \pm 0.68$ | 4 | c |
| | 1.10 | $-1.70 \pm 0.17$ | $-21.45^{+0.28}_{-0.28}$ | $30.94^{+7.85}_{-7.85}$ | $5.50 \pm 1.40$ | 4 | c |
| | 0.63 | $-1.25 \pm 0.17$ | $-21.38^{+0.21}_{-0.18}$ | $42.00^{+4.00}_{-3.00}$ | $2.60 \pm 0.22$ | 5 | |
| | 0.96 | $-1.25 \pm 0.17$ | $-21.67^{+0.15}_{-0.13}$ | $40.00^{+3.00}_{-2.00}$ | $3.24 \pm 0.20$ | 5 | |
| | 1.36 | $-1.25 \pm 0.17$ | $-22.01^{+0.13}_{-0.13}$ | $24.00^{+2.00}_{-2.00}$ | $2.66 \pm 0.22$ | 5 | |
| B | 0.04 | $-1.24 \pm 0.01$ | $-20.12^{+0.05}_{-0.05}$ | $34.99^{+0.69}_{-0.69}$ | $0.72 \pm 0.12$ | 6 | a |
| | 0.07 | $-1.24 \pm 0.10$ | $-20.09^{+0.04}_{-0.04}$ | $23.96^{+1.73}_{-1.73}$ | $0.49 \pm 0.04$ | 2 | d |
| R | 0.04 | $-0.54 \pm 0.02$ | $-20.15^{+0.05}_{-0.05}$ | $33.96^{+1.72}_{-1.72}$ | $0.55 \pm 0.04$ | 6 | a |
| | 0.07 | $-0.76 \pm 0.10$ | $-19.91^{+0.10}_{-0.10}$ | $35.96^{+2.06}_{-2.06}$ | $0.47 \pm 0.03$ | 2 | e |
| | 0.33 | $-1.00$ | $-21.00^{+0.19}_{-0.19}$ | $7.10^{+2.20}_{-2.20}$ | ... | 7 | f |
| | 0.90 | $-1.00$ | $-21.75^{+0.15}_{-0.15}$ | $6.80^{+1.90}_{-1.90}$ | ... | 7 | f |

NOTES.—Col. (1): Sample: All galaxies (A), Blue (B), or Red (R). Col. (2): Median redshift of sample. Col. (3): Schechter function faint-end slope and error. Col. (4): Characteristic luminosity and errors. Col. (5): Schechter function normalization and errors. Col. (6): Luminosity density and error. Col. (7): References. Col. (8): Additional notes. All quantities are converted to the ($H_0$, $\Omega_M$, $\Omega_\Lambda$) cosmology of this paper and are calculated for $B_{Johnson}$ using the transformations listed in the individual footnotes. Those involving SDSS magnitudes and colors come from B04, using average colors $(g - r) = 0.82$, 0.69, and 1.01 for All, Blue, and Red galaxies, respectively.

[a] $B_{Johnson} = b_j + 0.21$.
[b] $B_{Johnson} = g + 0.115 + 0.370 \times 0.82$.
[c] $\phi^*$ inferred from fits to VVDS data points fixing $\alpha$ and $M_B^*$.
[d] $B_{Johnson} = g + 0.115 + 0.370 \times 0.69$.
[e] $B_{Johnson} = g + 0.115 + 0.370 \times 1.01$.
[f] Fixed $\alpha$.

REFERENCES.—(1) Norberg et al. 2002; (2) Bell et al. 2003; (3) Blanton et al. 2003; (4) Ilbert et al. 2005; (5) Gabasch et al. 2004; (6) Madgwick et al. 2002; (7) Im et al. 2002.

combine the Poisson errors in $\phi(M)$ with the cosmic variance estimated from the field-to-field variations.

Also shown in the top row of Figure 6 are $1/V_{max}$ data points by Ilbert et al. (2005; VVDS), represented by blue diamonds. This sample uses ~11,000 spectroscopic redshifts from the VVDS to $I_{AB} = 24$ (7800 redshifts are termed "secure"). Finally, the gray dashed lines show Schechter fits to local red and blue SDSS samples at $z \sim 0.05$ from Bell et al. (2003), who divided galaxies both by color and by concentration, getting similar results. The exact Schechter parameters used in other papers are given in Table 5.

The conclusions from Figure 6 are as follows:

1. *All galaxies* (*top row*).—Measurements of the All galaxy luminosity function from all four surveys agree well out to $z \sim 1$ and down to the apparent magnitude limit of DEEP2 and COMBO-17 ($R \sim 24$). Below this, VVDS claims to see a steepening in faint-end slope from $\alpha \sim -1.2$ at $z = 0.05$ to $\alpha \sim -1.5$ at $z = 1$. Neither DEEP2 nor COMBO-17 goes deep enough to test this, but, as noted in § 1, Gabasch et al. (2004; FDF) go 2.5 mag fainter and do not see it, getting $\alpha = -1.25$ at all redshifts. Relative to the local Schechter function, the All data brighten back in time ($M_B^*$) but stay roughly constant in number density ($\phi^*$). This visual assessment is confirmed by quantitative Schechter fits in § 4.2. In short, for the All sample, galaxies are getting dimmer with time, but their characteristic number density near $L^*$ has remained much the same since $z \sim 1$.

2. *Blue galaxies* (*middle row*).—The results found above for the All sample are replicated for the Blue sample, as expected since blue galaxies account for the majority of objects at all redshifts. Results here are available only from DEEP1, DEEP2, and COMBO-17 (since VVDS does not divide their samples by color), and these data sets agree well. Relative to the local blue Schechter function (*dashed gray line*), $M_B^*$ brightens back in time while $\phi^*$ remains constant, again confirmed by Schechter fits in § 4.2.

3. *Red galaxies* (*bottom row*).—Before considering red galaxies, we review again the conclusions of B04, which offered the first analysis of evolution in $\phi^*$ and $M_B^*$ for red galaxies, based on COMBO-17. Their main finding was that $M_B^*$ for red galaxies dims over time by ~1.5 mag from $z = 1$ to 0 and that $\phi^*$ *rises* by at least a factor of 2. This evidence for evolution based on the luminosity function was further bolstered by consideration of the total $B$-band luminosity density of red galaxies, $j_B$, which can be measured with smaller (formal) errors than $M^*$ or $\phi^*$ separately. The quantity $j_B$ was found to hold nearly constant since $z = 1$. Since models of stellar evolution for red galaxies predict a rise in $B$-band stellar mass-to-light ratio by 1–2 mag since $z = 1$ (as discussed further in § 5), constant $j_B$ implies that the total stellar mass contained in red galaxies has at least doubled since $z = 1$, providing further evidence for significant growth in the total stellar mass in red galaxies over this epoch.

The finding by Bell et al. (2003) of recent strong evolution among red galaxies disagrees with the classic scenario for red galaxy formation, in which E/S0 galaxies assembled their mass and formed stars very early and have been passively fading ever since (e.g., Eggen et al. 1962; Larson 1975). This so-called monolithic collapse picture predicts constant $\phi^*$ accompanied

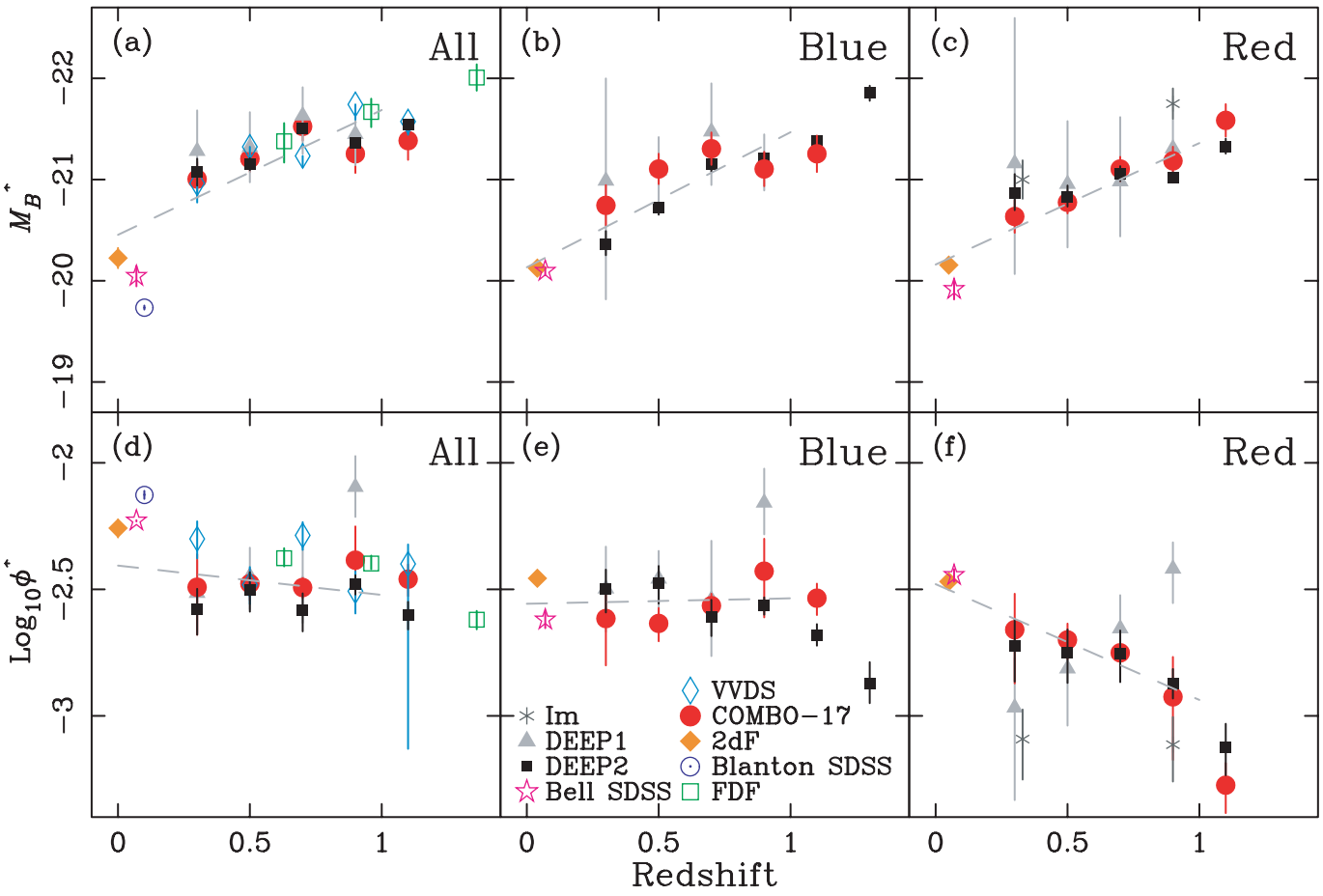


FIG. 7.—Evolution with redshift of the Schechter function parameters $M_B^*$ (*top row*) and $\phi^*$ (*bottom row*) for the All, Blue, and Red galaxy samples. Data values for DEEP2 and COMBO-17 come from Tables 2–4. These parameters were calculated keeping the faint-end slope parameter $\alpha$ fixed to the "quasi-local" COMBO-17 values (−1.3 [All], −1.3 [Blue], and −0.5 [Red]). Error bars on DEEP2 and COMBO-17 are Poisson 68% values for $M_B^*$ and Poisson errors convolved in quadrature with cosmic variance for $\phi^*$ (see text). Also shown are the Schechter parameters from the other works summarized in Table 5. Estimates for distant galaxies come from Ilbert et al. (2005, VVDS, panels [*a*] and [*d*]) and Gabasch et al. (2004, FDF, panels [*a*] and [*d*]). Previous DEEP1 values from Im et al. (2002) are discussed in the text. Local values come from Bell et al. (2003) and Blanton et al. (2003) using SDSS and from Norberg et al. (2002) and Madgwick et al. (2003) using 2dF. The dashed gray lines represent linear fits vs. $z$ to the evolution of $M_B^*$ and $\phi^*$ shown in Table 6; the data fitted are the local surveys plus COMBO-17 and DEEP2 (out to $z = 1$). $M_B^*$ brightens by ~1.2–1.3 mag at $z = 1$ for all colors, but galaxy number density ($\phi^*$) differs markedly with color: Blue number densities remain roughly constant after $z = 1$, Red number densities rise with time, while the All sample is a blend of the two.

by equal dimming in both $M_B^*$ and $j_B$, but neither of these trends was seen by B04. Checking these conclusions by remeasuring these quantities with both DEEP2 and COMBO-17 was a major goal of the present study.

The bottom row of Figure 6 presents the new data for red galaxies. As before, DEEP2 and COMBO-17 agree well. The most striking impression is the relative *lack* of evolution in the Red luminosity function, especially when compared to the large shift to brighter magnitudes seen in the Blue function. What evolution there is, is quantified in § 4.2 by fitting Schechter functions, which are shown in Figure 6 as the black lines. These fits indicate a formal dimming of $M_B^*$ over time, accompanied by a rise in number density, $\phi^*$. However, the magnitude of these shifts is such that the data translate roughly *along* the observed luminosity function, leaving the raw counts at fixed absolute magnitude relatively constant (Fig. 9 below shows this more explicitly). Since the raw counts are not changing very much, the fitted values of $M_B^*$ and $\phi^*$ come from slight curvature in the data, which at high redshifts could be unreliable. We return to the accuracy of the Schechter fits again in § 5, where the constancy of the red counts is considered from various points of view. For now we simply note that both the raw data and the fitted Schechter parameters from DEEP2 and COMBO-17 agree well and that the formal values of $\phi^*$ from both data sets agree with the rise in red number density found by B04.

Another important result in Figure 6 is the marked turnover in the slope of the Red luminosity function at the faint end. This turnover is well established in both DEEP2 and COMBO-17 at intermediate redshifts and is also seen by Cross et al. (2004) and Giallongo et al. (2005) at higher redshifts. However, DEEP2 and COMBO-17 appear to disagree with one another in the lowest redshift bin ($z = 0.2$–$0.4$), where the number of faint red galaxies continues to turn over according to DEEP2 but flattens according to COMBO-17. This is noteworthy because it is the *only significant discrepancy* between DEEP2 and COMBO-17, but the error bars on COMBO-17 are large, reflecting field-to-field variations. Other local data sets also yield conflicting values for the red faint-end slope. For example, Bell et al. (2003) found only a modest turnover using early-type galaxies in SDSS identified by concentration and color, whereas Madgwick et al. (2002) identified red galaxies spectroscopically in 2dF and found a strong turnover like that in DEEP2. We return to faint-end slope evolution in §§ 5 and 6 when discussing Schechter parameter errors and galaxy formation scenarios.

In passing, we note the gray triangles in Figure 6, which show luminosity functions from DEEP1 based on data from the original Groth strip (Im et al. 2002). These agree fairly well with DEEP2 and COMBO-17 except in bin $z = 0.8$–$1.0$, where DEEP1/Red in particular is a factor of 1.5 too high. Two "walls" due to large-scale structure appear in the Groth strip in that redshift bin, one at $z \sim 0.81$ and a larger one at $z \sim 0.98$ (Le Fèvre et al. 1994; Koo et al. 1996; see also Fig. 7). However, the observed fluctuation is not much larger than the expected cosmic variance limits, which are $\sim$30%.

### 4.2. *Schechter Fits*

This section presents the results of fitting Schechter functions to DEEP2 and COMBO-17 using the STY79 method. Aside from the possible low-redshift flattening of the Red function in COMBO-17, mentioned in the previous section, we see no variations in faint-end slopes in our data that are statistically significant, motivating the use of constant $\alpha$-values obtained from averaging over several redshift bins. (Technically, small changes are expected in the shape of the All function because the shapes of the Red and Blue functions differ and their relative numbers are changing with redshift; however, this effect is small.) We decided to adopt the average faint-end slopes for $z = 0.2$–$0.6$ from COMBO-17 (because of their larger number of galaxies in this redshift range), which yielded $\alpha = -0.5$ for the Red sample and $\alpha = -1.3$ for the All and Blue samples (these values were also used for DEEP2 in Paper I). The latter slope agrees well with the value $\alpha = -1.25$ found for all galaxies by FDF, while the former is close to the average value $-0.59$ found for distant red galaxies by Giallongo et al. (2005).

Schechter function parameters for both DEEP2 and COMBO-17 are presented in Tables 2–4 for the All, Blue, and Red samples. (See note to Table 2 for description of columns.) As explained in § 3, we adopted the minimal weighting scheme for DEEP2/Blue and the average weighting scheme for DEEP2/Red because we think that failed redshifts in the two color classes have different redshift distributions. The All sample combines each of these populations with its preferred weighting scheme (called "optimal" in Table 2).

For DEEP2, the 68% errors are Poisson estimates for $M_B^*$ and $\phi^*$ and are taken from the $\Delta\chi^2 = 1$ contour levels in the ($M_B^*$, $\phi^*$)-plane, computed from the $1/V_{\rm max}$ residuals and their errors. Errors for $j_B$ are conservatively calculated by adding the fractional Poisson errors for $M_B^*$, $\phi^*$, and cosmic variance in quadrature; these are overestimates because they neglect correlated errors in $M_B^*$ and $\phi^*$, which tend to conserve $j_B$. However, the biggest error term is usually cosmic variance so the overestimate is small. For COMBO-17, the 68% errors in $M_B^*$, $\phi^*$, and $j_B$ are rms estimates from field-to-field variations, which are particularly large for the redshift bin centered at $z = 0.9$, caused by a big downward fluctuation in CDF-S. The tabulated cosmic variance error estimates for both samples take exact volumes and field geometries into account and use separate bias ($b$) values for All, Blue, and Red galaxies. The DEEP2 values were described in § 4.1 and shown in Figure 6.

The resulting Schechter fits for DEEP2 are shown as the solid black lines in Figure 6. All fits use only the magnitude ranges of the data actually displayed. The close match between the fitted curves and all data suggests that the Schechter formula, and in particular the assumed $\alpha$-values, are a good match to the luminosity function shapes over the magnitude ranges where the data exist. The goodness of the Schechter match to red galaxies was explored quantitatively in Appendix B of Paper I and is reviewed again under errors here in § 5.

Evolutionary trends in fitted Schechter function parameters are shown in Figure 7. Besides DEEP2 and COMBO-17, this figure adds data from other recent surveys (2dF, Norberg et al. 2002; Madgwick et al. 2002; SDSS, Blanton et al. 2003; Bell et al. 2003; VVDS, Ilbert et al. 2005; FDF, Gabasch et al. 2004; DEEP1, Im et al. 2002). The Schechter parameters from these other surveys are tabulated for reference in Table 5. Since the various surveys use different values for $\alpha$, changing them to the same values used by DEEP2 and COMBO-17 would cause small shifts in $M_B^*$ and $\phi^*$. For example, if local All and Blue values were corrected to match DEEP2 and COMBO-17, $M_B^*$ would brighten by $\sim$0.2 mag and $\phi^*$ would decline by $\sim$0.1 dex; these would act to *reduce* the gaps visible in Figure 7 between the local and distant values. For Red galaxies, the changes are opposite: $M_B^*$ would dim by $\sim$0.15 mag while $\phi^*$ would increase by $\sim$0.08 dex, which would act to *increase* the gaps. All these corrections are small, and we ignore them.

Figure 7 contains the principal results of this paper. The first conclusion (from the top row) is that $M_B^*$ has dimmed by roughly the same amount for All, Blue, and Red samples since $z = 1$. COMBO-17 (*red circles*) agrees well with DEEP2 (*black squares*) in all three color bins, and VVDS and FDF agree well with them for All galaxies (the latter do not subdivide by color). The agreement is impressive given that the samples were selected and measured in different ways: COMBO-17 and DEEP2 are $R$-band selected to $R = 24$, VVDS is $I$-band selected to $I_{\rm AB} = 24$, and FDF is $I$-band selected to $I_{\rm AB} = 26.8$. VVDS and DEEP2 use spectroscopic redshifts, COMBO-17 uses high-precision photometric redshifts based on 17 filters, and FDF uses photo-$z$'s derived from photometry in nine bands including $J$ and $K$. Despite these differences, values of $M_B^*$ for all four distant surveys typically agree to within $\pm$0.1 mag. Agreement for the two local surveys as analyzed by Bell et al. (2003; SDSS) and Norberg et al. (2002; 2dF) is also good. The Blanton et al. (2003) value for SDSS/All is dimmer than these by 0.4 mag, but their estimate of magnitude evolution *within* SDSS (not shown) is consistent with the slope in Figure 7*a* to within the errors. In short, a consistent picture for the evolution of $M_B^*$ for All, Blue, and Red galaxies since $z = 1$ seems to be emerging.

Table 6 (second, third, and fourth columns) shows the results of fitting functions to the evolution of $M_B^*$ in Figure 7. Local data from SDSS and 2dF and distant data from COMBO-17 and DEEP2 were used in these fits, with the COMBO-17 and DEEP2 data truncated at $z = 1$. The goal of these fits is to derive a best value for the evolution in $M_B^*$ from $z = 1$ to now, which is taken to be the slope of the fitted line (the $Q$ parameter in Table 6). Two sorts of fits are shown: one is linear in $z$ (upper part of Table 6), the other is linear in $\log_{10}(1 + z)$ (lower part of Table 6) (we thank the referee for suggesting this second fit). The unweighted rms scatter in magnitudes about the fitted functions is shown in the column labeled "rms." The $x$-coordinates in the two fits have been zero pointed and scaled to make both intercepts refer to redshift $z = 0.5$, and both slopes represent magnitude evolution from $z = 1$ to 0 (see notes to Table 6). The fits to $z$ are shown as the dashed gray lines in Figure 7.

Three conclusions emerge. First, the fitted values for the coefficients hardly differ between the linear and logarithmic fits, changing by much less than the quoted error of measurement. Second, the rms scatter is similar for the two types of fit but is slightly smaller (10%) for the logarithmic fits. The differences are small but are repeated in fits to $\phi^*$ and $j_B$ below, and so the logarithmic fits look slightly better. They give a total dimming since $z = 1$ of $1.23 \pm 0.19$ mag for the Red sample, $1.35 \pm 0.19$ mag for the Blue sample, and $1.34 \pm 0.33$ mag for the All

TABLE 6
EVOLUTION OF $M^*$, $\phi^*$, AND $j_B$ FROM SDSS, 2dF, COMBO-17, AND DEEP2

| Sample | $M_B^*$ | $Q$ | rms[a] | $\log_{10}\phi^{*}$[b] | $P$ | rms[a] | $\log_{10} j_B$[c] | $H$ | rms[a] |
|---|---|---|---|---|---|---|---|---|---|
| All[d] | $-21.07 \pm 0.10$ | $-1.23 \pm 0.36$ | 0.29 | $-2.46 \pm 0.04$ | $-0.12 \pm 0.14$ | 0.11 | $8.24 \pm 0.01$ | $0.44 \pm 0.05$ | 0.04 |
| Red[d] | $-20.76 \pm 0.06$ | $-1.20 \pm 0.21$ | 0.20 | $-2.71 \pm 0.02$ | $-0.46 \pm 0.06$ | 0.06 | $7.72 \pm 0.02$ | $0.00 \pm 0.07$ | 0.06 |
| Blue[d] | $-20.80 \pm 0.06$ | $-1.34 \pm 0.22$ | 0.20 | $-2.55 \pm 0.03$ | $0.02 \pm 0.09$ | 0.08 | $8.05 \pm 0.02$ | $0.62 \pm 0.07$ | 0.06 |
| All[e] | $-21.10 \pm 0.09$ | $-1.34 \pm 0.33$ | 0.26 | $-2.47 \pm 0.04$ | $-0.15 \pm 0.14$ | 0.11 | $8.25 \pm 0.01$ | $0.46 \pm 0.04$ | 0.03 |
| Red[e] | $-20.80 \pm 0.06$ | $-1.23 \pm 0.19$ | 0.17 | $-2.72 \pm 0.02$ | $-0.46 \pm 0.06$ | 0.05 | $7.72 \pm 0.02$ | $0.01 \pm 0.07$ | 0.06 |
| Blue[e] | $-20.84 \pm 0.06$ | $-1.35 \pm 0.19$ | 0.18 | $-2.55 \pm 0.03$ | $0.01 \pm 0.09$ | 0.08 | $8.06 \pm 0.01$ | $0.65 \pm 0.05$ | 0.04 |

[a] The rms is the unweighted average rms residual.
[b] The units of $\phi^*$ are galaxies Mpc$^{-3}$.
[c] The units of $j_B$ are $L_{B,\odot}$ Mpc$^{-3}$.
[d] These are linear fits of the indicated quantity in the table vs. $z$. The data used come from Figs. 7 and 8 and are the two local surveys plus COMBO-17 and DEEP2 (below $z = 1$). The zero points shown are calculated at $z = 0.5$, so that the errors in slope and zero point are nearly independent. The fitted functions are therefore $y = a_0(z = 0.5) + a_1(z - 0.5)$, where $M_B^*$, $\log_{10}\phi^*$, and $\log_{10} j_B$ are the zero points and $Q$, $P$, and $H$ are the slopes.
[e] Identical to the upper fits but fitting vs. $\log_{10}(1 + z)$ instead of $z$. To make the numbers comparable to those in the top half, the $x$-coordinate has been normalized such that its total range from $z = 0$ to $z = 1$ is 1 and the zero points again apply to $z = 0.5$. The fitted functions are therefore $y = a_0(z = 0.5) + a_1[\log_{10}(1 + z) - \log_{10}(1 + 0.5)]/\log_{10}(2)$.

sample. (This last is not simply a weighted mean of the first two values because the functions for red and blue galaxies have different shapes.) Thus, our third conclusion is that the magnitude evolution in $M_B^*$ for Red, Blue, and All galaxies has been very similar since $z = 1$.

Based on DEEP2 alone, we wondered in Paper I whether $M_B^*$ for red galaxies in fact evolved very much, and indeed the slope derived from DEEP2 (*black squares in* Fig. 7) is rather shallow. However, adding the points from COMBO-17 has steepened the slope for the high-redshift data, and this has been further bolstered by the addition of the local values from SDSS and 2dF. We return to this topic in § 5 when discussing uncertainties in the Red fits.

The bottom row of Figure 7 is a similar plot of $\phi^*$ versus redshift for the three color classes. Agreement is again very good among the data sets, but now red and blue galaxies evolve quite differently. The number density of blue galaxies remains nearly flat to $z = 1$, whereas the number density of red galaxies rises with time. This rise, already noted in connection with Figure 6, repeats very closely the pattern found by B04, whose data showed a gradual rise in $\phi^*$ since $z \sim 0.8$ by a factor of $\sim$2, preceded by a steeper rise before that near $z = 1$. The new data from DEEP2, which are completely independent, show the same trend, namely, a steep rise near $z = 1$ followed by a shallower rise after that.

It is desirable to estimate the increase in Red $\phi^*$ since $z = 1$ more quantitatively. We have done this in two ways, both of which yield similar results. Method 1 averages the DEEP2 and COMBO-17 values of $\phi^*$ at $z = 1$ and compares them to the local values from SDSS and 2dF. The mean value of $\phi^*$ at $z = 1$ is $0.95 \times 10^{-3} \pm 14\%$, where this value comes from interpolating DEEP2 and COMBO-17 data at $z = 0.9$ and 1.1 (see Table 4) and the error reflects assumed uncertainties of 20% in both DEEP2 and COMBO-17 separately. The local value of $\phi^*$ is $3.44 \times 10^{-3} \pm 20\%$, where the two local values have been averaged and the error comes from a conservative estimate of their errors individually. Method 1 then yields a formal value for the rise in $\phi^*$ from $z = 1$ to now of $3.6 \pm 24\%$ ($0.56 \pm 0.09$ dex).

A drawback of method 1 is that it relies on COMBO-17 and DEEP2 data at $z = 1.1$, which are at the very limits of both surveys. Recent work (Brown et al. 2007, discussed in § 6.4) suggests that these last data points may be too low. Hence, we recompute the evolution in $\phi^*$ more conservatively using method 2, which utilizes linear and logarithmic fits to the data only below $z = 1$, as was done above for $M_B^*$. These fits are shown in the fifth, sixth, and seventh columns of Table 6, where the $P$ parameter represents the evolutionary change (in dex) to $\phi^*$ since $z = 1$. Both linear and logarithmic fits give the same value of $2.88 \pm 14\%$ ($0.46 \pm 0.06$ dex) for the rise in $\phi^*$ since $z = 1$. This value is 20% smaller than that gotten by method 1, but the error bars overlap. For future discussion, we average the two methods by saying that all data over the interval $z = 0$–1 formally indicate a rise in $\phi^*$ of $\sim$0.5 dex per unit redshift.

Parenthetically, we note that this rise disagrees with earlier DEEP1 results by Im et al. (2002), in which $\phi^*$ for red galaxies was claimed to hold constant after $z \sim 1$. The two relevant redshift bins from Im et al. (2002) are plotted as crosses in Figure 7, where they are seen to be both low and constant back in time. Im et al. (2002) applied a very stringent cut to define their sample, targeting only morphologically normal, spheroid-dominated E/S0s having red colors consistent with passively fading stellar populations. Their numbers therefore have to be corrected upward by $\sim$30% to account for non-E/S0 contamination on the distant red sequence (Bell et al. 2004a; Weiner et al. 2005). However, the actual difference between Im et al. (2002) and DEEP2 is nearly a factor of 2 based on counts by DEEP2 over the same region. The reason for this bigger discrepancy has not yet been unravelled and suggests that the sample used by Im et al. (2002) may not have been as complete or as well defined as they thought. Furthermore, Im et al. (2002) used an earlier estimate for the number density of *nearby* spheroidal galaxies that is considerably lower than the newer values used here. When all of these factors are combined and coupled with new and larger cosmic variance estimates, it is plausible that Im et al. (2002) reached the no-evolution conclusion they did.

We end this section by comparing to other published luminosity functions divided by color classes. The discovery of color bimodality is rather new, and the study by Giallongo et al. (2005) is one of only two distant luminosity function studies to divide galaxies by rest-frame color. Unfortunately, no quantitative comparison can be given since Giallongo et al. (2005) did not present any numbers for $z \sim 1$ and our data do not go out to $z = 2$. However, their plots agree qualitatively with ours in showing similar dimming for both red and blue galaxies, a roughly constant number of blue galaxies, and a significant rise in the number of red galaxies since $z = 1$. Furthermore, although the Giallongo et al. (2005) sample is much smaller than ours, it goes roughly 2 mag fainter and is therefore valuable for establishing that the *turnover* we see in the faint end of the red luminosity

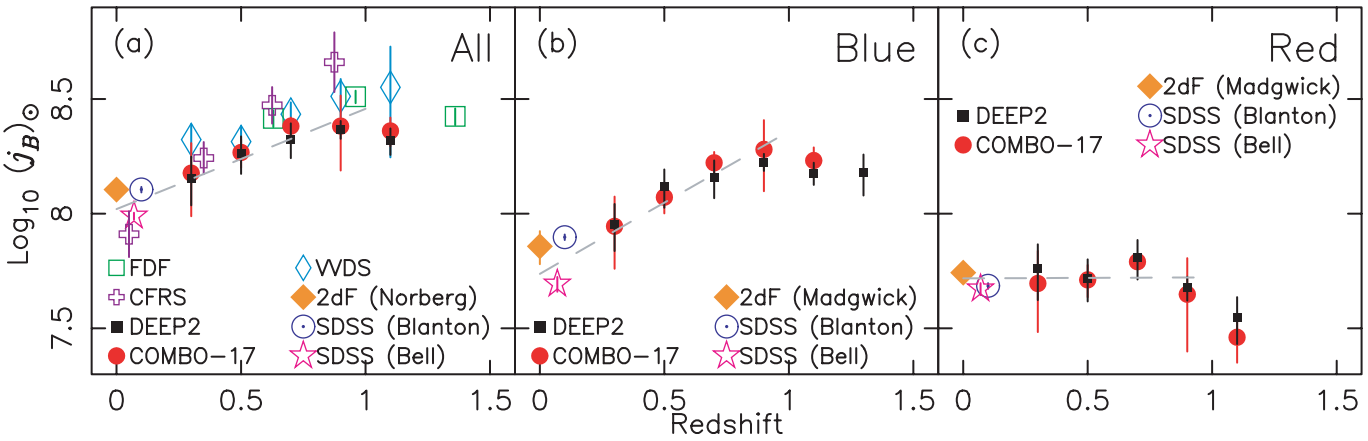


FIG. 8.—Evolution of the comoving $B$-band luminosity density in units of solar luminosities per Mpc$^3$, vs. redshift. Data values for COMBO-17 and DEEP2 come from Tables 2–4. References and symbols are the same as in Fig. 7 except for CFRS (*blue crosses*), which comes from Lilly et al. (1996). The blue and red estimates from Blanton et al. (2003) use the total luminosity density from that paper corrected by a contribution due to red galaxies of 38% from Hogg et al. (2002; see text). The dashed gray lines are as in Fig. 7 and show the linear fits to $z$ from Table 6; data used include the local surveys plus COMBO-17 and DEEP2 (out to $z = 1$). The luminosity density of blue galaxies has decreased by about a factor of 4.2 since $z = 1$, while that for red galaxies has remained roughly constant, with a possible rise before that.

function at intermediate redshifts (Fig. 6) extends as well to $z \sim 1$.

The second high-redshift study is by Cross et al. (2004), who counted both red-selected galaxies and galaxies morphologically selected to be spheroids regardless of color based on ACS images. Their counts agree well with ours despite their very small sample (72 galaxies). They also find an even steeper turnover in red faint-end slope near $z \sim 1$, where they obtain $\alpha = \sim +0.3$, declining to $\alpha \sim -0.5$ when blue spheroids are included.

Several older studies attempted to count galaxies in various ways back in time to see whether spheroids are disappearing at early epochs. Reviews can be found in Schade et al. (1999) and Im et al. (2001). Motivated by the predictions of semianalytic models, Kauffmann et al. (1996) reanalyzed CFRS data and claimed a drop in spheroid density to $z \sim 1$, but their conclusions were later disputed by Totani & Yoshii (1998). Schade et al. (1999) and Menanteau et al. (1999) counted morphologically normal $R^{1/4}$ law objects in *HST* images out to $z \sim 1$ and concluded that there was indeed no drop. However, sample and field sizes were very small in both cases and no color cuts were applied, with the result that half or more of all distant objects were blue. When these are removed, there is no contradiction in principle with the present study, although the prevalence (again) of distant blue spheroids is interesting.

Our final reference is to CFRS, the pioneering study that first attempted to calculate luminosity functions for distant red and blue galaxies (Lilly et al. 1995b). For blue galaxies, CFRS claimed a steepening in total faint-end slope back in time to $z = 1$. As noted, we have refrained from drawing any strong conclusions about faint-end slope evolution from our data despite the fact that DEEP2 and COMBO-17 have many more galaxies and go 1.5 mag deeper than CFRS. In retrospect, the CFRS data were probably not deep enough to support that conclusion. For red galaxies, CFRS found no evolution in either $M_B^*$ or $\phi^*$, whereas we find a dimming of $M_B^*$ by $\gtrsim 1$ mag and a rise in $\phi^*$ by a factor of $\sim 0.5$ dex since $z = 1$. Part of the difference may be that, lacking knowledge of color bimodality, CFRS used a nonevolving color cut that did not quite hit the valley at high redshifts. For whatever reason, CFRS projected an overall picture in which the red galaxy population has been rather static since $z = 1$, whereas the blue population has been significantly evolving. The picture here is different: the blue population is rather static in number density over this time (although individual blue galaxies may be evolving), whereas red galaxies are actively being created. In the broadest terms, the impression in CFRS of a strongly evolving blue population versus a static red population is essentially opposite to what we find.

### 4.3. *Luminosity Density*

The luminosity density provides an estimate of the total amount of light emitted by galaxies per unit volume. The luminosity density (in Johnson $B$ band) in this work is obtained assuming the Schechter form of the luminosity function:

$$j_B = \int L\phi(L)\, dL = L^*\phi^*\Gamma(\alpha + 2), \qquad (2)$$

where $j_B$ is calculated in solar units using $M_{B_\odot} = 5.48$ (Binney & Merrifield 1998) and $\Gamma$ is the Gamma function. Use of this expression entails extrapolation over faint magnitudes that are not observed, the more so at high redshifts. However, fitting a given bright-end data set assuming different values of $\alpha$ tends to leave the product $L^*\phi^*$ unchanged, which means that most of the uncertainty in applying equation (2) comes from $\Gamma$. For example, changing $\alpha$ from $-1.3$ to $-1.7$, as suggested by VVDS for their All sample at $z = 1.1$, changes $\Gamma$ by 230%. This case is extreme, however. Values of $\alpha$ for Blue and All galaxies from nearly all other studies range between $-1.0$ and $-1.3$, which implies a total change in $\Gamma$ of only 30%. Plausible red $\alpha$-values range from $-0.5$ to $-1.0$, which changes $j_B$ by only 11%. We conclude that, as long as $\alpha$-values remain below $-1.3$, uncertainties in $j_B$ are relatively small.

The resultant values of $j_B$ are plotted versus redshift in Figure 8. The two local surveys that divide by color are plotted in the All, Blue, and Red panels (Norberg et al. 2002; Bell et al. 2003). A third triplet of local values has been obtained by multiplying the total SDSS luminosity density from Blanton et al. (2003) by 62% and by 38% to obtain the fraction of $B$-band light in blue and red galaxies separately, based on fractional light contributions by Hogg et al. (2002). The latter are rough because they refer to $r$ band, not $B$ band, and because the Hogg et al. (2002) selection criteria were quite restrictive and probably did not include all red sequence galaxies. Since these effects tend to cancel, we have not tried to correct them.

The local SDSS and 2dF values in Figure 8 agree quite well for all three color classes. Relative to them, DEEP2, COMBO-17, and FDF for All galaxies show at most a mild decline with time in $j_B$. The fall in VVDS is nearly twice as large, probably due to their claimed steeper faint-end slope at high redshifts. Figure 8 shows All data from CFRS (Lilly et al. 1996), which also show a steep decline. Some of this is probably due to *their* claimed steep faint-end slope (noted in the previous section), but some also comes from an overly low nearby value, which they took from Loveday et al. (1992). The overly steep decline in *B*-band CFRS found here is consistent with recent UV analyses by Baldry et al. (2005) and Schiminovich et al. (2005), who also found that CFRS declines too steeply in UV light.

The evolutionary trends in $j_B$ can be quantified by fitting lines to the data in Figure 8 as we did for $M_B^*$ and $\phi^*$ in § 4.2. The resulting coefficients are given in the eighth, ninth, and tenth columns of Table 6, where the *H* parameter now represents the change in $j_B$ (in dex) from $z = 1$ to now. The linear and logarithmic fits are again nearly identical; taking the latter and assuming no $\alpha$ evolution, we find that $j_B$ for All galaxies (Fig. 8*a*) has fallen by the factor $2.88 \pm 10\%$ ($0.46 \pm 0.04$ dex) since $z = 1$. Blue luminosity density (Fig. 8*b*) falls faster, declining by $4.47 \pm 12\%$ ($0.65 \pm 0.05$ dex) since $z = 1$. This is consistent with the rather constant value of $\phi^*$ and the fade of 1.35 mag found for these objects in § 4.2. Finally, Red galaxies (Fig. 8*c*) show essentially *no change* in $j_B$ since $z = 1$, to within 17% (Table 6). This agrees with B04, who concluded that *B*-band luminosity density of red galaxies has remained essentially *flat* since $z \sim 1.0$ (possibly rising before that). The flat slope is caused by the simultaneous dimming of $M_B$ while $\phi^*$ is rising, and the two cancel out.

To summarize, DEEP2 agrees with both old and new analyses of COMBO-17 in showing that the *B*-band luminosity density for red galaxies has remained nearly constant since $z \sim 1$ with a possible rise just before that. Despite the fact that only the upper part of the luminosity function is observed at $z \sim 1$, DEEP2 and COMBO-17 agree within 20%, and extrapolation errors are small because the red function is known to turn over at high redshift (Cross et al. 2004; Giallongo et al. 2005). Barring actual loss of galaxies from both DEEP2 and COMBO-17 (see § 5), the constancy of $j_B$ for red galaxies after $z \sim 1$ should be well established. Stellar mass-to-light ratios are reviewed in § 5, where it is shown that both data and plausible models indicate an increase in $M/L$ by 1–2 mag since $z = 1$. The constancy of $j_B$ thus implies that the stellar mass bound up in red galaxies has increased by the same amount over that time, as first argued by B04. Given the strong implications of this result for galaxy formation, it is advisable to go back and review the errors and assumptions, which we do in the next section. Readers not interested in these details should skip to § 6.

## 5. ERRORS, ASSUMPTIONS, AND UNCERTAINTIES

This section focuses on the Red luminosity function, although many of the conclusions apply also to the Blue and All functions. The first issue is whether the apparent rise in the number density of bright red galaxies with time is due to the loss of high-redshift galaxies at various stages of the analysis. A second issue is the extent to which the conclusions are sensitive to fitting the counts to Schechter functions using the *same* $\alpha$ at all redshifts. These effects and others are discussed in this section:

1. *Completeness of the photometric catalogs*.—The COMBO-17 photometric catalog has a 5 $\sigma$ detection limit down to $R_{\rm AB} \sim 26$, nearly 2 mag below what is needed for the luminosity function surveys ($R_{\rm AB} \sim 24$). The DEEP2 5 $\sigma$ limit is $R = 24.5$ (Coil et al. 2004), which should still be adequate. DEEP2 makes an additional cut in surface brightness when designing the DEIMOS masks that delete low surface brightness galaxies in the last half-magnitude bin (Paper I, § 2). However, this should be largely corrected for by calculating weights as a function of both color and magnitude and furthermore does not affect early-type galaxies, which have high surface brightness.

Errors in star-galaxy separation may result in either too few or too many galaxies depending on the kind of error. Star-galaxy separation in COMBO-17 is based on 17 color photometry and is in general highly efficient; red counts near $z = 1$ may be $\sim$10% too high owing to K star interlopers (W04), but this would tend to *over*estimate red galaxies at that redshift. Star-galaxy separation for DEEP2 was checked in § 3.4 of Paper I using high-resolution *HST* images that cover part of the DEEP2 region in the GSS. Misclassification errors (of red galaxies classified as stars and vice versa) were found to be small, of order 10%. Finally, checks of both data sets show that nearly all galaxies to $R = 24$ have available photometry in all bands and the few ($\sim$1%) DEEP2 galaxies that do not have *B*-band photometry ("*B* dropouts") are corrected for statistically in the weights (Paper I, § 3.4).

2. *Dividing red galaxies from blue ones*.—This is done using rest-frame values of $U - B$ in DEEP2 and $U - V$ in COMBO-17. Errors in the zero points of these systems do not matter even if they vary with redshift since the dividing line is adjusted empirically to fit the color valley in each redshift bin. The local samples have been divided in various ways, but the results are not sensitive to method. For example, Madgwick et al. (2002) separated 2dF galaxies by spectral type, whereas Bell et al. (2003) separated SDSS galaxies by both concentration and optical color, but results are similar.

A second concern is that bluer than average (star-forming) red sequence galaxies may be missed at high *z* due to an improper *K*-correction. Rest-frame $U - B$ values for high-redshift galaxies are determined by observed $R - I$, and $R$ falls at $\sim$3300 Å at $z \sim 1$ and at bluer wavelengths beyond that. *GALEX* has shown that many nearby red sequence galaxies lie off the red sequence to bluer colors when viewed in the UV (Yi et al. 2005). However, the effect is strong only in *GALEX* NUV (2300 Å) and nearly absent in SDSS *u* (3550 Å; Schawinski et al. 2007), which is closer to our *R* band.

We have checked for this effect by making color-color plots for red sequence galaxies at $z = 1.1$ using $B - R$ versus $R - I$ for DEEP2 galaxies and $V - R$ versus $R - I$ for COMBO-17. These plots are a stringent test of our color separation because the bluer color in each pair is bluer than the color we actually use. The plots do show more scatter in the bluer color, indicating possible ongoing or recently quenched star formation. However, all color distributions are still strongly bimodal, and the valley isolates nearly the same samples regardless of whether the blue or red color is used. If anything, we find that the DEEP2 color cut includes *too many* blue valley galaxies at high *z*, and thus the loss of red galaxies due to ongoing or recent star formation appears to be small.

3. *Photometric systems*.—Weiner et al. (2005) checked DEEP2 rest-frame values of $M_B$ against values derived from GIM2D photometry of Groth strip *HST* images by Simard et al. (1999). GIM2D fitted model bulge+disk profiles to *V* and *I* images to find total magnitudes, whereas the DEEP2 CFHT photometry approximates each object by a Gaussian profile on *BRI* ground-based images and measures total light within an aperture of radius 3 times the Gaussian radius. Despite these different methods plus uncertainties in the *HST* WFPC2 photometric zero points

and charge transfer inefficiency corrections, the zero points of both $M_B$ systems agreed to within 0.07 mag. Furthermore, any mismatch in the magnitude systems for distant and local surveys would cause mainly an error in the evolution of $M_B$, not $\phi^*$, since the slope of the luminosity function near $L^*$ is shallow. COMBO-17 luminosities have never been independently checked. However, the detailed SED information allows a precise calculation of the rest-frame $B$-band luminosity at all $z < 1$ without extrapolation. The main source of error should be the photo-$z$ error, which translates into luminosity errors of 0.1–0.2 mag for most objects. The photometric systems of local surveys are claimed to be accurate to 0.1–0.02 mag (for photographic 2dF and CCD SDSS magnitudes, respectively). All of these errors are fairly small.

4. *Photometric errors for bright spheroidal galaxies*.—A much bigger error may be uncertainties in the total magnitudes of very bright spheroidal galaxies. Such magnitudes are hard to measure on account of the extended envelopes, which may be growing with time due to galaxy-galaxy interactions. Simply fitting such galaxies with de Vaucouleurs $R^{1/4}$ profiles is not appropriate because many profiles (at least locally) are even more extended than that (e.g., Graham et al. 2001). Total magnitude errors may therefore actually be larger for nearby galaxies than distant ones. For example, the total luminosities of nearby Abell brightest cluster galaxies (BCGs) can vary by *many tenths* of a magnitude (Gonzalez et al. 2005) depending on the profile fitting method used, and Lauer et al. (2007) find errors of up to a magnitude in SDSS luminosities for such galaxies. These are very large errors when one considers that a change of only 0.2 mag at $4L^*$ translates to a change in number density of a *factor of 2* in the Schechter function. Stellar masses have even larger errors because they depend on assumed evolution models for the fade in $M/L_B$, which add several more tenths of a magnitude uncertainty.

For now, we emphasize that our claim for the rise in the number of red galaxies comes from data *near* $L^*$, where envelopes are tamer, photometric errors are therefore smaller, and the slope of the luminosity function is shallower. The importance of magnitude errors for luminous spheroids is discussed further under recent work in § 6.3.

5. *R-band selection effect*.—The use of the $R$ band for selecting DEEP2 and COMBO-17 corresponds to rest-frame 3300 Å at $z = 1$, where the SEDs of red galaxies are rather dim. It is sometimes claimed that red galaxies are being "missed" on that account. In practice, this is fully allowed for by calculating limiting absolute magnitudes as a function of both redshift *and* color using slanting boundaries like those shown in Figure 4 (see also Fig. 4 of Paper I). The limiting $M_B^*$ magnitude to which the counts are complete in each redshift and color bin is well understood.

6. *Redshift completeness and accuracy*.—Redshift completeness has been simulated for COMBO-17 using Monte Carlo methods (W01, W03, W04). From these, it appears that redshifts are highly complete for red galaxies in COMBO-17 but substantially incomplete for blue galaxies in the last magnitude bin. This is consistent with the finding that nearly all failed COMBO-17 galaxies are faint blue galaxies. Testing the COMBO-17 completeness model independently is difficult. However, we have predicted total galaxy number counts from the best-fit luminosity functions, including extrapolations to the faint end and to somewhat higher redshifts, and find good consistency between predicted and observed COMBO-17 number counts. Of course, the power of this test to assess the completeness of a subsample in any particular redshift bin is limited.

Redshift completeness in DEEP2 is discussed in § 3.3 of Paper I. Using the minimal versus the average model (see § 3 above) typically results in no change in $M_B$ and a change in $\phi^*$ of 10%–20%. The average model, which is used for red galaxies, yields *higher* numbers of distant galaxies and minimizes the observed red galaxy evolution. Paper I also considered a third, extreme model for red galaxies in which all failed red galaxies were assumed to be located in *whatever redshift bin was under consideration*. It is possible to do this without redshifts because red sequence galaxies near $z = 0.7$–1.1 have apparent $R - I > 1.25$ and populate a well-defined ridge in the *apparent* CMD (see Fig. 1 of Paper I). This test amounts to counting all possible red galaxies and dumping all those with unknown redshifts into a *single* redshift bin. Even this extreme approach hardly affects results to $z = 0.9$ (although it does increase both counts and $j_B$ significantly at $z = 1.1$). Ultimately, this point will be thoroughly resolved with deeper data, and the DEEP2 team has started to compile deeper samples based on photometric redshifts.

Errors in measured DEEP2 redshifts are negligible ($<10^{-4}$ in $z$), and catastrophic failures are at the level of 1%. The accuracy of COMBO-17 photo-$z$'s has been studied using simulations, yielding an estimated rms error of 0.03, which agrees with the spectroscopic cross-check in W04. The effect of such errors on the Red luminosity function was simulated by B04 and shown to be small.

7. *Formal Schechter fit errors and cosmic variance*.—The errors in $\phi^*$ for red galaxies given in Table 4 include both Poisson noise and cosmic variance. In the two most distant bins, these errors are comparable and give an rms error in number density of about 20% per survey, or 14% for the two surveys together. The error in the local zero point of $\phi^*$ for red galaxies is conservatively set at 20%, yielding a formal 1 $\sigma$ error of 24% for the method 1 difference in $\phi^*$ between $z = 1$ and 0. Method 2 is based on fitting a slope to only $\phi^*$ data below $z = 1$ and agrees with method 1 to within 20%. The difference and errors are small compared to the claimed formal rise in $\phi^*$ since $z = 1.0$ of $\sim$0.5 dex.

This completes the list of known observational errors and selection effects. We turn now to various theoretical and model assumptions:

8. *The assumption of constant Schechter function shape at all redshifts*.—This amounts to assuming (1) that the Schechter formula is a good match to the bright end of the luminosity function at all redshifts and (2) that the faint-end slope $\alpha$ does not vary with redshift. A breakdown in either one will produce a mismatch between the data and the model, causing errors in both $M_B$ and $\phi^*$. If the shape of the real function is constant with redshift but is not well fitted by the model, the fitted parameters will drift spuriously with $z$ as the data are limited to progressively brighter magnitudes at higher redshifts. Any real evolution in shape will cause additional errors.

Inspection of Figure 6 suggests that our Schechter model (with the adopted value of $\alpha = -0.5$) *looks* like a good fit for red galaxies. Appendix B of Paper I tested this quantitatively by truncating the DEEP2 data in nearby bins at bright magnitudes corresponding to the observational limits in more distant bins. For red galaxies, a drift of $M_B^*$ of $\sim$0.1 mag toward fainter values was seen with more truncation, whereas the measured evolution is a brightening of $M_B^*$ by 1.2 mag back in time. The quantity $\phi^*$ drifted upward by $\sim$0.10 dex, whereas the measured evolution is a fall of $\sim$0.5 dex to $z = 1.0$. High-redshift bins cannot be tested in the same way, but visual

inspection indicates that the match between data and model remains good.

On the other hand, certain recent data suggest that the shape of the Red luminosity function *is* changing with time, which would invalidate the assumption of strictly constant $\alpha$. De Lucia et al. (2004) see a deficit in the number of faint red galaxies in rich clusters at $z = 0.8$ compared to Coma, and Kodama et al. (2004) detect a similar deficit of faint red galaxies in overdense field regions at $z \sim 1$. As noted in § 4.3, Cross et al. (2004) report a stronger turnover at $z \sim 1$ for distant faint red galaxies than seen locally. These studies at high redshift all go 1–2 mag fainter than DEEP2/COMBO-17 and are thus better measures of $\alpha$ in distant samples. Added to this is the potential flattening of faint-end slope seen by COMBO-17 in its nearest redshift bin (see Fig. 6), which resembles the flattish faint-end slope seen in local SDSS data by Bell et al. (2003) (although DEEP2 and 2dF [Madgwick et al. 2002] both disagree with this; see Table 5).

A flatter faint-end slope with time suggests that smaller red sequence galaxies may be forming later than larger ones and *filling in* the red sequence at faint luminosities. In addition to the luminosity functions just mentioned, further evidence for this includes (1) greater recent growth in the number of red sequence galaxies below $M^*$ (Bundy et al. 2005), (2) faster surface brightness fading of small red sequence galaxies from the magnitude-radius relation (McIntosh et al. 2005) and fundamental plane (van der Wel et al. 2005), (3) faster fading in the mass-to-light ratios of smaller galaxies (di Serego Alighieri et al. 2006), (4) later arrival on the red sequence of small spheroidal galaxies (Treu et al. 2005a, 2005b), (5) the fact that distant blue spheroidal galaxies are significantly smaller than red ones and would preferentially populate the low-mass end of the red sequence if they were fading toward it (Im et al. 2001; Cross et al. 2004), and (6) the fact that stellar populations in small red sequence galaxies seem to be systematically younger than in massive ones (Proctor & Sansom 2002; Caldwell et al. 2003; Thomas et al. 2005; Nelan et al. 2005; Schiavon 2007; Graves et al. 2007). Also relevant is the discovery that nearby faint red sequence galaxies actually populate denser regions than their brighter red sequence counterparts (Hogg et al. 2003). A plausible explanation is that many of these fainter objects are starved, stripped, or harassed satellites in large clusters. Since such clusters form late, this quenching mode might have become more important recently and filled in the lower end of the red sequence at late times.

In short, recent data do seem to support a gradual filling in of the lower red sequence with time, such that small spheroidal galaxies are forming later than large ones. However, even if this is occurring, the effect on our Schechter parameters is not large. Suppose that $\alpha$ is evolving from $-0.5$ at $z \sim 1$ to $-1.0$ (flat) locally, the largest change that the data permit (see Table 5). As an experiment, we have refitted local data[24] using $\alpha = -1.0$ and find that $M_B^*$ brightens by 0.3 mag, $\phi^*$ declines by 0.18 dex, but $j_B$ declines by only 2%. This last change is particularly tiny compared to the claimed evolution and illustrates the power of $j_B$ as a robust gauge of evolution. We conclude that the red faint-end slope is sufficiently flat that total luminosity density is determined quite well by data only down to $L^*$, which is achieved at all redshifts here.

9. *Using color as a surrogate for morphological type.*—In focusing on red galaxies, we are implicitly assuming that rest-frame color is a good way of finding spheroid-dominated, E/S0 types at all redshifts. The method works well at low redshifts, where only 15%–20% of nearby red sequence galaxies have Hubble types later than S0, being mostly edge-on and dust-reddened spirals (Strateva et al. 2001; Weiner et al. 2005). However, contamination by nonspheroidal galaxies is larger at higher redshifts, amounting to 30% at $z \sim 0.75$ (Bell et al. 2004a; Weiner et al. 2005), and may increase beyond that (Cimatti et al. 2002a, 2003; Yan & Thompson 2003; Gilbank et al. 2003; Moustakas et al. 2004). Because of this rise back in time, our measured increase in the number of red galaxies is actually a *lower limit* to the rise in morphologically normal E/S0s. Assuming that contamination on the red sequence amounts to 30% at $z = 1$ would mean that the real rise is 0.06 dex larger than our value and could be even larger since contamination at $z = 1$ may be higher than at $z = 0.75$.

10. *Uncertainties in evolving stellar mass-to-light ratios.*—These come into play when converting luminosity density into the more fundamental quantity stellar mass. As noted, $j_B$ for red galaxies is nearly constant out to $z \sim 1$ and may be lower before that. Since stellar mass-to-light ratios are increasing with time, this means that the stellar mass bound up in red sequence galaxies must also increase, but by how much? B04 investigated this using single-burst passively evolving models, but these are only one option. We have investigated further possibilities, such as $\tau$ models, "frosting" models with a continuing low level of star formation (e.g., Gebhardt et al. 2003), and "quenched" models in which star formation is shut down abruptly at some epoch (Harker et al. 2006). Models have been set up to match the average color of red sequence galaxies today, together with the relatively small amount of color evolution since $z = 1$ [$\Delta(U - B) = 0.15$–$0.25$ mag; B04; Weiner et al. 2005; Koo et al. 2005; Harker et al. 2006]. Recipes that satisfy these constraints yield fadings of 1–2 mag in $M/L_B$.

Observationally measured brightenings are consistent with these model estimates. The fundamental plane zero point brightens by 1–2 mag (van Dokkum et al. 2000; Gebhardt et al. 2003; van Dokkum & Ellis 2003; Treu et al. 2005a, 2005b; van der Wel et al. 2005), the magnitude-radius zero point brightens by 1–1.6 mag (Trujillo & Aguerri 2004; McIntosh et al. 2005), and $M_B^*$ for red galaxies brightens by 1.2 mag (this paper). These shifts do not necessarily represent pure fading if galaxies are also evolving in radius, mass, and/or $\sigma$. Nevertheless, it seems highly significant that the amount of fading from the various scaling laws is close to the fading seen in $L_B^*$ and that this in turn is in the range predicted by stellar population models. Combining all results together, we adopt 1.0 mag (0.4 dex) as the *minimum* increase in the mass-to-light ratio of a typical massive red galaxy since $z = 1$. Since $j_B$ has remained constant, this is also the minimum increase in red stellar mass over the same period.

We now collect together the three known potential numerical corrections to our previous estimate of $\Delta\phi^*$ for red spheroidal galaxies from $z = 1$ to now. A positive sign means that the previously estimated growth in $\phi^*$ would be even bigger than we quoted. The factors are as follows: a possible mismatch between the adopted Schechter function shape and the actual bright end of the luminosity function, +0.10 dex; a possible nearby flattening of $\alpha$ from $-0.5$ to $-1.0$, $-0.18$ dex; contamination by distant non-E/S0s, +0.06 dex. Each effect is small, and collectively they tend to cancel. For these reasons, we do not apply any of these corrections to the formal rise of $\sim$0.5 dex in $\phi^*$ since $z = 1$ computed in § 4.2.

[24] For example, using sample data available at http://www.mpia-hd.mpg.de/homes/bell/data/glfearlycol.out.

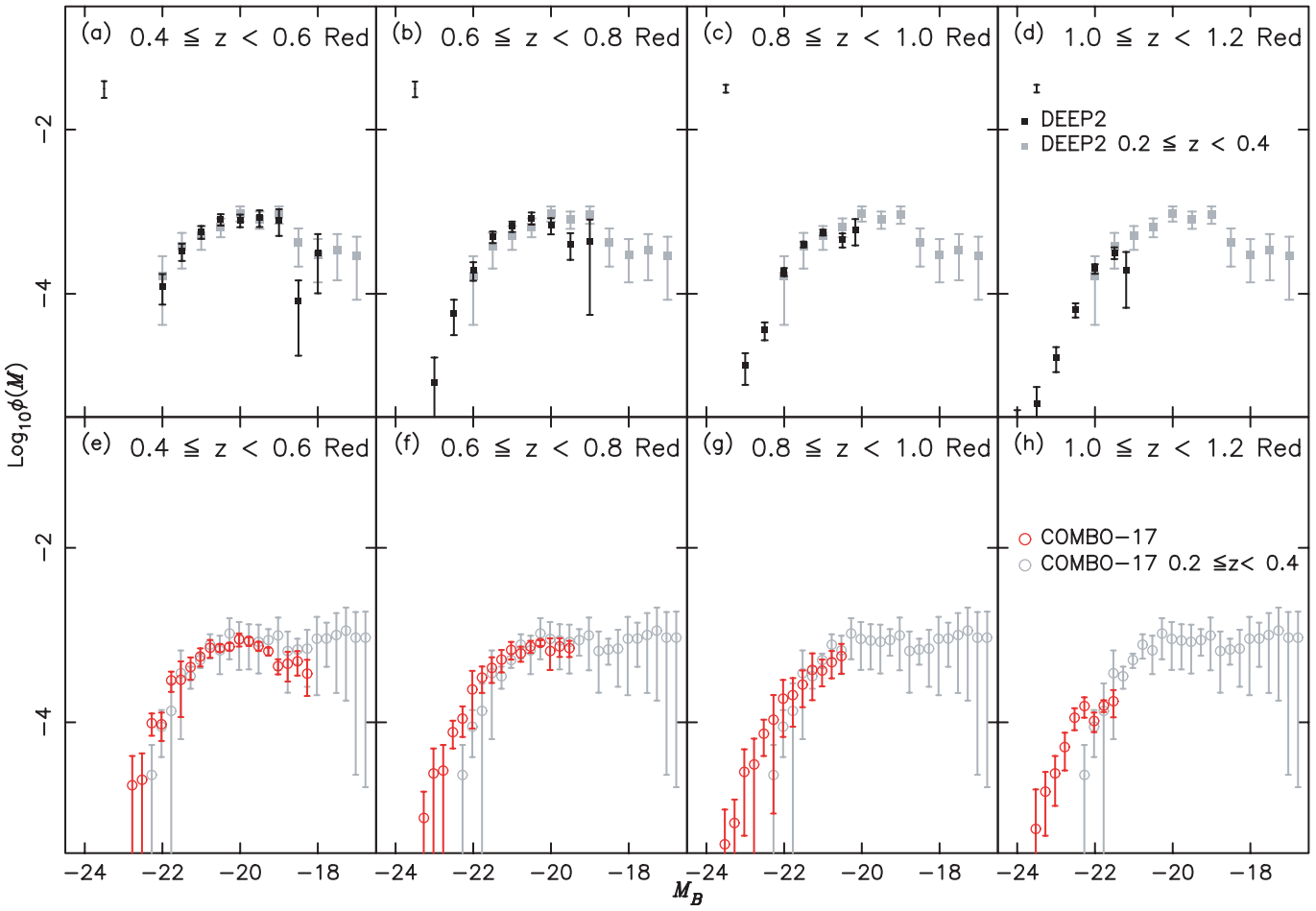


FIG. 9.—This figure overplots Red counts from the lowest redshift bin ($z = 0.2$–$0.4$; *gray symbols*) on top of counts at high redshift, for both DEEP2 and COMBO-17. The purpose is to illustrate how the Red counts do not evolve very much internally to each survey. The luminosity functions either stay fixed or translate parallel to themselves such that there is little change in number at constant absolute magnitude. This conclusion is strongest near $L_B^*$ ($M_B^* = -21.5$), which is well probed at all redshifts. Fitted values of $\phi^*$ are decreasing and $M_B^*$ are increasing throughout this range; although formally significant, these values depend on subtle curvature in the data, and independent confirmation is desirable. This comes from stellar mass-to-light ratios, which, if taken into account, indicate that the number density of galaxies *at fixed stellar mass* is falling approximately as $\phi^*$ (see text).

We have thus far not uncovered any "smoking gun" that suggests why the counts of red galaxies in DEEP2 or COMBO-17 might be seriously in error. Nevertheless, there is a worrisome feature of the data, and that is the fact that neither survey shows much *internal* evolution in red $\phi^*$ over most of their well-measured range. This point was mentioned in Paper I (§ 4) in connection with DEEP2, and it is visible again in Figure 7, which plots both DEEP2 and COMBO-17. In both data sets, there is a jump in $\phi^*$ of $\sim$0.2 dex between the distant surveys and the local surveys and another jump of $\sim$0.3 dex between $z = 0.9$ and 1.1. In the middle, $\phi^*$ tends to plateau. This stagnation is illustrated differently in Figure 9, which overplots $1/V_{\rm max}$ data points from the lowest bin at $z = 0.2$–$0.4$ from both surveys on top of the data points for distant bins. As noted, this figure shows that the red counts at bright magnitudes tend to translate *parallel* to themselves, and one might even conclude that *no evolution* in the luminosity function (and thus in number density) had occurred. Both DEEP2 and COMBO-17 are similar. This degeneracy could be broken by having fainter data, but our two surveys do not go deep enough.

At this point, the argument involving stellar mass-to-light ratios becomes critical. Imagine replotting Figure 9 versus *stellar mass* instead of $M_B$. To account for the evolution in mass-to-light ratio, the counts at $z \sim 1$ would have to be shifted over to the right by at least 1 mag, which would produce a vertical offset with respect to the low-redshift counts by about a factor of 4 (0.6 dex) near $M_B = -21.5$, where all curves superimpose. This is nearly identical to our previous falloff of $\sim$0.5 dex based on $\phi^*$. Thus, once mass-to-light ratio evolution is allowed for, the number of massive red galaxies *at fixed stellar mass* is increasing about as fast as the formal fit for $\phi^*$. This argument is similar to the one applied by B04 to *total* red luminosity density, but we apply it here specifically to galaxies near $L^*$ ($M_B^* \sim -21.5$ at $z = 1$). The distinction is a small one, but the present version of the argument does not rely on any assumptions about faint unseen galaxies below $L^*$, but only on objects that have been seen and measured.

As the final point in this section, we estimate both the minimum and maximum rise in the number density of red $L^*$ galaxies that are consistent with the data. The minimum rise is estimated in two ways. The first way drops the risky near and far redshift bins and uses only DEEP2 and COMBO-17 data between $z = 0.2$ and 1.0. A linear least-squares fit to $\log_{10}\phi(z)$ versus $z$ for our data over this range has slope $0.32 \pm 0.07$ dex per unit redshift. Taking the 1 $\sigma$ minimum slope of 0.25 dex per unit redshift yields a total increase of a factor of 1.8 from $z = 1$ to now. The second way fits $\log_{10} j_B$ using DEEP2 and COMBO-17 data over the same redshift range, which gives

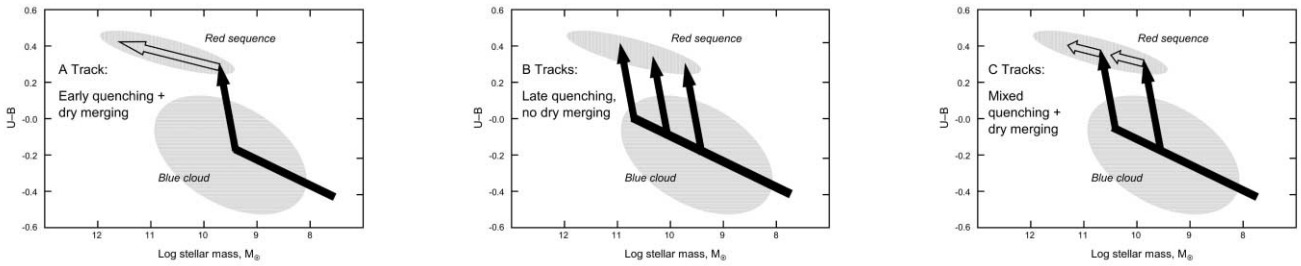


FIG. 10.—Schematic arrows showing galaxies migrating to the red sequence under different versions of the merging hypothesis. Evolutionary tracks are plotted in the color-mass diagram. Here it is assumed that red galaxies arise from blue galaxies when star formation is quenched during a major merger, causing the galaxy to double in mass, but the exact nature of the quenching mechanism is not crucial. Quenching tracks are shown by the nearly vertical black arrows. The mergers would be gas-rich (or "wet") because the progenitor galaxies are blue objects making stars and hence contain gas. Once a galaxy arrives on the red sequence, it may evolve more slowly along it through a series of gas-poor, or "dry," mergers. These are shown as the white arrows. They are tilted upward to reflect the aging of the stellar populations during the more gradual dry merging. A major variable is the time of mass assembly vs. the time of quenching. Three possibilities are shown. Track A represents very early quenching while the fragments of the galaxy are still small. In that case, most mass assembly occurs in dry mergers along the red sequence. Track B is the other extreme, having maximally late quenching. In that case, galaxies assemble most of their mass while still blue and then merge once to become red with no further dry merging. Track C is intermediate, with contributions from both mechanisms. This "mixed" scenario best matches the properties of both distant and local ellipticals. In addition to the merging scenario illustrated here, the gas supply of some disks may simply be choked off or stripped out without mergers, to produce disky S0s. Such tracks would be vertical, but aside from this their histories are similar. S0s dominate on the red sequence below $L^*$, ellipticals above (Marinoni et al. 1999).

slope $0.06 \pm 0.09$ dex per unit redshift ($j_B$ rising with time). Taking the 1 $\sigma$ minimum slope of $-0.03$ dex per unit redshift (falling with time) and assuming a minimum change in mass-to-light ratio $M^*/L_B$ of 1.0 mag gives a rise in total red stellar mass of a factor of 2.3. The geometric mean of these two numbers gives a minimum increase of a *factor of 2* in the number of red $L^*$ galaxies from $z = 1$ to now, the same as claimed by B04.

To obtain the maximum rise, we take the formal difference in $\phi^*$ estimated in § 4.2 between $z = 0$ and 1 using method 1 and all data ($0.56 \pm 0.09$ dex) and *add* the 1 $\sigma$ error bar. This yields a maximum rise of 0.65 dex, or a factor of 4.5. However, this maximum still does not contain a correction for the likely growing contamination by dusty galaxies at $z \sim 1$, which could add another 30% or more, for a factor of about 6.

## 6. DISCUSSION

### 6.1. *A "Mixed" Scenario for the Formation of Spheroidal Galaxies*

The most arresting conclusion to emerge so far from the study of luminosity functions is the growth in the number of red $L^*$ galaxies since $z = 1$, as shown in Figure 7. Barring mergers among a large and undiscovered population, which would have to be tiny and/or highly obscured to avoid detection in present surveys, this rise means that the ancestors of a large fraction of today's red $L^*$ galaxies must be visible *in existing blue samples* at $z = 1$ and later. The implications of this were discussed by B04. We build on their arguments by adding data on the blue luminosity function (measured here by DEEP2 and COMBO-17 for the first time) and the properties of local E galaxies, which we argue also have strong implications for formation scenarios. Our discussion focuses on typical *field* galaxies at high redshift, since DEEP2 and COMBO-17 sample all galaxies regardless of location. The red sequence in distant clusters has also been extensively studied, but we do not try to fold these data into the picture at this time.

It is well established that residence on the red sequence (in the absence of dust) requires that star formation be quenched or at least strongly reduced. Stellar populations become red enough to join the red sequence just 1–2 Gyr after star formation is stopped (e.g., Newberry et al. 1990; Barger et al. 1996; Bower et al. 1998; Poggianti et al. 1999), but in order for them to stay there, the star formation rate must remain low. Gebhardt et al. (2003) explored a "frosting model" with an early high rate of star formation followed by a slowly decaying $\tau$ component. Based on colors, they found that only 7% of the total stellar mass could be formed in the $\tau$ component; similar limits on present-day star formation rates are set by *GALEX* observations (Yi et al. 2005; Salim et al. 2005). In short, the large buildup in red stellar mass after $z = 1$ could not have arisen from star formation within red galaxies themselves (see also B04). Rather, the stellar mass near $L^*$ on the red sequence must have *migrated* there via one of three processes: (1) the quenching of star formation in blue galaxies, (2) the merging of less luminous already quenched red galaxies, or (3) some combination of the two. In the following discussion, we focus on galaxies arriving on the red sequence near $L^*$ because the data are complete there and photometric errors are not as serious as they are for brighter spheroids. Galaxies may of course also be migrating to the lower end of the red sequence, and the data reviewed in § 5 (point 8) suggest that this is also happening.

It is helpful to visualize this mass migration as the movement of progenitor galaxies through the CMD or, more fundamentally, the color-mass diagram. Sample tracks are shown in Figure 10. Two parent regions are illustrated, a narrow red locus corresponding to the red sequence and a broader blue clump, which we call the "blue cloud." The rather constant morphology of the CMD since $z = 1$ (B04; Weiner et al. 2005; Paper I) suggests that these parent regions are relatively stable in size and location. In reality, they are also moving as galaxies evolve, but this will not be too important if individual galaxies move through them more rapidly. With that assumption, we show the clumps as fixed and the galaxies as moving through them with time.

Each final galaxy today is represented by its most massive progenitor at any epoch. Stellar mass is migrating toward the upper left corner, where luminous red galaxies reside. For a galaxy to get there, two things must happen: the mass composing the final galaxy must be assembled via gravitational collapse, and star formation must be quenched. A key question in the formation of red sequence galaxies therefore is, did quenching occur early in the process of mass buildup, midway, or late? If extremely early, the pieces that would become the final galaxy

migrated to the red sequence while still small, producing a large number of small galaxies on the lower red sequence that must later merge along the sequence in a series of "dry," i.e., purely stellar, mergers. This is track A. If extremely late, the progenitors grew in mass hierarchically while still making stars within the blue cloud. On quenching, the most massive of them moved to near the head of the red sequence and took up residence there without any further dry mergers. This late-stage quenching scenario (for various masses) is shown as the tracks labeled B. *Mixed* scenarios are also possible involving a moderate amount of mass assembly during the star-forming stage, followed by quenching and continued (but limited) dry merging along the red sequence. These are the tracks labeled C.

Strictly speaking, dry mergers increase the stellar mass of a galaxy but leave its color unchanged. The arrows for an instantaneous dry merger should therefore be horizontal in Figure 10, which has traditionally been thought to add objectionable scatter to the color-magnitude relation (e.g., Bower et al. 1992). But now there is an additional source of scatter, which is caused by the different mean ages of stars in galaxies with the same stellar mass but that have quenched at different times. With suitable assumptions, dry merging might even reduce this second source of scatter. Actual dry merging would probably proceed rather slowly, in which case stellar populations would age and redden as they grow in mass, causing dry merging tracks to be tilted upward. This is how we have drawn them in Figure 10. Given a preexisting color-magnitude relation, the process of dry merging might therefore tend to move galaxies *along* this relation rather than off it, reducing scatter. Evidently, the net scatter induced by dry merging will depend not only on the amount of dry merging that occurs but also on how fast it happens and whether there is an underlying color-magnitude relation due to, for example, inherent mass-age and/or mass-metallicity trends. We return to the origin of tilt and scatter on the color-magnitude relation at the end of this subsection.

The simplest picture for the formation of a red sequence galaxy involves the fading of a *single* blue galaxy without any merging at all. However, we do not consider this to be viable by itself for explaining red $L^*$ galaxies because many objects today near $L^*$ (and above) are *spheroid-dominated* Es and E/S0s (the ratio of Es to S0s crosses near $L^*$; above $L^*$, Es dominate; Marinoni et al. 1999). Since distant blue galaxies are mainly disks (Bell et al. 2004a; Weiner et al. 2005), fading alone cannot transform them into spheroids: a major merger at some point is needed. There also are not enough massive blue galaxies in the distant CMD with masses comparable to those of the brightest red galaxies (B04; Weiner et al. 2005; Paper I, Fig. 4). Hence, in order both to boost mass and also to create spheroids, a process involving both quenching *and* merging of blue galaxies seems to be required. Two different versions of this "quenching/merging" picture are discussed below. (On the other hand, quenching of pure disks without merging may well feed the *lower* red sequence below $L^*$, where S0s dominate. Evidence for late infill of the lower red sequence via such processes was reviewed in § 5, point 8. Some fraction of the S0s near $L^*$ may also form this way.)

Yet another process by which galaxies might migrate to the red sequence is *unveiling*, whereby a dusty starburst is cleansed of its interstellar medium and the underlying galaxy is revealed. Such a process might cause the galaxy to brighten as dust absorption is removed, but also to redden as the starburst ages. However, there is no need to discuss this case separately because it is already subsumed under the previous ones. If the starburst is an episode in the life of a single disk galaxy (e.g., Hammer et al. 2005), then the object today is still a late-type spiral and is irrelevant to the red sequence. If the starburst has been induced by a merger, then the dusty phase is a temporary stage between the original blue precursor and the final red remnant, which does not alter our fundamental model of blue galaxies merging and turning into red galaxies. The arrows in Figure 10 are meant to connect initial and final states, not represent the detailed track whereby an object moves from blue to red. The only assumption that we have made concerning the transition is that merger remnants move quickly to the red sequence without lingering very long as bright blue starbursts. This is required by the fact that few if any bright blue starbursts are visible in the CMD (B04; Weiner et al. 2005; Fig. 4 of Paper I). It is also supported by radiative transfer models of dust in merging galaxies, which indicate that the burst itself is heavily cloaked by dust and is optically nearly invisible (Jonsson et al. 2006). Thus, starbursting galaxies are hard to tell optically from nonstarbursting galaxies, and both types populate the blue cloud, as assumed in Figure 10.

The above quenching models could be represented equally well by tracks in the CMD as in the color-mass diagram, and the former would be closer to raw data. However, stellar mass is the more fundamental parameter, its behavior under merging is easier to predict than light (because dust and starbursts are not a problem), and mass estimates for samples of distant galaxies are becoming standard (e.g., Drory et al. 2004, 2005; Fontana et al. 2004; Bundy et al. 2005). With mass as the size parameter, the motions of galaxies moving onto the red sequence via mergers are described by vectors moving both upward (redder) and to the left (more massive).

Yet another perturbation to the basic model is the possibility that the most massive progenitor might take up residence on the red sequence and then later accrete fresh gas, perhaps by swallowing another blue galaxy. The resultant starburst could briefly move the remnant back to the blue cloud, followed by subsequent decay back onto the red sequence (e.g., Charlot & Silk 1994). However, such events (while they last) would create massive blue galaxies, which we have argued are rare. The events must therefore be short lived and should not greatly distort our basic assumption that, once the most massive progenitor galaxy enters the red sequence, the galaxy remains there permanently.

We make three generic points before considering tracks A, B, and C in more detail. First, since the number of massive spheroids (and their associated stellar mass) has been growing since $z \sim 1$, the makeup of the population is not stable over that time, and mean properties such as average color, stellar age, etc., are constantly being skewed by recent arrivals (the so-called progenitor bias phenomenon of van Dokkum & Franx 2001). The population as a whole therefore cannot be modeled using passively fading single-burst, monolithic collapse models, even though certain properties such as $L_B$ and color seem to be moderately well fitted by such models (but for a closer discussion of colors see Harker et al. 2006). This similarity is a coincidence, and such models should be abandoned.

The second point pertains to what we mean by the "age" of a galaxy. In the monolithic picture, the age of a spheroidal galaxy is well determined and corresponds to the epoch at which the mass collapsed and the stars were formed (both are the same). In the new picture, each spheroidal galaxy has at least *four* potential characteristic ages: the epoch of major mass assembly, the epoch when the first stars were formed, the epoch of major star

formation, and the epoch of quenching, which might all be different.[25]

The third point is the power of nearby E galaxies to constrain formation models for the *upper* red sequence. Five properties of these galaxies are relevant:

1. The most obvious property is that nearby red galaxies are spheroid dominated, which motivated the argument above that quenching is coupled to spheroid formation (particularly for massive galaxies). We can now say more about specific mechanisms to accomplish this. We start with the fact that *major mergers* can morphologically transform disks to spheroids (Toomre & Toomre 1972; Toomre 1977; Mihos & Hernquist 1994, 1996; Barnes & Hernquist 1996). Many nearby merger remnants are known whose properties are consistent with their evolving into spheroidal galaxies once the acute merger phase is over (e.g., Schweizer 1982, 1986; Hibbard 1995). The incidence of spheroid-dominated galaxies is also higher in denser regions (e.g., Dressler 1980; Postman & Geller 1984; Hogg et al. 2003; Balogh et al. 2004; Baldry et al. 2004), where mergers are (or were) more frequent.

However, mergers by themselves need to be augmented with quenching in order to create suitably red colors. Fortunately, several gas removal mechanisms exist within the merger framework itself, such as starburst heating (Mihos & Hernquist 1994, 1996; Sanders & Mirabel 1996), radiation-driven winds operating on dust (Murray et al. 2005), orbital energy injected during the merger (Cox et al. 2006), and active galactic nucleus (AGN) feedback (e.g., Granato et al. 2004; Springel et al. 2005). A "unified" model has been proposed that incorporates all of these mechanisms to build spheroids, QSOs, and central black holes via major mergers at the same time (e.g., Hopkins et al. 2006). (This is the model that motivated the tracks drawn in Figure 10, which assume that stellar mass doubles on quenching.)

An alternative quenching model that does not explicitly involve merging has galaxies falling into massive dark halos above $M_{\rm crit} \sim 10^{12}\,M_{\odot}$ (e.g., Rees & Ostriker 1977; Birnboim & Dekel 2003; Dekel & Birnboim 2006), where further gas accretion is halted by inefficient cooling. However, this model is likewise incomplete and must be augmented with merging to create spheroidal morphologies. Such mergers may be common, as halos may pass over the threshold halo mass $M_{\rm crit}$ by merging with another similar-sized halo, in which case the merger of their central galaxies would soon follow (A. Cattaneo et al. 2007, in preparation). (Those cases in which mergers do not occur may produce luminous S0s.)

Finally, neither of the above quenching mechanisms may be able to *maintain* spheroids gas-free over long times: more gas is expected to fall in eventually, creating large numbers of massive blue galaxies that are not seen (e.g., Kauffmann et al. 1999; Benson et al. 2003). The problem is especially acute for the central gas in massive X-ray clusters, which looks like it should be cooling on a very short timescale yet instead is apparently being heated by a central radio galaxy (for a review see Fabian 2005). Recent models have invoked this long-term low-level "radio mode" for keeping central galaxies gas-free after the initial quenching is accomplished (Croton et al. 2006).

To summarize, the exact mechanism(s) that cause galaxies to quench and migrate to the red sequence are not known. However, candidates exist that naturally combine the necessary ingredients of major mergers (for morphological transformation) and quenching (for shutting off the gas supply). Any of these would suffice to create the massive spheroids that dominate the upper red sequence near $L^*$ and above.

2. The second important property of local E galaxies is that they populate rather tight *stellar population scaling relations* linking population properties to galaxy size and $\sigma$. Examples are the color-magnitude relation (Baum 1959; Faber 1973; Sandage & Visvanathan 1978; Bower et al. 1992), the color-$\sigma$ relation (Bernardi et al. 2005), and the Mg-$\sigma$ relation (Bender et al. 1992; Bernardi et al. 1998; Trager et al. 1998; Colless et al. 1999; Worthey & Collobert 2003; Bernardi et al. 2005). A viable formation theory must explain the origin and small scatter of these relations.

3. Next is the fact that the mean light-weighted stellar population ages of local Es vary widely, from over 10 Gyr down to just a few Gyr (e.g., Gonzalez 1993; Trager et al. 2000a; Jørgensen 1999; Terlevich & Forbes 2002; Caldwell et al. 2003; Thomas et al. 2005; Schiavon 2007), with most being younger than predicted by classic single-burst models (11.4 Gyr if $z_{\rm form} = 3$). The large number of intermediate-age systems allows room for late quenching, as required by the late growth in $\phi^*$. However, a problem arises in that the *scatter* in both age and metallicity at a given mass and $\sigma$ is quite large (Trager et al. 2000b; Caldwell et al. 2003; Thomas et al. 2005). To keep the stellar population scaling relations tight, Worthey et al. (1995) posited that an *anticorrelation* must exist between age and metallicity at constant mass and $\sigma$, and this was later detected by Jørgensen (1999), Trager et al. (2000b), and Bernardi et al. (2005). An explanation is needed for the origin of this age-$Z$ anticorrelation.

4. The fourth property is the recent discovery that, despite the scatter, both age and $Z$ vary smoothly along the stellar population scaling relations in the sense that massive red sequence galaxies tend to be *both older and more metal-rich* than smaller ones (Thomas et al. 2005; Nelan et al. 2005; Schiavon 2007; Graves et al. 2007). The stellar population scaling relations are thus not caused by either metallicity or age alone but by both in combination. A proper theory for spheroid formation should explain this.

5. The fifth and final property is that nearby Es populate a *structure sequence* in which smaller Es rotate strongly and have disky isophotes and steep central surface brightness profiles, whereas massive Es rotate weakly and have boxy isophotes and core-type central profiles (e.g., Davies et al. 1983; Bender et al. 1992; Faber et al. 1997). At the low-mass end, these properties connect smoothly with S0s and, through them, to the remainder of the Hubble sequence. Kormendy & Bender (1996) have suggested that the structure sequence can be explained if smaller Es were assembled via mergers of "wet," gas-rich progenitors while more massive Es were produced by progressively drier, stellar mergers of smaller red sequence galaxies. Final assembly of the most massive Es, such as BCGs, was almost completely via dry mergers. If this picture is correct, the structure sequence of nearby E galaxies implies that the gas content of the mergers that made those galaxies must have *declined systematically* with increasing galaxy mass.

With these five properties of local Es as background, we return to the tracks in Figure 10. The early quenching scenario (track A) has most of its mass assembly occurring in dry mergers *along* the red sequence. This can be ruled out on two grounds. First, to produce the large amount of stellar mass bound up in massive red sequence galaxies would require a huge reservoir of

[25] Our use of the word "age" here is not meant to obscure the fact that mass assembly and star formation are both prolonged processes, so that three of the above "ages" are the mean of events that may have lasted over a long time.

small, faint galaxies on the lower red sequence. This excess is not detected at any redshift: the local red sequence luminosity function is at most flat ($\alpha \sim -1.0$) and if anything turns over more steeply at higher redshifts (Cross et al. 2004; Kodama et al. 2004; Giallongo et al. 2005; see also Fig. 6). The required reservoir of small red galaxies does not exist.

Second, building up massive red galaxies from purely dry mergers along the red sequence would yield stellar populations whose metallicities are uncorrelated with stellar age and whose ages and metallicities would converge to a single value at high mass after many mergers had occurred. This fails to match the large spread in age and $Z$ at fixed size even among massive galaxies (Trager et al. 2000b; Terlevich & Forbes 2002; Caldwell et al. 2003; Thomas et al. 2005), the trends in age and $Z$ with mass along the sequence, or the age-$Z$ anticorrelation.

The late quenching scenario (track B) has *no* dry merging at all along the red sequence. In this picture, massive present-day spheroidals were formed via a single merger of two very massive *gas-rich* progenitors. The main reason for ruling this out is the structure sequence among local Es, which, as noted, suggests that more massive Es were formed by drier, gas-poor mergers. The signatures of such mergers are distinctive because the precursors are dynamically hot, yielding fuzzy tidal tails without sharp boundaries. Many examples of such mergers can be seen in local catalogs (e.g., Arp 1966; van Dokkum 2005). These purely dry mergers are not present in the late quenching scenario, and so track B does not fit the data. Track B also cannot produce the extremely high stellar masses of today's BCGs, which exceed the stellar mass of any known spiral.

The mixed scenario (track C) involves early mass assembly and star formation, followed by quenching and further (but limited) dry merging. This scenario seems most able to explain the properties of both near and far E/S0 galaxies. First, the final mergers making small spheroidal galaxies would be mostly gas-rich, while later mergers along the red sequence would be progressively more gas-poor, as required by the structure sequence. Second, the break point between boxy and disky Es would correspond to the *largest blue galaxies that have migrated onto the red sequence recently*. That break point today is in the range $M_B = -20$ to $-21$, where boxy and disky galaxies coexist (Faber et al. 1997; Lauer et al. 2007). With mean $M/L_B \sim 6$ (from Gebhardt et al. 2003, adjusted to the $B$ band and $H_0 = 70$), this translates to stellar masses of $(1–2) \times 10^{11}\ M_\odot$, or blue progenitor masses of $(0.5–1) \times 10^{11}\ M_\odot$ for equal-mass mergers. These are at the upper end of blue stellar masses today (Bell et al. 2003), as required.

Third, the mass-metallicity relation for E/S0 galaxies arises naturally as a consequence of the same relation that already existed among the blue star-forming precursors. This mass-metallicity relation is strong among nearby blue galaxies (Tremonti et al. 2004) and is visible among star-forming galaxies back to $z = 1$ and earlier (e.g., Kobulnicky et al. 2003). If the amount of dry merging is not too large, this trend will survive to form the metallicity contribution to the E/S0 stellar population scaling relations seen today, with larger galaxies being more metal-rich. The mass-metallicity relation of today's E/S0s may therefore simply be the *fossil relic* of a preexisting relation that existed among the blue progenitors.

Finally, the mixed scenario might even go some way toward explaining the age-$Z$ anticorrelation. Consider a selection of red sequence galaxies at a fixed stellar mass today. In the mixed scenario, these galaxies could have arrived there via different routes: some will have been produced by recent gas-rich mergers of two blue galaxies, while others will have quenched earlier and evolved along the red sequence via dry mergers for a longer time. These routes will produce different outcomes: galaxies that quenched early from small blue progenitors will have low metallicities (reflecting their small progenitors), but their average stellar age will be high (since multiple dry mergers take time). In contrast, galaxies that quenched late and arrived on the red sequence near their present mass will have high metallicities (reflecting more massive progenitors), but their average stellar ages will be younger (because they quenched more recently). This is the required age-$Z$ anticorrelation. Moreover, the more dry merging that takes place along the red sequence, the more the underlying mass-metallicity correlation of the progenitors will be smeared out, to be replaced by a corresponding (inverse) age scatter. The amount of scatter in age and $Z$ at fixed mass might therefore be used to quantify the amount of dry merging that could have occurred, as suggested by Bower et al. (1998) in their discussion of the formation histories of cluster early-type galaxies.

Note that the above discussion has focused for definiteness on the creation of $L^*$ ellipticals via quenching plus mergers. However, the situation is essentially similar for S0s near $L^*$, which may be created via simple massive halo quenching without mergers. These objects will not display the boxy-disky structure sequence of ellipticals, but their mass-metallicity relation and stellar population scaling relations would otherwise be similar.

In conclusion, the mixed scenario with track C seems able to explain the metallicity component of the nearby E/S0 galaxy stellar population scaling relations, and the *multiplicity of routes* that is inherent in this scenario also seems compatible with both the spread in age and $Z$ and the age-$Z$ anticorrelation. However, we have not yet addressed the *age* component of the stellar population scaling relations, i.e., the fact that larger red sequence galaxies are not only metal-rich, but their stars are also older. This question is discussed under the topic of downsizing in the next section.

### 6.2. *Downsizing*

There are many different kinds of downsizing that can affect the stellar population scaling relations and the luminosity and mass functions of nearby E/S0 galaxies. We focus here on the version of downsizing that was introduced by Cowie et al. (1996) to describe their finding that actively star-forming galaxies at low redshifts have smaller masses than actively star-forming galaxies at $z \sim 1$. This suggests that star formation is stronger at later times in smaller galaxies, hence "downsizing."

The downsizing of mean stellar ages was already strongly implied by existing data on nearby galaxies. For example, early-type galaxies are more luminous and more massive than later type galaxies (de Vaucouleurs 1977; Binggeli et al. 1988), and their stellar populations are older (Tinsley 1968; Searle et al. 1973). Color and gas fraction vary systematically along the Hubble sequence (de Vaucouleurs 1977; Roberts 1969) and indicate progressively slower, less efficient star formation in later Hubble types. The blue end of the Hubble sequence is a mass sequence (van den Bergh 1976; de Vaucouleurs 1977), with low-mass Irr galaxies having the smallest fraction of stars and the highest fraction of gas ( Roberts 1969). Abundant evidence thus indicated (even then) that massive galaxies made most of their stars early while small ones formed theirs relatively late. Recent analyses of the star-forming histories of both local galaxies from SDSS (Heavens et al. 2004, revised and updated in Panter et al. 2007) and distant galaxies from the Gemini Deep Deep Survey (Juneau et al. 2005) have confirmed this basic picture.

Blumenthal et al. (1984) offered a reason for this mass-dependent sequence by suggesting that early-type galaxies arose from higher $\sigma$ density perturbations in a cold dark matter (CDM) universe. Such perturbations would collapse first, start making stars early, and grow to higher masses. Moreover, because of the nonwhite nature of the CDM power spectrum, these high-$\sigma$ perturbations would be embedded preferentially within larger high-$\sigma$ perturbations (Bardeen et al. 1986), which caused them to end up in groups and clusters. The accelerated growth of high-$\sigma$ perturbations was demonstrated in early hydrodynamical simulations by Cen & Ostriker (1993), which showed the first galaxies collapsing at the intersections of filaments, forming stars rapidly, and assembling later into groups and clusters. They identified these early-forming objects with E/S0s.[26]

This downsizing of mean stellar age across *all* galaxies may provide a natural explanation for the second component of the stellar population scaling relations, namely, the trend of increasing age with mass. We argued in the previous section that the metallicity part of the relations might be a fossil relic of the similar metallicity-mass trend among blue star-forming galaxies (e.g., Tremonti et al. 2004). In the same way, the age trend might also be a second fossil relic, as downsizing across all blue star-forming galaxies will cause more massive blue precursors to form their stars earlier, which makes them older. This age-mass trend will be impressed on all newly quenched red galaxies as they arrive on the red sequence, setting the stage for the tendency of larger E/S0 galaxies to have older stars today.

We close this section by noting that red sequence galaxies can have many different kinds of downsizing, each one with a different timescale. Thus far we have linked downsizing to the *mean epoch of star formation*. However, there are other timescales, such as the epoch of *quenching* and the epoch of *mass assembly.* These timescales might all vary differently with mass, thereby generating different kinds of downsizing (or even *up*sizing).

Quenching is especially complicated because the various quenching mechanisms likely affect different masses of galaxies at different times. For example, the massive halo quenching model predicts a *fairly constant* quenching mass for central galaxies over recent times, since the critical halo mass remains constant near $M_{\rm crit} \sim 10^{12}\ M_{\odot}$ after $z \sim 2$ (Dekel & Birnboim 2006), and central galactic stellar mass tracks halo mass at the moment of quenching in this model (Cattaneo et al. 2006). The unified merger/AGN/starburst model, on the other hand, implies a *downsizing* of quenching mass because stellar host galaxy masses scale with QSO masses in this model, and the latter are observed to be falling with time (Hopkins et al. 2006). Finally, *satellite* quenching has yet a different effect. This process, which apparently fills in the lower red sequence, would tend to pull down the *average* quenching mass at late times, but this would not impact the characteristic quenching mass of centrals.

[26] It has sometimes been said in the recent literature that CDM predicts that massive galaxies form late and should therefore have younger stars, which is opposite to what the Hubble sequence shows. This remark demonstrates confusion between the formation of galaxies and their dark matter halos. Massive halos indeed form late, but they are making clusters today, not galaxies. The slow cooling of gas in massive halos (Rees & Ostriker 1977; Birnboim & Dekel 2003; Keres et al. 2005; Dekel & Birnboim 2006) means that halo mass can continue to grow without adding to galaxy stellar mass. Moreover, if there is a critical quenching mass above which dark halos do not cool, massive galaxies will have passed over it earlier, which means that star formation in them will have shut down earlier. For all of these reasons (and possibly others), the history of dark halo mass assembly and the history of star formation in galaxies are different.

In summary, blue galaxies may enter the red sequence via several different processes (e.g., mergers, massive halo quenching, satellite quenching), each of which operates at a different characteristic mass and may evolve differently in time. Thus, the red sequence may be built up in different ways at different times and masses, and the concept of a single process that is "downsizing" (or upsizing) probably does not apply.

### 6.3. *Related Topics*

The finding that the majority of red spheroidal stellar mass was quenched *after* $z = 1$ amounts to a paradigm shift with wide repercussions over a range of issues in galaxy formation. This section briefly lists three important questions that are raised by the late quenching picture.

First, where does the increase of mass on the red sequence come from? To answer this, we convert the fits to luminosity density evolution in Table 6 to stellar mass density evolution using mass-to-light ratio values based on optical colors. An empirical formula was given by Lin et al. (2007) that fits stellar $M/L_B$ values from Bundy et al. (2006) (based on SED fitting) to $U - B$, $B - V$, and redshift. Observed colors come from figures in Weiner et al. (2005; $U - B$) and B04 ($U - V$). We find that total stellar mass density has roughly doubled since $z = 1$, which is fairly consistent with literature values between 1.4 and 2.0 (Fontana et al. 2004; Rudnick et al. 2003; Drory et al. 2004, 2005; Borch et al. 2006; but see also Bundy et al. [2005] and Panella et al. [2006], who give smaller rises). Red stellar mass has nearly tripled, but blue stellar mass has increased by only 15%. At $z = 1$, red galaxies comprised only 50% of the total stellar mass, while at $z = 0$ they comprise 70% (cf. Bell et al. [2003], who quote 50%–75%). The total growth in total stellar mass since $z = 1$ is therefore dominated by the growth of stellar mass in galaxies on the red sequence. These numbers are almost identical to those of Borch et al. (2006), which is not surprising since their study was based on COMBO-17 luminosity functions, which we have shown here agree well with DEEP2.

Given the large amount of recent growth in red galaxies, most of it must have occurred via new stellar mass *cycling through* the blue population. The relative constancy of blue stellar mass is therefore due to a (fortuitous?) balance between stellar mass being lost to the red sequence and the creation of new blue stellar mass coming from in situ star formation and continuing mass accretion onto blue galaxies.

A second issue is reconciling the rise in red sequence galaxies with the rate of mergers needed to create them. Estimated pair fractions among $L^*$ galaxies hover around 7% going back to $z \sim 1$, falling slightly with time (Patton et al. 2002; Conselice et al. 2003; Lin et al. 2004; Bundy et al. 2004). Given that some of these mergers are between red sequence galaxies, not blue ones, and assuming a pair visibility time of 0.5 Gyr, we estimate a conversion rate per blue galaxy of roughly 10% per Gyr. Acting over several Gyr, this rate would be large enough to convert a substantial fraction of blue galaxies into red spheroids, as required. A similar conclusion was reached based on counts of merger candidates by Lotz et al. (2006).

A final question is the impact of late quenching on the relationship between spheroids and black holes. The masses of present-day black holes correlate closely with the total stellar masses (Kormendy & Richstone 1995; Häring & Rix 2004) and velocity dispersions (Gebhardt et al. 2000; Ferrarese & Merritt 2000) of their parent spheroids. As long as all spheroids formed early, it was possible to imagine that this relationship is ancient with roots going back to $z \gtrsim 2$, when black hole accretion was at its peak (e.g., Richstone et al. 1998). However, if many spheroids

emerged late from spirals, there is a possible disconnect between the epoch of peak black hole formation (early) and the birth of many spheroids (later). Perhaps the two can be kept in step by invoking downsizing of black holes and spheroids together, as in the unified model of Hopkins et al. (2006). In any case, the late emergence of many spheroids adds an important new challenge to the black hole/galaxy coevolution story.

### 6.4. *Recent Work*

The field of distant luminosity functions is advancing rapidly, and several new papers have appeared since our paper was first submitted. We briefly mention the most relevant developments.

Brown et al. (2007) measured the evolving space density of red galaxies to $z \sim 1$ using broadband photometric redshifts of 40,000 galaxies from the NOAO Deep Wide-Field Survey and *Spitzer* IRAC Shallow Survey. A careful investigation of the photometry uncovered a probable systematic error of $\sim$0.15 mag in DEEP2 magnitudes for spheroidal galaxies in the sense that our magnitudes are too faint. This would cause us to underestimate the number of very bright galaxies, where the luminosity function is steep, and indeed Brown et al. (2007) found more bright galaxies at high $z$ than we do, and thus little increase in the number of *very* bright $4L^*$ galaxies with time. They also counted twice as many red galaxies at $z = 0.9$ as we do (based on $\phi^*$), which is not explained by small magnitude errors. Despite these differences, they concluded that the amount of stellar mass in red sequence galaxies has approximately doubled since $z \sim 1$, which is the same as our minimum increase. A collaboration has started between our teams to observe areas of sky in common and compare results.

Zucca et al. (2006) used VVDS redshifts to determine the luminosity functions of galaxies divided by SED type out to $z \sim 1$. They concluded that stellar mass in red spectral type galaxies roughly doubled from $z = 1$ to now, but a closer comparison is not possible because of their different way of selecting galaxies.

Ilbert et al. (2006) measured distant luminosity functions divided by galaxy morphologies classified from *HST* images. The number of red spheroidal galaxies increased by roughly three from $z = 1$ to now, and $\phi^*$ for blue disks remained constant. Both findings agree with our results. However, $M_B^*$ for disk galaxies faded by only $\sim$0.5 mag, less than half our value.

Ferreras et al. (2005) counted morphologically normal spheroidal galaxies of all colors in the GOODS-S field and found that the number grew by a factor of 5 since $z = 1$. Their sample included both red and blue galaxies but was heavily dominated by red ones. They find a somewhat larger increase than we do, but their field is small and their value might be influenced by cosmic variance.

Cimatti et al. (2006) used the DEEP2 and COMBO-17 red luminosity functions from this paper, added Subaru data at $z \sim 1$ from Yamada et al. (2005), and corrected all functions to $z = 0$ assuming a linear fade of 1.15 $B$ magnitudes per unit redshift. In other words, these authors actually executed the *thought experiment* suggested in § 5 (Fig. 9) to convert luminosity functions to mass functions. They found a large fall in the number of galaxies back in time near $M^*$, as we do, but little change in the number of very massive ellipticals, from which they concluded that massive early-type galaxies must have formed first ("downsizing") and that dry merging after $z = 1$ to form the very largest ellipticals must be limited. We comment further below on present uncertainties in the counts of very luminous ellipticals.

Wake et al. (2006) measured color-selected very luminous red galaxies (LRGs) having spectroscopic redshifts in the SDSS, together with an additional sample of photometrically selected SDSS galaxies for which 2dF redshifts had been added. The sample was limited to luminous objects with $M_{0.2r} < -23$ ($M_B \lesssim -22.2$) over the redshift range $z = 0.15$–$0.6$. After correcting for $M/L_B$ evolution in the manner of Cimatti et al. (2006), they found good agreement with the COMBO-17 luminosity function in the range where the data overlap ($M_B \sim -22$). They also saw little change in the number density of very luminous red galaxies well above $L^*$, in agreement with Brown et al. (2007) and Cimatti et al. (2006).

Cirasuolo et al. (2006) measured $K$-band luminosity functions in the range $z = 0.5$–$2$ split by rest-frame $U - B$. If extrapolated, their $\log \phi^*$ trends show a 30% growth in the number of blue galaxies and an increase in red galaxies of a factor of 2.7 from $z = 1$ to now, in good agreement with our results.

Several works have now measured stellar mass functions based on SED fitting. Bundy et al. (2006) analyzed DEEP2 redshift data (augmented by photometric redshifts) to derive mass functions for red and blue galaxies to $z = 1.4$. The number of bright red galaxies above $M^*$ doubled from $z \sim 1.1$ to 0.55 in their data, but faint red galaxies below $M^*$ grew even more, which they took as evidence for downsizing of the quenching mass. Bright blue galaxies also tended to disappear, which they took as further evidence for downsizing. Total stellar mass remained sensibly constant, and the growth of red stellar mass was largely generated at the expense of blue stellar mass.

Panella et al. (2006) used photometric redshifts and broadband SEDs to estimate stellar masses in GOODS-S and the FDF. Like Bundy et al. (2006), they saw a doubling of mass in bright red galaxies, a decline in the stellar mass of blue galaxies, and only a slight increase in total stellar mass overall.

Borch et al. (2006) measured red and blue stellar mass functions based on COMBO-17 SEDs. Unlike the previous authors, they found that the bright blue mass function was virtually constant, which they took as evidence *against* the downsizing of the quenching mass. Total stellar mass doubled from $z = 1$ to now, the extra mass coming mostly from the growth of red galaxies. We noted in § 6.3 that the Borch et al. (2006) results agree well with ours.

In summary, although certain discrepancies remain, two themes stand out. First, *all* authors claim an increase in total red stellar mass on the red sequence of at least a factor of 2 since $z = 1$, in agreement with the present paper. Second, many authors also claim small or no growth in the number of *very* luminous galaxies well above $L^*$. The evidence for this is weak in our opinion. In § 5 we noted that a photometric error of only 0.2 mag changes the derived number density *by a factor of 2* at $4L_B^*$. To derive stellar masses, $M/L$ needs to be known to the same accuracy. Paradoxically, it may be the magnitudes and masses of *nearby* spheroids that are most in question. Gonzalez et al. (2005) found that BCG luminosities could vary by up to a full magnitude depending on the assumed outer brightness profiles. Lauer et al. (2007) found that SDSS magnitudes of BCG galaxies are systematically too faint by up to a magnitude, and recent work has uncovered a similar underestimate in Two Micron All Sky Survey luminosities (T. Lauer 2006, private communication). The latter data sets are the backbone of local luminosity function determinations (e.g., Bell et al. 2003). Magnitude errors of this size are in the sense that nearby very bright spheroids have been significantly undercounted, leading to an underestimate in late mass assembly due to dry merging. Indeed, the same dry merging would drastically alter the light profiles, making it all but impossible to define the luminosities of bright spheroidal galaxies consistently at all redshifts. Until these fundamental issues

are settled, we think that it is premature to conclude, as some papers have, that very luminous spheroidals were fully assembled by $z = 1$ and have not continued to grow in mass since then.

## 7. SUMMARY

The evolution of *B*-band galaxy luminosity functions since $z \sim 1$ has been determined using a total sample of 39,000 galaxies to $R \sim 24$ mag from the DEEP2 and COMBO-17 surveys. DEEP2 data come from Paper I, while the COMBO-17 data come originally from W03 but have been substantially reworked using improved photo-*z*'s and new color classes. Evolution is examined for blue and red samples separately by dividing galaxies using color bimodality; this is the first study aside from Paper I to compare distant blue and red galaxies in this way. Cosmic variance is reduced to 7%–15% per redshift bin by combining the results of the surveys. DEEP2 counts agree well with COMBO-17 in all color classes at nearly all redshifts.

Luminosity functions of blue and red galaxies evolve differently with redshift; the blue counts shift to brighter magnitudes at fixed number density back in time, whereas red counts are nearly constant at fixed absolute magnitude. Schechter function parameters are fitted to the data assuming constant $\alpha$, and results are compared to recent measurements from other distant surveys. Good agreement is found between DEEP2 and COMBO-17 at all redshifts, and between these and the total luminosity functions of other large, recent surveys. Results dividing galaxies by color are not yet available from these other surveys.

Combining distant Schechter parameters with local ones, we solve for the fading over time of characteristic luminosity $M_B^*$ for All, Red, and Blue samples. All classes fade by nearly the same amount, showing fadings (per unit redshift) of $1.23 \pm 0.19$ mag for red galaxies, $1.35 \pm 0.19$ mag for blue galaxies, and $1.34 \pm 0.33$ mag for all galaxies. In contrast, $\phi^*$ evolves differently for blue and red galaxies, holding steady for blue galaxies since $z = 1$, while rising by $\sim$0.5 dex for red galaxies (a formal value based on two different data treatments). The evolution of luminosity density, $j_B$, also differs with color; for blue galaxies it falls by $\sim$0.6 dex after $z \sim 1$, while for red galaxies it remains virtually constant.

The simplest interpretation of these results is that the number density of blue galaxies has remained nearly constant since $z = 1$, whereas the number density of red galaxies has increased. The latter conclusion is subjected to close scrutiny, and a wide range of possible errors is considered. Two conservative methods set a firm *lower limit* to the rise in red $\phi^*$ of at least a factor of 2. This is further supported by the constancy of red $j_B$, together with a rise of at least 1 mag in the mass-to-light ratios ($M/L_B$) of red stellar populations since $z = 1$. Thus, both the new DEEP2 data and the reanalysis of COMBO-17 strongly support a rise in red number density of *at least a factor of 2* since $z \sim 1$, as found in COMBO-17 by B04. More recent work by other authors is reviewed and supports this minimum value. The rise in morphologically pure E/S0s is even larger if increasing contamination by non-E/S0s at higher redshifts is allowed for.

We stress that our claim of a rise in red number density refers to galaxies near $L_B^*$, not to much more luminous galaxies. To count galaxies on the steep part of the Schechter function requires highly accurate photometry. In our opinion, the requisite accuracy has not yet been attained, for either nearby or distant samples.

The implications of the late formation of many red $L^*$ spheroids are examined. The key point is that the precursors of at least half of all modern-day $L^*$ spheroids *must be visible* in the blue galaxy population at $z \sim 1$, i.e., they are disk galaxies not unlike today's disks in the blue cloud. This lateness of the rise of spheroids is inconsistent with the classic monolithic collapse model for elliptical formation, which predicts constant numbers of spheroidal galaxies over this epoch. Instead, it appears that most present-day E/S0s near $L^*$ arose from blue galaxies with ongoing star formation that were "quenched" at or after $z \sim 1$ and then migrated to the red sequence. The properties of nearby E galaxies are reviewed and found to support a "mixed" scenario in which quenched galaxies enter the red sequence via wet, gas-rich mergers, followed by a limited number of dry, stellar mergers along the sequence. Massive Es are built up during the last stages of dry merging and are visible today as boxy ellipticals. The most extreme of these are BCGs. S0s near $L^*$ can form via quenching without mergers (e.g., via massive halo quenching), but aside from that their histories are similar.

Considerable evidence is reviewed that points to the fact that small galaxies well below $L^*$ have arrived on the red sequence later than larger ones and via a different mechanism. Many of these may be satellites that have been starved or stripped by falling into massive halos. This is consistent with the fact that fainter red sequence galaxies more frequently have disky (i.e., S0) morphologies and populate denser regions than their brighter counterparts. However, ellipticals, which predominate above $L^*$, are strongly *spheroid dominated*, and their formation requires major mergers. A variety of current models that combine merging, stellar feedback, AGN feedback, and inefficient cooling in massive halos may be able to combine the necessary merging and quenching components that are needed to explain them.

The realization that many $L^*$ E/S0s were blue disk galaxies not long ago prompts asking whether the color-magnitude and other stellar population scaling laws for these galaxies might have arisen from the properties of their precursors. The answer is a promising yes. It is now known that these relations signal a rise in both age and metallicity versus mass, together with an anticorrelated scatter in age and *Z* at fixed mass. The metallicity and age trends should both be present in the stellar populations of blue progenitors and would therefore be impressed on all quenched galaxies when they arrive on the red sequence. The age-*Z* anticorrelated scatter could also arise naturally as a consequence of the different merging and star formation histories of red sequence galaxies winding up with the same stellar mass today.

The paper concludes with a discussion of downsizing, taking care to distinguish among the several different kinds that might apply to spheroidal galaxies. Each characteristic time, such as stellar mass assembly time, star formation time, and quenching time, generates its own possible downsizing (or upsizing), and these are not easily predictable without a detailed theory. Two points stand out: the downsizing of star formation efficiency is ubiquitous across all types of galaxies, and its presence among the blue progenitors can explain the older stellar ages of larger nearby E/S0s. Second, there are two fundamentally different types of quenching: gas starvation or stripping of satellites that fall into massive halos, and quenching processes that inject central galaxies onto the red sequence near $L^*$. Downsizing of the one may occur without the other, and the filling in of the lower red sequence may reflect mainly satellite starvation, not necessarily downsizing of the main injection mass. Separating the various processes will prove challenging.

We would like to thank the anonymous referee for a very helpful report that resulted in substantial improvements to the paper. C. N. A. W. thanks G. Galaz, S. Rauzy, M. A. Hendry, and

K. D'Mellow for extensive discussions on the measurement of the luminosity function; E. Bell, J. Brinchmann, A. Gabasch, and G. Galaz for providing electronic versions of their data; S. Lilly for correspondence on the CFRS luminosity function, and G. Blumenthal, J. Cohen, and L. Cowie for useful discussions. S. M. F. thanks R. Somerville, J. Primack, and T. Lauer for extensive discussions concerning the origin of spheroidal galaxies. The DEEP team thanks C. Steidel for sharing unpublished redshift data. The authors thank the Keck Observatory staff for their constant support during the many observing runs of DEEP1 and DEEP2; the W. M. Keck Foundation and NASA for construction of the Keck telescopes; and Bev Oke and Judy Cohen for their tireless work on LRIS that enabled the spectroscopic observations of DEEP1 galaxies. We also wish to recognize and acknowledge the highly significant cultural role and reverence that the summit of Mauna Kea has always had within the indigenous Hawaiian community; it is a privilege to be given the opportunity to conduct observations from this mountain.

The DEEP1 and DEEP2 surveys were founded under the auspices of the NSF Center for Particle Astrophysics. The bulk of the work was supported by National Science Foundation grants AST 95-29098 and 00-71198 to UCSC and AST 00-71048 to UCB. Additional support came from NASA grants AR-05801.01, AR-06402.01, and AR-07532.01 from the Space Telescope Science Institute, which is operated by AURA, Inc., under NASA contract NAS 5-26555. DEIMOS was funded by NSF grant ARI92-14621 and by generous grants from the California Association for Research in Astronomy and from UCO/Lick Observatory. *HST* imaging of the Groth strip was planned, executed, and analyzed by Ed Groth and Jason Rhodes with support from NASA grants NAS5-1661 and NAG5-6279 from the WFPC1 IDT. S. M. F. would like to thank the California Association for Research in Astronomy for a generous research grant and the Miller Institute at UC Berkeley for the support of a Visiting Miller Professorship. C. W. was supported by a PPARC fellowship. N. P. V. acknowledges support from NASA grant GO-07883.01-96A and NSF grants NSF-0349155 from the Career Awards Program and NSF-0123690 via the ADVANCE Institutional Transformation Program at NMSU. K. G. was supported by Hubble Fellowship grant HF-01090.01-97A awarded by the Association of Universities for Research in Astronomy, Inc., for NASA under contract NAS5-26555. J. A. N. acknowledges support from NASA through Hubble Fellowship grant HST-HF-01165.01-A awarded by the Space Telescope Science Institute, which is operated by the Association of Universities for Research in Astronomy, Inc., for NASA, under contract NAS 5-26555. M. I. was supported by grant R01-2005-000-10610-0 from the Basic Research Program of the Korea Science, and Engineering Foundation Computer hardware gifts from Sun Microsystems and Quantum, Inc. are gratefully acknowledged. This research has made use of the NASA/IPAC Extragalactic Database (NED), which is operated by the Jet Propulsion Laboratory, California Institute of Technology, under contract with the National Aeronautics and Space Administration. Finally, we acknowledge NASA's Astrophysics Data System Bibliographic Services.

## REFERENCES

Arp, H. A. 1966, ApJS, 14, 1
Baade, D., et al. 1999, Messenger, 95, 15
Baldry, I. K., Glazebrook, K., Brinkmann, J., Ivezić, Z., Lupton, R. H., Nichol, R. C., & Szalay, A. S. 2004, ApJ, 600, 681
Baldry, I. K., et al. 2005, MNRAS, 358, 441
Balogh, M. L., Baldry, I. K., Nichol, R., Miller, C., Bower, R. G., & Glazebrook, K. 2004, ApJ, 615, L101
Bardeen, J. M., Bond, J. R., Kaiser, N., & Szalay, A. S. 1986, ApJ, 304, 15
Barger, A. J., Aragón-Salamanca, A., Ellis, R. S., Couch, W. J., Smail, I., & Sharples, R. M. 1996, MNRAS, 279, 1
Barnes, J., & Hernquist, L. 1996, ApJ, 471, 115
Baum, W. A. 1959, PASP, 71, 106
Bell, E. F., McIntosh, D. H., Katz, N., & Weinberg, M. D. 2003, ApJS, 149, 289
Bell, E. F., et al. 2004a, ApJ, 600, L11
———. 2004b, ApJ, 608, 752 (B04)
Bender, R., Burstein, D., & Faber, S. M. 1992, ApJ, 399, 462
Benson, A. J., Bower, R. G., Frenk, C. S., Lacey, C. G., Baugh, C. M., & Cole, S. 2003, ApJ, 599, 38
Bernardi, M., Sheth, R. K., Nichol, R. C., Schneider, D. P., & Brinkmann, J. 2005, AJ, 129, 61
Bernardi, M., et al. 1998, ApJ, 508, L143
———. 2003, AJ, 125, 1849
Bertin, E., & Arnouts, S. 1996, A&AS, 117, 393
Binggeli, B., Sandage, A., & Tammann, G. A. 1988, ARA&A, 26, 509
Binney, J., & Merrifield, M. 1998, Galactic Astronomy (Princeton: Princeton Univ. Press)
Birnboim, Y., & Dekel, A. 2003, MNRAS, 345, 349
Blanton, M. R., et al. 2001, AJ, 121, 2358
———. 2003, ApJ, 592, 819
Blumenthal, G. R., Faber, S. M., Primack, J. R., & Rees, M. J. 1984, Nature, 311, 517
Bolzonella, M., Pelló, R., & Maccagni, D. 2002, A&A, 395, 443
Borch, A., et al. 2006, A&A, 453, 869
Bower, R. G., Kodama, T., & Terlevich, A. 1998, MNRAS, 299, 1193
Bower, R. G., Lucey, J. R., & Ellis, R. S. 1992, MNRAS, 254, 601
Brinchmann, J., et al. 1998, ApJ, 499, 112
Bromley, B. C., Press, W. H., Lin, H., & Kirshner, R. P. 1998, ApJ, 505, 25
Brown, M. J. I., Dey, A., Jannuzi, B. T., Brand, K., Benson, A. J., Brodwin, M., Croton, D. J., & Eisenhardt, P. R. 2007, ApJ, 654, 858
Bundy, K., Ellis, R. S., & Conselice, C. 2005, ApJ, 625, 621
Bundy, K., Fukugita, M., Ellis, R. S., Kodama, T., & Conselice, C. 2004, ApJ, 601, L123
Bundy, K., et al. 2006, ApJ, 651, 120
Caldwell, N., Rose, J. A., & Concannon, K. D. 2003, AJ, 125, 2891
Cattaneo, A., Dekel, A., Devriendt, J., Guiderdoni, B., & Blaizot, J. 2006, MNRAS, 370, 1651
Cen, R., & Ostriker, J. P. 1993, ApJ, 417, 415
Charlot, S., & Silk, J. 1994, ApJ, 432, 453
Chen, H.-W., et al. 2003, ApJ, 586, 745
Cimatti, A., Daddi, E., & Renzini, A. 2006, A&A, 453, L29
Cimatti, A., et al. 2002a, A&A, 381, L68
———. 2002b, A&A, 392, 395
———. 2003, A&A, 412, L1
Cirasuolo, M., et al. 2006, MNRAS, submitted (astro-ph/0609287)
Cohen, J. G. 2002, ApJ, 567, 672
Coil, A. L., et al. 2004, ApJ, 617, 765
Colless, M., Burstein, D., Davies, R. L., McMahon, R. K., Saglia, R. P., & Wegner, G. 1999, MNRAS, 303, 813
Conselice, C., Bershady, M. A., Dickinson, M., & Papovich, C. 2003, AJ, 126, 1183
Cowie, L. L., Songaila, A., Hu, E. M., & Cohen, J. G. 1996, AJ, 112, 839
Cox, T. J., Jonsson, P., Primack, J. R., & Somerville, R. S. 2006, MNRAS, 373, 1013
Cross, N. J., et al. 2004, AJ, 128, 1990
Croton, D. J., et al. 2006, MNRAS, 365, 11
Cuillandre, J.-C., Luppino, G., Starr, B., & Isani, S. 2001, in Proceedings of Semaine de l'Astrophysique Franaise, ed. F. Combes, D. Barret, & F. Thévenin (Les Ulis: EdP Sciences), 605
Davies, R. L., Efstathiou, G., Fall, S. M., Illingworth, G., & Schechter, P. L. 1983, ApJ, 266, 41
Davis, M., & Huchra, J. P. 1982, ApJ, 254, 437
Davis, M., et al. 2003, Proc. SPIE, 4834, 161
Dekel, A., & Birnboim, Y. 2006, MNRAS, 368, 2
de Lapparent, V., Arnouts, S., Galaz, G., & Bardelli, S. 2003, A&A, 404, 831
De Lucia, G., et al. 2004, ApJ, 610, L77
de Vaucouleurs, G. 1977, in Evolution of Galaxies and Stellar Populations, ed. B. M. Tinsley & R. Larson (New Haven: Yale Univ. Press), 43
di Serego Alighieri, S., Lanzoni, B., & Jørgensen, I. 2006, ApJ, 647, L99
Dressler, A. 1980, ApJ, 236, 351
Drory, N., Bender, R., Feulner, G., Hopp, U., Maraston, C., Snigula, J., & Hill, G. J. 2003, ApJ, 595, 698
———. 2004, ApJ, 608, 742

Drory, N., Salvato, M., Gabasch, A., Bender, R., Hopp, U., Feulner, G., & Panella, M. 2005, ApJ, 619, L131
Eales, S. 1993, ApJ, 404, 51
Efstathiou, G., Ellis, R. S., & Peterson, B. A. 1988, MNRAS, 232, 431
Eggen, O. J., Lynden-Bell, D., & Sandage, A. R. 1962, ApJ, 136, 748
Faber, S. M. 1973, ApJ, 179, 731
Faber, S. M., et al. 1997, AJ, 114, 1771
———. 2003, Proc. SPIE, 4841, 1657
Fabian, A. C. 2005, Philos. Trans. R. Soc. London A, 363, 725
Felten, J. E. 1976, ApJ, 207, 700
Ferrarese, L., & Merritt, D. 2000, ApJ, 539, L9
Ferreras, I., Thorsten, L., Carollo, C. M., Lilly, S., & Mobasher, B. 2005, ApJ, 635, 243
Fioc, M., & Rocca-Volmerange, B. 1997, A&A, 326, 950
Folkes, S., et al. 1999, MNRAS, 308, 459
Fontana, A., et al. 2004, A&A, 424, 23
Fried, J. W., et al. 2001, A&A, 367, 788
Gabasch, A., et al. 2004, A&A, 421, 41
Gebhardt, K., et al. 2000, ApJ, 543, L5
———. 2003, ApJ, 597, 239
Giallongo, E., et al. 2005, ApJ, 622, 116
Gilbank, D. G., Smail, I., Ivison, R. J., & Packham, C. 2003, MNRAS, 346, 1125
Gonzalez, A. H., Zabludoff, A. I., & Zaritsky, D. 2005, ApJ, 618, 195
Gonzalez, J. J. 1993, Ph.D. thesis, Univ. California, Santa Cruz
Graham, A. W., Erwin, P., Caon, N., & Trujillo, I. 2001, ApJ, 563, L11
Granato, G. L., de Zotti, G., Silva, L., Bressan, A., & Danese, L. 2004, ApJ, 600, 580
Graves, G. L., Faber, S. M., Schiavon, R. P., & Yan, R. 2007, ApJ, submitted
Groth, E. J., et al. 1994, BAAS, 26, 1403
Hammer, F., Flores, H., Elbaz, D., Zheng, X. Z., Liang, Y. C., & Cesarsky, C. 2005, A&A, 430, 115
Häring, N., & Rix, H.-W. 2004, ApJ, 604, L89
Harker, J. J., Schiavon, R. P., Weiner, B. J., & Faber, S. M. 2006, ApJ, 647, L103
Heavens, A., Panter, B., Jimenez, R., & Dunlop, J. 2004, Nature, 428, 625
Heyl, J., Colless, M., Ellis, R. S., & Broadhurst, T. 1997, MNRAS, 285, 613
Hibbard, J. E. 1995, Ph.D. thesis, Columbia Univ.
Hogg, D., et al. 2002, AJ, 124, 646
———. 2003, ApJ, 585, L5
Hopkins, P. F., Hernquist, L., Cox, T. J., Robertson, B., Di Matteo, T., & Springel, V. 2006, ApJS, 163, 1
Ilbert, O., et al. 2005, A&A, 439, 863
———. 2006, A&A, 453, 809
Im, M., et al. 2001, AJ, 122, 750
———. 2002, ApJ, 571, 136
Jonsson, P., Cox, T. J., Primack, J. R., & Somerville, R. S. 2006, ApJ, 637, 255
Jørgensen, I. 1999, MNRAS, 306, 607
Juneau, S., et al. 2005, ApJ, 619, L135
Kauffmann, G., Charlot, S., & White, S. D. M. 1996, MNRAS, 283, L117
Kauffmann, G., Colberg, J. M., Diaferio, A., & White, S. D. M. 1999, MNRAS, 303, 188
Kauffmann, G., et al. 2003a, MNRAS, 341, 33
———. 2003b, MNRAS, 341, 54
Keres, D., Katz, N., Weinberg, D. H., & Davé, R. 2005, MNRAS, 363, 2
Kinney, A. L., Calzetti, D., Bohlin, R. C., McQuade, K., Storchi-Bergmann, T., & Schmitt, H. R. 1996, ApJ, 467, 38
Kobulnicky, H. A., et al. 2003, ApJ, 599, 1006
Kodama, T., et al. 2004, MNRAS, 350, 1005
Koo, D. C., et al. 1996, ApJ, 469, 535
———. 2005, ApJS, 157, 175
Kormendy, J., & Bender, R. 1996, ApJ, 464, L119
Kormendy, J., & Richstone, D. 1995, ARA&A, 33, 581
Larson, R. B. 1975, MNRAS, 173, 671
Lauer, T. R., et al. 2007, ApJ, 662, 808
Le Fèvre, O., Crampton, D., Hammer, F., Lilly, S. J., & Tresse, L. 1994, ApJ, 423, L89
Le Fèvre, O., et al. 2005, A&A, 439, 845
Lilly, S. J., Hammer, F., Le Fèvre, O., & Crampton, D. 1995a, ApJ, 455, 75
Lilly, S. J., Le Fèvre, O., Hammer, F., & Crampton, D. 1996, ApJ, 460, L1
Lilly, S. J., Tresse, L., Hammer, F., Crampton, D., & Le Fèvre, O. 1995b, ApJ, 455, 108
Lin, H., et al. 1999, ApJ, 518, 533
Lin, L., et al. 2004, ApJ, 617, L9
———. 2007, ApJ, 660, L51
Lotz, J. M., et al. 2006, ApJ, submitted (astro-ph/0602088)
Loveday, J., Peterson, B. A., Efstathiou, G. P., & Maddox, S. J. 1992, ApJ, 390, 338
Madgwick, D., et al. 2002, MNRAS, 333, 133
———. 2003, ApJ, 599, 997
Marinoni, C., Monaco, P., Giuricin, G., & Constantini, B. 1999, ApJ, 521, 50
Marzke, R. O., & da Costa, L. N. 1997, AJ, 113, 185
Marzke, R. O., da Costa, L. N., Pellegrini, P. S., Willmer, C. N. A., & Geller, M. J. 1998, ApJ, 503, 617
Marzke, R. O., Huchra, J. P., & Geller, M. J. 1994, ApJ, 428, 43
McIntosh, D. H., et al. 2005, ApJ, 632, 191
Menanteau, F., Ellis, R. S., Abraham, R. G., Barger, A. J., & Cowie, L. L. 1999, MNRAS, 309, 208
Mihos, C. J., & Hernquist, L. 1994, ApJ, 427, 112
———. 1996, ApJ, 464, 641
Moustakas, L., et al. 2004, ApJ, 600, L131
Murray, N., Quataert, E., & Thompson, T. A. 2005, ApJ, 618, 569
Nelan, J. E., et al. 2005, ApJ, 632, 137
Newberry, M. V., Boroson, T. A., & Kirshner, R. P. 1990, ApJ, 350, 585
Newman, J. A., & Davis, M. 2002, ApJ, 564, 567
Norberg, P., et al. 2002, MNRAS, 336, 907
Oke, J. B., et al. 1995, PASP, 107, 375
Panella, M., et al. 2006, ApJ, 639, L1
Panter, B., Jimenez, R., Heavens, A. F., & Charlot, S. 2007, MNRAS, in press (astro-ph/0608531)
Patton, D. R., et al. 2002, ApJ, 565, 208
Poggianti, B., et al. 1999, ApJ, 518, 576
Poli, F., Menci, N., Giallongo, E., Fontana, A., Cristiani, A., & D'Odorico, S. 2001, ApJ, 551, L45
Postman, M., & Geller, M. J. 1984, ApJ, 281, 95
Pozzetti, L., et al. 2003, A&A, 402, 837
Press, W. H., Flannery, B. P., Teukolsky, S. A., & Vetterling, W. T. 1992, Numerical Recipes in C (2nd ed.; Cambridge: Cambridge Univ. Press)
Proctor, R. N., & Sansom, A. E. 2002, MNRAS, 333, 517
Ratnatunga, K. U., Griffiths, R. E., & Ostrander, E. J. 1999, AJ, 118, 86
Rees, M. J., & Ostriker, J. P. 1977, MNRAS, 179, 541
Richstone, D., et al. 1998, Nature, 395, 14
Roberts, M. 1969, AJ, 74, 859
Rudnick, G., et al. 2003, ApJ, 599, 847
Salim, S., et al. 2005, ApJ, 619, L39
Sandage, A. R., Binggeli, B., & Tammann, G. A. 1985, AJ, 90, 1759
Sandage, A. R., Tammann, G. A., & Yahil, A. 1979, ApJ, 232, 352 (STY79)
Sandage, A. R., & Visvanathan, N. 1978, ApJ, 225, 742
Sanders, D. B., & Mirabel, I. F. 1996, ARA&A, 34, 749
Schade, D., et al. 1999, ApJ, 525, 31
Schawinski, K., et al. 2007, ApJ, in press (astro-ph/0601036)
Schiavon, R. P. 2007, ApJS, 171, 146
Schiminovich, D., et al. 2005, ApJ, 619, L47
Schmidt, M. 1968, ApJ, 151, 393
Schweizer, F. 1982, ApJ, 252, 455
———. 1986, Science, 231, 227
Searle, L., Sargent, W. L. W., & Bagnuolo, W. G. 1973, ApJ, 179, 427
Simard, L., et al. 1999, ApJ, 519, 563
———. 2002, ApJS, 142, 1
Somerville, R. S., Lee, K., Ferguson, H. C., Gardner, J. P., Moustakas, L. A., & Giavalisco, M. 2004, ApJ, 600, L171
Springel, V., Di Matteo, T., & Hernquist, L. 2005, ApJ, 620, L79
Strateva, I., et al. 2001, AJ, 122, 1861
Takeuchi, T. T., Yoshikawa, K., & Ishii, T. T. 2000, ApJS, 129, 1
Terlevich, A. I., & Forbes, D. A. 2002, MNRAS, 330, 547
Thomas, D., Maraston, C., Bender, R., & Mendes de Oliviera, C. 2005, ApJ, 621, 673
Tinsley, B. M. 1968, ApJ, 151, 547
Toomre, A. 1977, in Evolution of Galaxies and Stellar Populations, ed. B. M. Tinsley & R. Larson (New Haven: Yale Univ. Press), 401
Toomre, A., & Toomre, J. 1972, ApJ, 178, 623
Totani, T., & Yoshii, Y. 1998, ApJ, 501, L177
Trager, S. C., Faber, S. M., Worthey, G., & Gonzalez, J. J. 2000a, AJ, 119, 1645
———. 2000b, AJ, 120, 165
Trager, S. C., Worthey, G. Faber, S. M., Burstein, D., & Gonzalez, J. J. 1998, ApJS, 116, 1
Tremonti, C. A., et al. 2004, ApJ, 613, 898
Tresse, L. 1999, preprint (astro-ph/9902209)
Treu, T., Ellis, R. S., Liao, T. X., & van Dokkum, P. 2005a, ApJ, 622, L5
Treu, T., et al. 2005b, ApJ, 633, 174
Trujillo, I., & Aguerri, J. A. L. 2004, MNRAS, 355, 82
Tyson, J. A., & Jarvis, J. F. 1979, ApJ, 230, L153
van den Bergh, S. 1976, ApJ, 208, L17
van der Wel, A., Franx, M., van Dokkum, P. G., Rix, H.-W., Illingworth, G. D., & Rosati, P. 2005, ApJ, 631, 145
van Dokkum, P. G. 2005, AJ, 130, 2647

van Dokkum, P. G., & Ellis, R. S. 2003, ApJ, 592, L53
van Dokkum, P. G., & Franx, M. 2001, ApJ, 553, 90
van Dokkum, P. G., Franx, M., Fabricant, D., Illingworth, G. D., & Kelson, D. D. 2000, ApJ, 541, 95
Vogt, N. P., et al. 2005, ApJS, 159, 41
Wake, D. A., et al. 2006, MNRAS, 372, 537
Weiner, B. J., et al. 2005, ApJ, 620, 595
Willmer, C. N. A., et al. 2006, ApJ, 647, 853 (Paper I)
Wolf, C., Meisenheimer, K., Rix, H.-W., Borch, A., Dye, S., & Kleinheinrich, M. 2003, A&A, 401, 73 (W03)
Wolf, C., Meisenheimer, K., & Röser, H.-J. 2001, A&A, 365, 660 (W01)
Wolf, C., et al. 2004, A&A, 421, 913 (W04)
Worthey, G., & Collobert, M. 2003, ApJ, 586, 17
Worthey, G., Trager, S. C., & Faber, S. M. 1995, in ASP Conf. Ser. 86, Fresh Views of Elliptical Galaxies, ed. A. Buzzoni, A. Renzini, & A. Serrano (San Francisco: ASP), 203
Yamada, T., et al. 2005, ApJ, 634, 861
Yan, L., & Thompson, D. 2003, ApJ, 586, 765
Yi, S. K., et al. 2005, ApJ, 619, L111
Zucca, E., et al. 2006, A&A, 455, 879